Investigating the use of printed circuit board leach residue as reductant in pyrometallurgical operations

by

Desmond Attah-Kyei

Thesis presented in partial fulfilment
of the requirements for the Degree

of

MASTER OF ENGINEERING
(EXTRACTIVE METALLURGICAL ENGINEERING)

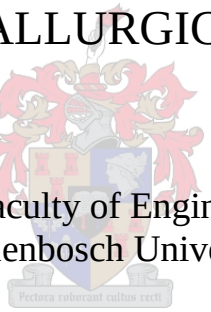

in the Faculty of Engineering
at Stellenbosch University

Supervisor
Prof. G. Akdogan

Co-*Supervisor*
Prof. C. Dorfling

April 2019

Declaration

By submitting this thesis electronically, I declare that the entirety of the work contained therein is my own, original work, that I am the sole author thereof (save to the extent explicitly otherwise stated), that reproduction and publication thereof by Stellenbosch University will not infringe any third party rights and that I have not previously in its entirety or in part submitted it for obtaining any qualification.

Date: April 2019

Plagiarism Declaration

1. Plagiarism is the use of ideas, material and other intellectual property of another's work and to present is as my own.

2. I agree that plagiarism is a punishable offence because it constitutes theft.

3. I also understand that direct translations are plagiarism.

4. Accordingly all quotations and contributions from any source whatsoever (including the internet) have been cited fully. I understand that the reproduction of text without quotation marks (even when the source is cited) is plagiarism.

5. I declare that the work contained in this assignment, except where otherwise stated, is my original work and that I have not previously (in its entirety or in part) submitted it for grading in this module/assignment or another module/assignment.

Student number: 21537992

Initials and surname: D. Attah-Kyei

Signature: 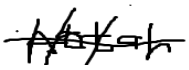

Date: April 2019

Abstract

In recent years, there has been an increase in the generation of waste electrical and electronic equipment (WEEE) due to the advancement of technology. In addition to the environmental benefits of recycling electronic waste (e-waste), it also provides certain economic value. Printed circuit board (PCB) is the main focus of electronic waste because of the inherently high value of contained metals such as gold, silver and copper. Hydrometallurgical processes, consisting of several leaching stages, are often the most preferred option for the recovery of metals from PCB waste. However, hydrometallurgy does not address the issue of non-metallic PCB fractions that may end up being dumped at landfill sites or incinerated. It is important to reduce the environmental impact and gain value from both the metallic and non-metallic fractions of PCB waste.

Several options for treatment of the non-metallic fraction including material recycling, where the residue may be used as inclusions in concrete or asphalt materials with minimal processing or chemical recycling, where chemicals and fuels are produced from the residue using techniques such as pyrolysis exist. Due to the complex composition of PCB leach residue, recovery by thermal treatment is likely to be the most feasible process route from technical and economical perspectives.

In this study, the utilisation of the non-metallic PCB waste fraction as reductant in primary metal smelting operations and solid state reduction was investigated. The organic component as well as the ash composition of the PCB were characterised using Fourier transform infrared spectroscopy (FTIR) and X-ray fluorescence spectroscopy (XRF) respectively. Proximate analysis on the PCB revealed the ash and volatile matter contents being 40.1% and 44.8%, which is higher than coal used in reductive smelting operations. The elemental analysis showed carbon and oxygen content of 30.43% and 20.72% respectively.

Thermodynamic modelling of chromite and iron smelting were performed using various blends of PCB and coal. The models showed that PCB residue might be used to partially replace the conventional reductants. The study revealed that in chromite smelting the optimal blend contains around 20 wt% PCB residue, with energy savings of 200 kWh/t of ore to achieve the same metal recovery.

Laboratory-scale experiments simulating solid state reduction of hematite (Fe_2O_3) was also performed using various blends of PCB and graphitic carbon. The tests were carried out in a Differential Scanning Calorimeter (DSC) from ambient temperature to 1200°C as well as in

Single particle reactor (SPR) at 900℃ and 1000℃. The product of each test was analysed using scanning electron microscope (SEM) and X-ray powder diffraction (XRD). The degree of reduction calculated from the mass lost during the test showed that PCB acts as better reductant at lower temperatures. However, at higher temperatures the advantage shift towards carbon.

Abstrak

In die laaste jare is daar ’n verhoging in die generasie van elektriese afval en elektroniese toerusting (WEEE) as gevolg van die verbetering van tegnologie. Buiten die omgewingsvoordele van die herwinning van elektroniese afval (e-afval), bied dit ook sekere ekonomiese waarde. Gedrukte stroombaanbord (PCB) is die hooffokus van elektroniese afval as gevolg van die inherente hoë waarde metale, soos goud, silwer en koper, wat daarin bevat word. Hidrometallurgiese prosesse, wat uit verskeie uitlogingfases bestaan, is dikwels die mees gewenste opsie vir die herwinning van metale uit PCB-afval. Hidrometallurgie spreek egter nie die probleem van nie-metaal PCB-fraksies wat op die ashoop kan beland, of veras kan word, aan nie. Dit is belangrik om die omgewingsimpak te verminder en waarde te kry uit beide die metaal en nie-metaalfraksies van PCB-afval.

Verskeie opsies bestaan vir die behandeling van die nie-metaalfraksies, insluitend materiaal herwinning waar die residu gebruik kan word as deel van beton of asfaltmateriaal met minimale prosessering of chemiese herwinning, of waar chemikalieë en brandstowwe vervaardig word uit die residu deur tegnieke soos piroliese te gebruik. As gevolg van die komplekse samestelling van PCB loogresidu, is herwinning deur termobehandeling waarskynlik die mees uitvoerbare prosesroete vanuit tegniese en ekonomiese oogpunte.

In hierdie studie is die gebruik van die nie-metaal PCB-afvalfraksies as reduseermiddel in primêre metaal smelting bedrywighede en vaste toestand reduksie ondersoek. Die organiese komponente sowel as die as-samestelling van die PCB is gekarakteriseer deur Fourier transform infrarooi spektroskopie (FTIR) en X-straal-fluoressensiespektroskopie (XRF), onderskeidelik, te gebruik. Kort analise op die PCB het gewys dat die as en vlugtige materie-inhoud 40.1% en 44.8% is, wat hoër is as die steenkool wat gebruik word in reduserende smelting bedrywighede. Die elementanalise het koolstof- en suurstofinhoud van 30.43% en 20.72%, onderskeidelik, gewys.

Termodinamiese modellering van chromiet en yster smelting is gedoen deur verskeie vermengings van PCB en steenkool te gebruik. Die modelle het gewys dat PCB-residu gebruik kan word om die konvensionele reduseermiddels gedeeltelik te vervang. Die studie het gewys dat in chromiet smelting, die optimale vermenging rondom 20 wt.% PCB-residu bevat, met energiebesparings van 200 kWh/t van erts om dieselfde metaalherwinning te bereik.

Eksperimente is op laboratoriumskaal uitgevoer wat vaste toestand reduksie van hematiet (Fe_2O_3) simuleer deur verskillende vermengings van PCB en grafitiese koolstof. Die toetse is

uitgevoer in ’n Differensiaal Skandeerder Kalorimeter (DSC) van omgewingstemperatuur tot 1200 °C sowel as in Enkel partikel reaktor (SPR) by 900 °C en 1000 °C. Die produk van elke toets is geanaliseer deur ’n skandeerder elektron mikroskoop (SEM) en X-straal-poeierdiffraksie (XRD) te gebruik. Die grade van reduksie wat bereken is uit die massa wat verlore gegaan het gedurende die toets het gewys dat PCB as ’n beter reduseermiddel optree by laer temperature. By hoër temperature skuif die voordeel egter na koolstof.

Acknowledgement

I would like to express my gratitude and appreciation to the following:

- Almighty God for His grace and protection
- My supervisors, Prof Akdogan and Prof Dorfling for their technical advice, guidance and support
- Staff at Pyromet division at Mintek especially Marcus and Quinn for their support
- Students and Staff at Ex Mente Technologies especially Johan, Marinda, Nigel and Zane
- Students and staff at Åbo Akademi especially Prof Lindberg
- My family, colleagues and friends especially Prince and Pat.

Table of Contents

List of Figures

List of Tables

List of Abbreviations

BFR	Brominated flame retardant
DSC	Differential Scanning Calorimetry
DTA	Differential Thermal Analysis
EDS	Energy Dispersive X-Ray Spectrometer
E- waste	Electronic waste
EEE	Electrical and Electronic Equipment
FTIR	Fourier transform infrared spectroscopy
HDPE	High Density Polyethylene
ICP-OES	Inductively coupled plasma optical emission spectroscopy
LOI	Loss on Ignition
MF	Metallic fraction
NMF	Non-metallic fraction
PBDE	Polybrominated diphenyl ethers
PCB	Printed Circuit Board
PE	Polyethylene
PET	Polyethylene terephthalate
PP	Polypropylene
PS	Polystyrene
PVC	Polyvinyl chloride
PU	Polyurethane
SEM	Scanning Electron Microscopy
SPR	Single Particle reactor
TBBPA	Tetrabromobisphenol-A

TCD	Thermal conductivity detector
TGA	Thermogravimetric Analysis
WEEE	Waste from electrical and electronic equipment
XRD	X-ray powder diffraction spectroscopy
XRF	X-ray fluorescence spectroscopy

1 Introduction

1.1 Statement of Research Problem

Printed circuit boards (PCBs) are often the focus of electronic waste recycling operations because of the inherently high value contained in metals such as gold and copper that are present in the PCBs. Hydrometallurgical processes, which typically consist of multiple leaching stages to selectively dissolve metals from the PCBs, are the preferred processing method for small scale recycling operations where the expected waste treatment rate would not justify the high capital and operating costs associated with a dedicated smelter. However, these hydrometallurgical processes do not consider the non-metallic fractions of the circuit boards, and often resort to disposal of these waste fractions by landfilling or combustion. Landfilling of the non-metallic fractions could lead to pollution due to leaching of heavy metals and flame retardants, while combustion could lead to the formation of dioxins and furans (Huang, Guo, & Xu, 2009). From an environmental management perspective, a zero-waste approach for PCB recycling should be developed to gain value from and reduce the environmental impact of both the metallic and non-metallic fractions of the PCB waste. This project focusses on the treatment of the solids residue recovered after the majority of metals had been leached from the PCBs.

1.2 Background

The non-metallic fractions of PCBs consist of a mixture of primarily woven glass fibre, thermosetting resins, and flame retardants (Guo, Guo, & Xu, 2009). Recycling of polymeric compounds are generally classified as material recycling, chemicals recycling, or energy recycling (i.e. combustion) (Fink, 1999; Fisher, 2006). Material recycling approaches refer to applications where the non-metallic fractions of the PCBs are used as inclusions or fillers in concrete, asphalt materials, or thermoplastic, resin, or similar matrix composites with minimal processing. Chemical recycling, on the other hand, refers to processes in which chemicals and fuels are produced from PCB leach residue using techniques such as pyrolysis, supercritical fluids depolymerisation or hydrogenolytic degradation. While material recycling is promising, it has found only limited industrial applications due to the diverse composition of circuit boards, poor compatibility between the non-metallic fractions and matrix materials, potential leaching of residual hazardous metals, and generally low public acceptance of products containing recycled PCBs. The high costs associated with chemical recycling methods, on the other hand,

often deter the adoption of these processes even though it is the most effective method to manage hazardous components and to fully utilise all elements (Guo, Guo, & Xu, 2009).

1.3 Aims and Objectives

The research project aims to determine the technical feasibility of using the non-metallic fraction of PCBs recovered after hydrometallurgical removal of metals as a reducing agent in ferroalloy production. The following objectives are set in order to achieve the project aim:

- Perform lab-scale experiments on specific pyrometallurgical operations to understand the behaviour of PCB as a reducing agent
- Perform thermodynamic modelling to investigate the effect of operating conditions (e.g. reducing agent blending ratios, furnace temperature, circuit board composition) on the alloy composition, off-gas composition, and energy balances for different pyrometallurgical operations and interpret.
- Compare thermodynamic modelling results with lab scale tests to prepare a suitable strategy for utilization of PCB residue in ferroalloy and iron making operations.

1.4 Thesis Outline

The thesis sets out as follows: Chapter 1 introduces the study by giving the research problem, background and objectives of this research. Chapter 2 forms the literature review which explores the composition of PCB, effect of disposing waste PCBs as well as methods of recycling. The use of polymer waste as pyrometallurgical operations as well as techniques used for characterising PCB leached residue are also included in Chapter 2. Chapter 3 highlights the experimental procedure, equipment and materials used in the leaching of PCB as well as the step-by-step procedure for reduction tests and thermodynamic simulations. The discussion of experimental results is included in Chapter 4, while Chapter 5 consists of the conclusions and recommendations.

2 Literature Review

2.1 Introduction

The world is currently faced with issues of environmental preservation. The growth of population and demand for wealth have caused the depletion of natural resources and the pollution of the environment. In order to solve this challenge and cause a sustainable society, secondary resources which lower the impact of pollution on the environment should be exploited. Recycling of waste should be given special attention instead of disposing of it. Apart from the shortage of landfill sites, there are other impacts of disposal of waste such as toxicity issue, global warming, effects on the external environment, etc (Legarth, Alting & Baldo, 1995).

One of the fastest growing sectors of the manufacturing industry in the world is the production of electrical and electronic equipment (EEE). Any product that relies on electricity to function is categorized as EEE. Due to technological innovation and intense marketing, these equipment are being replaced rapidly forcing consumers to dispose electronic waste at the same rate. Khaliq et al., 2014 defines electronic waste (E-waste) as a broad and growing range of electronic devices such as cell phones, computers, refrigerators, air conditioners and so on which have been discarded by users. This proliferation of technology has shortened the lifespan of EEE from about 5 years to 2-3 years (Yamane et al., 2011; Ning et al., 2017). Considering that the lifespan of a mobile phone is approximately one year and that of a computer is 2-5 years, it is estimated that about 100 million mobile phones and 17 million computers are discarded annually as a result of malfunctioning equipment or due to technologies becoming obsolete (Yamane et al., 2011). According to Cui & Anderson (2016), there were approximately 41.8 million tonnes of electronic waste generated through the world in 2014 and it is expected that the amount of electronic waste will reach 49.8 million tonnes in 2018, with an annual growth rate of four to five percent.

The UN Environmental Programme estimates that the world generates 20-50 million tonnes of waste from electrical and electronic equipment (WEEE) each year and the amounts are rising three times faster than other forms of municipal waste (Huang et al., 2009). Zhao et al., (2016) predicted based on the gray model that, by 2031, WEEE generation in China which represents about 14% of the world total weight will reach 13 million tonnes**.** Legarth, Alting & Baldo (1995) grouped the sources of environmental problems associated with the disposal of WEEE into three, namely the cathode ray tubes containing heavy metals, the technical thermoplastics

containing various problematic additives and the printed circuit board (PCB) with their complex mixture of chemicals. PCB, ubiquitous in modern EEE, constitutes a significant proportion of WEEE and it represents about 8% by weight of WEEE collected from small appliances and 3% of the mass of global WEEE (Luda, 2011). Recycling of e-waste through appropriate technologies is considered to be a profitable business as the PCBs contain the precious metals (including gold, silver etc.). PCBs, the most valuable part of electronic waste contain more abundant base and precious metal than their ores, normally ten times or higher than rich renewable sources. According to Cui & Anderson (2016), the gold content in PCBs is 35-50 times higher than gold ore. As a result of its high concentration, e-waste recycling and metal recovery is an appealing prospect from economic, technical, and environmental points of view (Cayumil et al., 2014). Printed circuit boards (PCBs) are among the most complex e-waste, containing significant quantities of hazardous and toxic materials leading to high levels of pollution if landfilled or processed inappropriately (Sohaili, Muniyandi & Mohamad, 2012). It is reported that 70% of the heavy metal in the landfill site come from WEEE disposal. The presence of precious metals, in addition to strict environmental regulation, has made the recovery methodologies very suitable (Widmer et al., 2005; Ning et al., 2017)

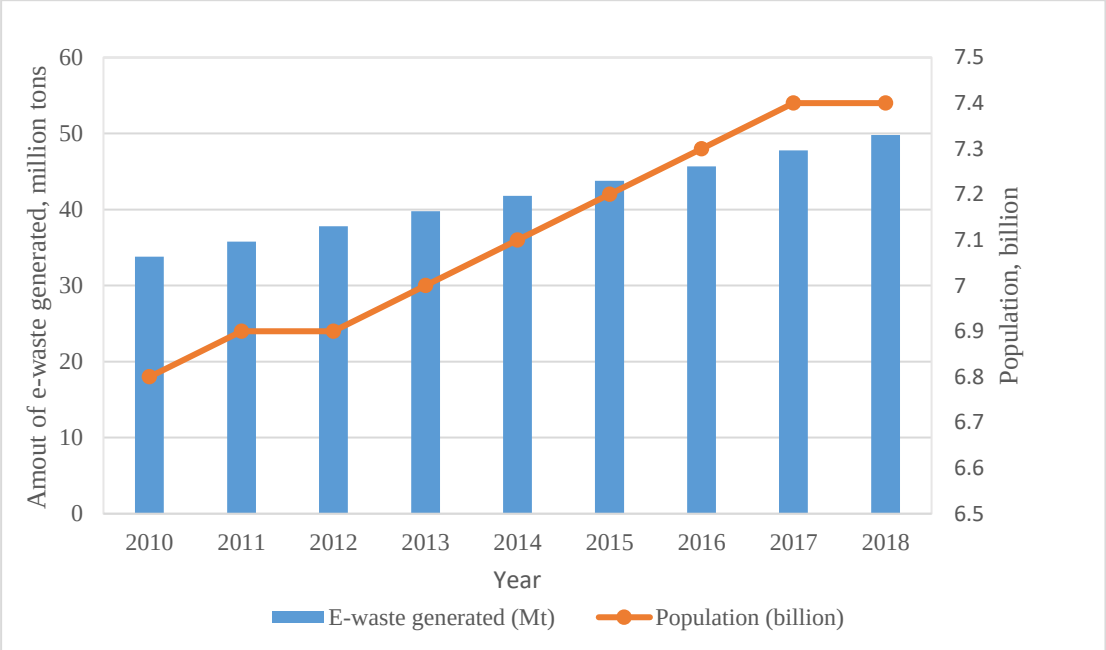

Figure 2.1: Global e-waste generation from 2010 to 2018 (data source (Baldé et al., 2015))

2.2 Composition of PCB

PCBs are platforms on which integrated circuits and other electronic devices and connections are installed. They mechanically support and electrically connect the components using conductive tracks, pads, and copper sheets laminated onto a non-conductive substrate. The components (eg. capacitors, resistors or active devices) are generally soldered on the PCB. Typically, PCBs present a heterogeneous and complex mixture of elements consisting of a 30% polymers, 30% refractories and 40% metals. The platforms of PCB represent about 23% of the weight of whole PCB (Silvas et al., 2015).

During the manufacturing of PCB, carbonaceous compounds such as brominated flame retardants and dyes are added in order to improve the flame resistance and visual recognition ability (Ning et al., 2017). The metals in PCBs consist of copper, iron, tin, nickel, lead, zinc, silver, gold and palladium, mixed with plastics, epoxy resins reinforced with glass fibre and ceramics. The components of circuit board assemblies are held on to the board via solder; so effective recovery of solder via electrochemical or thermal methods would in turn lead to the separation of the components from the board itself. Some of these materials have toxic effects on human health and on environment (for example lead). In spite of hazardous nature of PCB, other materials have added value, as is the case of precious metals and base metals such as gold and copper, respectively (Sohaili, Muniyandi & Mohamad, 2012; Silvas et al., 2015).

The non-metallic materials refer to the residue after separating the copper and other metals either physically or chemically from the waste PCB. They consist of 40% organic substance and 60% inorganic substance. The common organic substances include epoxy resin, brominated flame retardants, dicyandiamide and so on. However, the common inorganic substance is glass fibre which is made from various oxides dominated by silicon oxide, aluminium oxide and calcium oxide (Cayumil et al., 2014; Guanghan et al., 2016). PCBs are manufactured with sophisticated technologies and due to the complex composition, PCBs recycling requires a multidisciplinary approach intended to separate metals and plastics and reduce environmental pollution (Sohaili, Muniyandi & Mohamad, 2012).

Table 2.1: Composition of PCB

Metallic Element, wt%	(Shuey & Taylor, 2005)	(Kim et al., 2004)	(Ogunniyi & Vermaak, 2009)	(Chatterjee, 2012)	(Yokoyama & Iji, 1997)	(Diaz et al., 2016)	(Xiang et al., 2010)
Cu	20	15.6	23.47	16	22	22.62	23.1
Al	2	-	1.33	5	-	-	2.6
Fe	8	1.4	1.22	5	3.6	-	0.8
Sn	4	3.24	1.54	3	2.6	3.075	1.88
Ni	2	0.28	2.35	1	0.32	13.49	0.19
Zn	1	0.16	1.51	1	-	-	1.75
Pb	2	1.35	0.99	2	1.55	-	2.89
Sb	0.4	-	-	-	-	-	0.035
Au	1	0.042	0.570	0.025	0.35	0.53	0.014
Ag	2	1.24	3.301	0.1	-	0.26	0.026
Pd	0.05	0.01	0.29	0.01	-		
Ceramic							
SiO_2	15	41.8	-	-	-	-	-
Al_2O_3	6	6.97	-	-	-	-	-
Alkali and alkaline earth oxides	6	CaO 9.95	-	-	-	-	-
Titanates and mica, etc.	3	-	-	-	-	-	-
Plastics					Total 16 wt%		-
Polyethylene	9.9	-	-	-	-	-	-
Polypropylene	4.8	-	-	-	-	-	-
Polyesters	4.8	-	-	-	-	-	-
Polyvinyl chloride	2.4	-	-	-	-	-	-
Polytetra flouro ethane	2.4	-	-	-	-	-	-
Nylon	0.9	-	-	-	-	-	-

2.3 Disposal of PCB

Hazardous substances present in WEEE, including heavy metals (e.g., mercury, cadmium, lead, etc.), flame retardants (e.g., pentabromophenol, polybrominated diphenyl ethers (PBDEs), tetrabromobisphenol-A (TBBPA), etc.) and other chemicals may pose significant human and environmental health risks, if improperly managed (Kaya, 2016). The non-metallic fractions of PCB are generally treated by incineration or landfilling. There is the formation of highly toxic polybrominated dibenzodioxins and dibenzofurans during incineration process. Moreover, landfilling leads to leaching of some toxic substances into the soil and underground water with time. (Kadari et al., 2017). Muniyandi et al. (2013) stated that the cost of disposal of these

hazardous residues is very expensive in developed countries in addition to the cost of packaging, segregation, transportation and others.

2.4 Recycling PCB

Recycling of waste is not merely reduction of waste but reuse of resources with better economic value or less environmental impact. The process of PCB manufacturing is extremely complicated requiring a large investment in equipment and over 50 separate steps (Duan et al, 2011). It is important to recycle PCBs in order to protect the society as well as recover valuable materials. Many researchers have used various mechanical methods to separate metals and non-metals from PCB waste, such as multi-crushing, grinding, electrostatic separation, gravity separation, density-based separation and magnetic separation.

Guo, Tang & Xu, (2010) used the non-metals of PCB in the production of wood plastic composites, and they discovered that the flexural strength of the composites was higher than those of the control specimen. Wang et al., (2010) reported that using of non-metallic powder from PCBs as an additive in polyvinyl chloride (PVC) substrate, increased the bending strength over the pure PVC with an incorporation of 20% PCB. Franz (2002) stated that the use of the non-metallic PCB for thermoplastics would be the perfect recycling solution. Muniyandi et al. (2013) investigated the feasibility of using non-metallic PCB as filler in recycled high-density polyethylene (HDPE) in the production of rHDPE/PCB composite. They found out that tensile strength, Young's modulus, flexural strength and flexural modulus increased steadily until reaching maximum at PCB content of 30 wt%.

Only 20% of the e-waste generated were recycled from 2003 to 2005. 2% was incinerated and the remaining 78% was dumped at landfill site (Kahhat et al., 2008). Ning et al. (2017) classified the treatment and recycling technique of waste PCB according to the recovery degree. Direct treatment including landfilling and incineration means that no or only the energy of waste PCB was recovered while primitive recycling means the simple recycling of metallic fraction (MF), while the non-metallic fraction (NMF) ended up in the disposal or limited non-hazardous treatment. Advanced recycling includes two parts: separation methods without damage to the NMF and the direct use or modification of NMF.

According to Xiang et al. (2007) there are two types of PCB that need to be recycled. One comes from electromechanical products and the other from the waste of PCB production process. There are three branches of waste recycling according to the different material recovering process. These are thermal processing, chemical processing, and physical

processing. These steps are geared towards removal of the toxic part, upgrading and then refining the required materials.

2.4.1 Physical Recycling

Disassembling of the PCB is the first and the most important stage in recycling because it helps to conserve scarce resources (eg. precious metals), establishes the reuse of components and eliminate toxic materials from the environment (Xiang et al., 2007). It is often referred to as the pre-treatment stage and it is carried out before physical recycling. Almost all current recycling technologies of PCBs include a sorting or disassembling stage. This may be carried out manually (using tools such as a hammer, chisel, screwdriver and bare hands) or in semi-automatic approach; where the application of heat in addition to shear force, impact and vibrations are used to open soldered connections. In some European countries such as Germany, PCB recycling does not include dismantling, but it is directly crushed (Duan et al., 2011; Robinson, 2009).

After dismantling of the PCBs, the physical recycling is carried out. The size of the PCBs is reduced in order to easily separate the metallic from the non-metallic components. The PCB is initially reduced to a size of about 1-2 cm^2 using shredders or granulators and subsequently reduced to 5-10 mm using cutting mills or centrifugal mills. Havlik et al. (2011) stated that crushing is necessary to expose the metal surface by removing the plastics that cover the surface of the metals. Shape separation is then performed using an inclined conveyor and inclined vibrating plate to recover copper from the PCB. After the shape separation, ferrous metals are separated from the PCB using magnet. Density-based and electrical conductivity based separations are used to separate the metals from the non-metallic component in the PCB (Sohaili, Muniyandi & Mohamad, 2012; Khaliq et al., 2014).

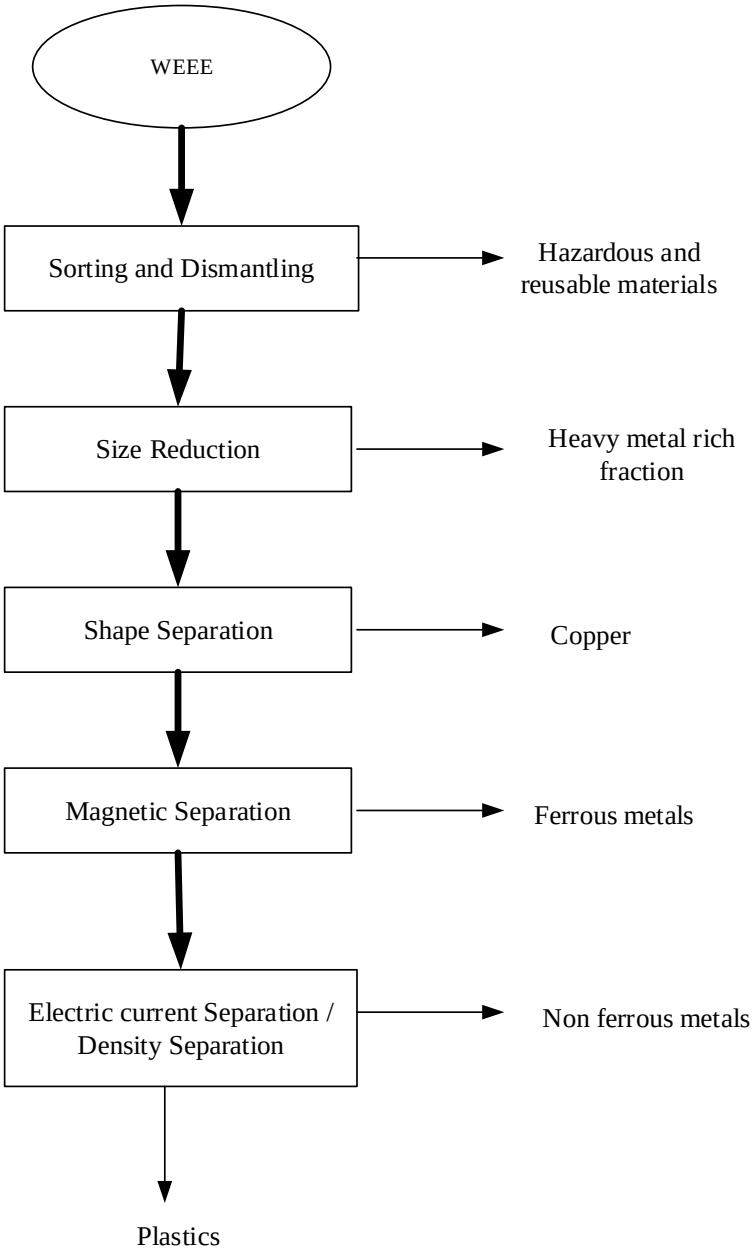

Figure 2.2: A block diagram showing the physical recycling of PCB (Sohaili, Muniyandi & Mohamad, 2012; Khaliq et al., 2014)

2.4.2 Chemical Recycling

In this recycling process, the metals are treated by hydrometallurgical techniques. It consists mainly of leaching, purification and recovery of metals. The constituents of PCB are dissolved to form a pregnant solution using a suitable lixiviant such as sulphuric cyanide, thiosulphate, halides. The metallic fraction is leached from the PCB. Hydrometallurgy is preferred because it is accurate, highly predictable and easily controlled. Hydrometallurgical treatment of e-waste has been proposed to be more efficient and environmentally friendly than other recovery

processes, such as physical separation and combustion. (Sohaili, Muniyandi & Mohamad, 2012; Diaz et al., 2016; Cui & Anderson, 2016).

Havlik et al. (2011) studied the leaching of metals from PCB using 1 M HCl at 80°C. It was discovered that up to 98% of copper was leached from the thermally pre-treated PCB while only 6% of copper was obtained from unburned PCB. He explained that the copper is covered by plastics which protect the copper from contact with the leaching agent. The effects of stirring speed, temperature, solid/liquid ratio and concentrations of HCl and H_2O_2 on the leaching of copper were investigated by Zhang et al. (2012). They concluded that the dissolution of copper from waste PCB in the HCl using H_2O_2 as oxidant was feasible. The increase in both H^+ and Cl^- ion as well as stirring speed enhanced the extraction of copper from the waste PCB.

Cui & Anderson (2016) classified the metallic fractions of PCB into base metals and precious metals. The base metals consist of metals such as copper, lead, zinc etc. whilst the precious metals were gold, silver and palladium. The base metal leaching was generally conducted by using acids such as H_2SO_4, HNO_3, aqua regia and HClO with various oxidants including H_2O_2, O_2, Fe^{3+} and Cl_2. Leaching of the precious metals was the second stage after leaching the base metals. The reagents used for the precious metal leaching include cyanide, thiourea and thiosulfate because of the stable metal complex formed.

Despite the advantages of the hydrometallurgical treatment methods, a serious issue is that they produce a lot of highly toxic wastewater containing cyanides, which might be hazardous for both soil and water bodies. Moreover, non-cyanide leaching solvents like thiourea or thiosulfate have disadvantages including low-stability, high cost, and high reagent consumption (Ning et al., 2017).

Another approach that proves promising in the metallurgical treatment of PCB is biometallurgy. Microbes can be used to recover some metals. These microbes have the ability to bind metal ions present in the external environment at the cell surface or to transport them into the cell for various intracellular functions. The two main areas in biometallurgy are bioleaching and biosorption. Bioleaching has been successfully applied for recovery of precious metals and copper from ores for many years. Faramarzi et al. 2004 carried out research on the bioleaching of metals from electronic wastes and demonstrated that when Chromobacterium violaceum is used, gold can be microbially solubilized from PCB. Bacterial consortium enriched from natural acid mine drainage could efficiently solubilized copper from waste PCBs in about 5 days (Xiang et al., 2010). Biosorption process is a passive physico-chemical interaction

between the charged surface groups of micro-organisms and ions in solution. Certain types of inactive, dead, microbial biomass bind and concentrate heavy metals from even very dilute aqueous solutions. Compared with the conventional methods, biosorption-based process offers a number of advantages including low operating costs, minimization of the volume of chemical/biological sludges to be handled and high efficiency in detoxifying (Sohaili, Muniyandi and Mohamad, 2012).

2.4.3 Thermal Recycling

This process aims at getting metal alloys using incineration or pyrometallurgy. The PCB is crushed and burned in a furnace to recover the precious metals. When PCB is pyrolysed, it leads to the formation of gases, oils and char which may be used as fuels. Pyrolysis degrades the organic part of the PCB and can be used as a method to separate the metallic from the non-metallic component (Sohaili, Muniyandi & Mohamad, 2012). This method is available and very simple. However, the non-metallic part cannot be reused, the waste gas produced as a result of incineration may contain certain toxic gases such as dioxin, lead fume and others. The presence of halogens in plastics (e.g. chlorine in PVC) and bromine in brominated flame retardant (BFR) treated plastics in the electronics scrap feedstock may lead to the formation of brominated and chlorinated dibenzofurans and dioxins in burning processes unless special installations and measures are present. High dioxin and furan formation potential were due to insufficient combustion.

Ortun et al. (2014) studied the pollutant emissions during pyrolysis and combustion of waste PCB before and after metal removal at temperatures 600 and 850 °C at two different atmospheres (nitrogen and sub-stoichiometric air). It was observed that hydrogen bromide is the main gaseous product emitted besides CO and CO_2 during the decomposition of the printed circuit boards, increasing its formation with increasing temperature. The emission of brominated pollutants is much higher than that of chlorinated. The metal enhances emission of halogenated compounds and an increase in the temperature produces the destruction of pollutants. They concluded that the emission trends of the compounds evolved depended mainly on operating conditions (temperature and oxygen ratio), but also on the presence of metals in the material.

The toxic gas emissions may be controlled by treating the off-gas or thermally decomposing at high temperatures (Stewart & Lemieux, 2003). Moreover, the metals obtained from this process need further refining using hydrometallurgical techniques. Bazargan et al., (2014) combined

acid treatment and thermal treatment to get porous silica from the non-metallic fraction of printed circuit board waste. Acid treatment was done using nitric, hydrochloric, and sulphuric acids to remove the metals. Afterwards, thermal treatment was used to remove the bromine and other volatiles from the samples. Higher heat treatment temperatures and longer durations lead to more crystalline SiO_2 with lower specific surface areas. The optimum porous silica sample produced at 500 ^oC showed relative silica content above 99% and a specific surface area as high as 300 m^2/g

Ning et al. (2017) compared pyrometallurgy to incineration of PCB in terms of dioxin and furan emission, bromine recovery, heat recovery and heavy metal recovery and recommended pyrometallurgy as a better approach.

2.4.4 Thermal Behaviour of PCB

When PCB is heated to high temperatures, it decomposes into smaller molecules. Several authors have studied the pyrolysis and combustion of PCB at high temperatures under various conditions. Pyrolysis is the process whereby a material decomposes into gases, oils and chars when it is heated to high temperatures under inert conditions. The products of pyrolysis may be used as chemical feedstock or fuels (Kanchanapiya et al., 2015; Yang et al., 2013). Evangelopoulos, Kantarelis & Yang (2015) studied the pyrolytic behaviour of PCB using thermogravimetric analysis and analytical pyrolysis. The experimental results showed that PCB decomposes at temperatures between 250℃ and 370℃ with production of varying amounts of aromatic compounds such as phenol, bromophenol, styrene and non-aromatic compounds such as acetone and bromomethane. It was discovered that temperature increase favours the production of aromatic hydrocarbons. Rajagopal, Rajarao and Sahajwalla (2016) investigated the kinetic behaviour of waste PCB obtained from monitor and processing boards of computer when heated from 40℃ to 700℃ under nitrogen atmosphere. In the study, pyrolysis occurred at temperatures between 250℃ and 405℃ with a weight loss of about 25%. They estimated activation energy range between 78.60 and 99.08 $kJmol^{-1}$. The weight loss can be ascribed to the thermal decomposition and volatilization of the epoxy resin in the PCB (Zhang et al., 2010). Quan, Li & Gao (2012) subdivided the pyrolysis of PCB into three stages. In the first stage at temperatures less than 293℃, the main products are CH_4, H_2O, CO_2, CO, CH_3COCH_3. Organic species with high molecular weight are produced in the second stage. Carbonization and char formation occur in the last stage at temperatures greater than 400℃.

According to Zhang et al. (2010), the thermal behaviour of PCB in CO_2 atmosphere is comparable to N_2. Nevertheless, when PCB is heated in air, two thermal decomposition steps are obtained. The first step is similar to the degradation in the N_2 atmosphere and the other indicated oxidation of the PCB.

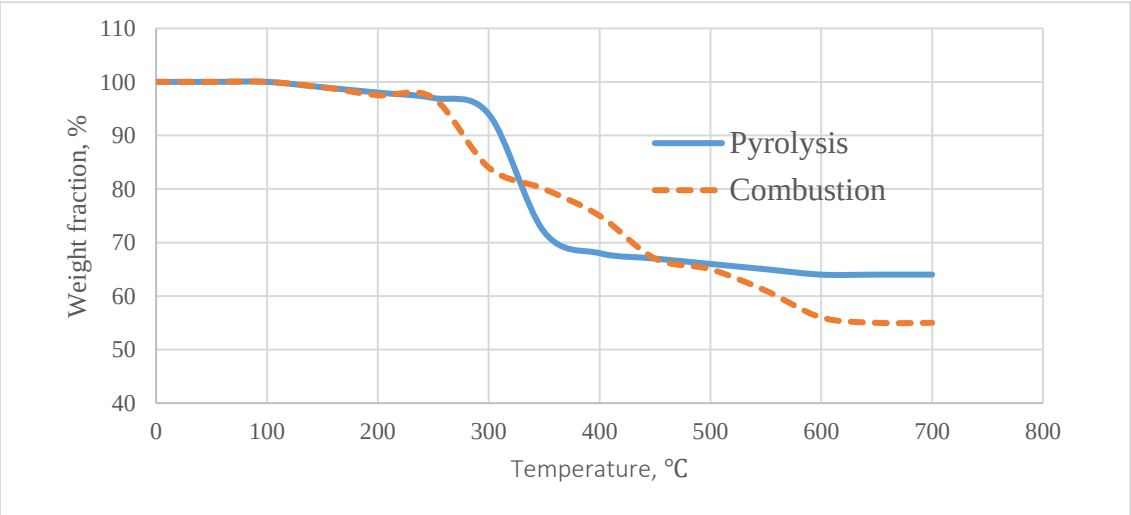

Figure 2.3: Thermogravimetric profile during the pyrolysis and combustion of PCB (Quan, Li, & Gao, 2013)

2.5 Polymer Waste as a Reductant in Pyrometallurgy

Smelting is a form of pyrometallurgy where heat is applied to ore to separate metals from waste fractions. Several metals including silver, iron, copper and other base metals are extracted from their ores using this technique. Smelting usually takes place above the melting point of the metal. Ore is charged in furnace together with a reductant to release the oxygen present in the ore as carbon dioxide. The most common reducing agent is a source of carbon, such as coal, coke, etc. There is a formation of slag during smelting operation. Both the slag produced and the ore that is charged contains oxygen. In order to improve the formation of slag and help in the melting of the oxides in the ore, flux, such as limestone may be added (Melorose, Perroy, & Careas, 2015).

There are various ways of recycling waste plastics: material, energy and feedstock recycling. Material recycling is carried out by melting and transforming the waste plastics into different products. It is often considered as the best method. Only about 22% of the material are of good quality to be recycled (PlasticsEurope, 2009). Energy can be recovered from the plastics by incineration or combustion in kilns. It is estimated that 1 kg of plastic waste has the same heating value as 1 litre of fuel oil. The cement industries consider polymer waste essentially as a substitute for conventional fuel. The third recycling method is aimed at generating chemical

feedstock by using processes such as pyrolysis. There is no sharp distinction between energy and feedstock recycling. For instance, the use of plastics in pyrometallurgical furnaces may be considered as both energy and feedstock recycling since the furnace makes use of both the reduction potential and the heating value of polymers (Fink, 1999; Kato, Nomura, & Uematsu, 2002).

Recycling of plastics as feedstock to reductive smelting operations has been investigated by several authors. One of the major applications in this field involves the use of polymer waste in blast furnaces for steelmaking, where plastics are substituted for coke, coal, or oil used for ore reduction and heating (Carpenter, 2010; PlasticsEurope, 2009). Injecting 1 kg of waste plastics replaced about 1.3 kg of pulverised coal in the blast furnace (BF) of JFE Steel, Japan, and about 1 kg of heavy oil at Stahlwerke Bremen, Germany (Carpenter, 2010). This technology was first implemented on an industrial scale by NKK Keihin Works in Japan after development by Bremen Steel Works in Germany (Zie & Stanek, 2001).

Some factors that influence the amount of polymer waste that can be added to blast furnace feeds include the hydrogen to carbon ratio, the energy content, supply rates required to sustain continuous operation, as well as the chloride and the residual non-ferrous metal content of the waste (Fink, 1999; Nourreddine, 2007). Plastics, compared to coal, have higher hydrogen to carbon ratio. Incorporating plastics in blast furnaces increases the amount of hydrogen gas. An increase in the hydrogen gas content decreases gas density, and therefore reduces the pressure drop or allows a greater gas flow for the same pressure. The reduction by hydrogen is less endothermic than the direct reduction by carbon, hence there is a decrease in energy requirements.

Plastics with high calorific values are required in reduction process. Generally, plastics have higher calorific value relative to coal. Polyethylene(PE) typically has a calorific value of around 46 MJ/kg; polypropylene (PP) 44 MJ/kg, polystyrene(PS) 40.5 MJ/kg, polyethylene terephthalate(PET) 23.5 MJ/kg and polyvinylchloride (PVC) 18.8 MJ/kg (although there are wide variations between rigid an flexible PVC) (Ida, 2006).

Fink (1999), Nourreddine (2007) and Zie & Stanek (2001) reported that the formation of dioxins is not problematic in these processing routes, but formation of chlorine-containing gases such as HCl might result in corrosion of equipment. The chlorine present in the plastic waste is as a result of PVC. Hence, the removal of PVC from the plastics before injection in the furnace is a good option (Carpenter, 2010). PVCs may be treated by heating at 300 °C to 400 °C in an

atmosphere without oxygen. HCl is released and the residual can be injected in furnace. The method is very effective, particularly for 100% PVC plastic. However, if the PVC is mixed in low range of approximately 2% to 30%, thermal decomposition can be carried out in a reaction vessel while agitating and moving forward the plastics by screws or paddles. Hydrochloride is generated at a comparatively low concentration and can be treated by neutralization (Hotta, 2003).

The presence of copper in the polymer waste may however, catalyse the formation of chlorodibenzodioxins; this could hold environmental risks if PCB waste undergoes thermal treatment without complete prior metal recovery. Residual metals in the non-metallic fraction of the PCB waste might also affect the reduction process and alloy quality; trace amounts of copper in steel, for example, results in a brittle product (Fink,1999). Several strategies have been proposed for feeding polymer wastes into the furnaces and could affect the waste's relative contribution to ore reduction (i.e. chemical recovery) and to energy recovery. Feeding strategies include direct mixing with the furnace feed, thermal pre-degradation of polymers into viscous liquids followed by direct injection, or gasification prior to injection (Fink, 1999).

According to Zie & Stanek (2001), injection of plastics in their solid state is usually the most feasible technically and economically. NKK also feed pulverised and granulated plastic solids through tuyeres located near the bottom of the furnace. Following this approach, Hotta (2003) reported that the plastics decomposed to CO and H_2, which acted as reducing agents; the role of H_2 as reducing agent reduced the CO_2 generation by 30 %.

It is reported that approximately 60% of the injected plastics fulfilled the role of reducing agents, while the remainder was used for energy recovery. It has been estimated that only 3% of the total carbon used as a reducing agent remains non-oxidised (Delgado, Barruetabeña, & Salas, 2007). Fisher (2006) also mentioned that direct addition of plastics as reductant to blast furnaces or reductive smelters effectively constitutes in-situ gasification which results in the formation of syngas. Dankwah et al. (2015) investigated the use of mixed plastic waste consisting of high density polyethylene, polypropylene, low density polyethylene, and polyethylene terephthalate as reductant in ironmaking, and reported improved reduction when using the mixed polymers compared to metallurgical coke or individual plastics. The relatively high oxygen content of polyethylene terephthalate was reported to be the cause for the increased CO_2 emissions observed when using the mixed polymers compared to metallurgical coke.

The use of polymer waste, and electronic scrap in particular, in non-ferrous metallurgy has been reported to lead to process disturbances and contamination of products (Fink, 1999). Mark & Lehner (2000) investigated the addition of PCB waste to a zinc fuming furnace, and concluded that the non-metallic fractions of the PCB were used primarily for chemical purposes (i.e. reduction of zinc oxide). It was furthermore reported that the participation of H_2 as reducing reagent might positively influence the reduction kinetics. Zie & Stanek (2001) performed energy balances to compare the impact of different supplementary reducing reagents on the energy efficiency of blast furnaces; it was concluded that the addition of plastic wastes resulted in more savings than when using pulverised coal, natural gas or coke oven gas as the supplementary reducing reagent. Other advantages of using waste plastics as supplementary reducing reagent to oil or coal include the reduction in the reducing agent's sulphur content (and hence improved desulphurisation, which could reduce process disturbances), energy savings of up to 40 %, easier metal/slag separation as well as improved carburisation (Dankwah & Koshy, 2014; Nourreddine, 2007)..

Despite significant research into the use of waste plastic as supplementary reducing agent in pyrometallurgical operations, very limited information about the use of the leached residue of PCBs for this purpose is available. The proposed study will therefore contribute significantly to the knowledge field and assist in expanding the basis for PCB waste recycling process design decisions. Rajarao et al., (2014) studied the use of lead free non-metallic PCB as reducing agent in iron making application. They pyrolysed PCB at temperatures between 750℃ and 1350℃. Analysis of the residue showed a high percentage of carbon (85-90%) and was found to be a promising reducing agent in iron making.

The use of plastics in as reductants in furnaces has several advantages and these are: Coal resources are conserved since there is a lower consumption of both coke and pulverized coal. There is a reduction in the amount of polymer waste being landfilled or incinerated which will help solve the environmental problems associated with the disposal methods. Energy resources are saved. Carpenter (2010) estimated that about 47 GJ/t is saved when plastic waste is used as reductants in blast furnaces. Hydrogen is a more favourable reducing agent than carbon. The regeneration of hydrogen is faster and less endothermic than carbon monoxide regeneration. Plastics generally have lower sulphur and alkalis contents than coal. Injectants with low sulphur contents are preferred because of the effects of sulphur on the quality of the hot metal. Polymer waste have little or no sulphur present in it. Low emissions of dioxins and furans, which are often associated with conventional waste incinerators (Carpenter, 2010).

3 Experimental Methods

3.1 Treatment of PCB

3.1.1 Dismantling

Several methods exist in dismantling of waste PCB. The most common way is manual dismantling where components are removed using pliers, screwdrivers, hammers, etc. Another approach exist where heat is applied to the boards in addition to shear force, impact and vibrations to open the soldered connection.

In this study, the waste PCBs from computers were disassembled by submerging it in 2 mol/dm^3 nitric acid for 24 hours to dissolve the soldered connections (Sharma et al., 2017). The large components, such as stainless steel heat sinks which could not be easily crushed and smaller components such as capacitors, batteries and piezo buzzers were removed after desoldering. The desoldered PCBs were washed with water and air dried.

3.1.2 Size Reduction

The size of the dismantled PCB were reduced in several stages as shown in Figure 3.1

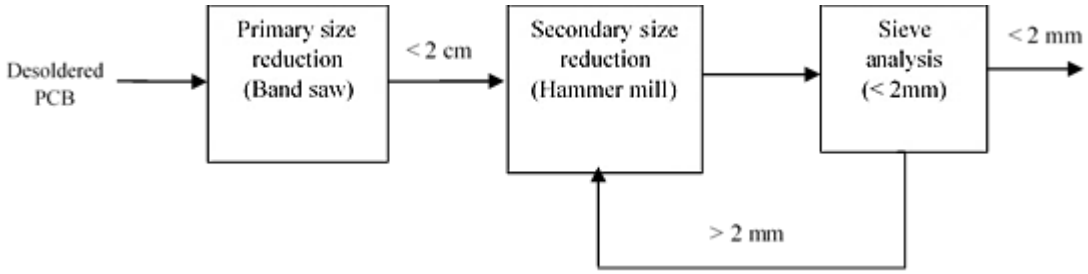

Figure 3.1: Schematic representation of procedure used for size reduction (Albertyn, 2017)

The boards were cut into sizes of about 2 cm by 2 cm using a band saw followed by crushing in a hammer mill. The pieces were gradually fed into the hammer mill and the product sieved to size less than 2 mm. The oversized materials were returned to the mill until the entire charge pass through the 2 mm sieve. The crushed PCBs were divided using a rotary splitter in order to get representative samples for the leaching test. Due to the formation of dust from cutting and the milling of the PCBs, minor feed loss occurred in both operations.

Figure 3.2 (a) shows the image of the PCB used for the study. It can be observed in (b) that the component are completely removed after it was desoldered in nitric acid solution and (c) shows the image of PCB crushed into size less than 2mm.

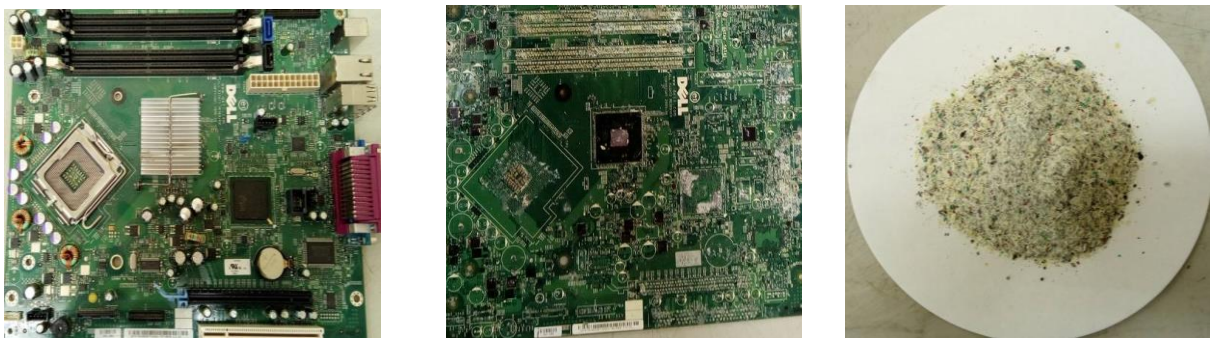

(a) (b) (c)

Figure 3.2: (a) printed circuit board (PCB); (b) Desoldered PCB; (c) crushed PCB

3.1.3 Leaching of PCB

The leaching of metals from PCBs was performed in two stages as shown in Figure 3.3.

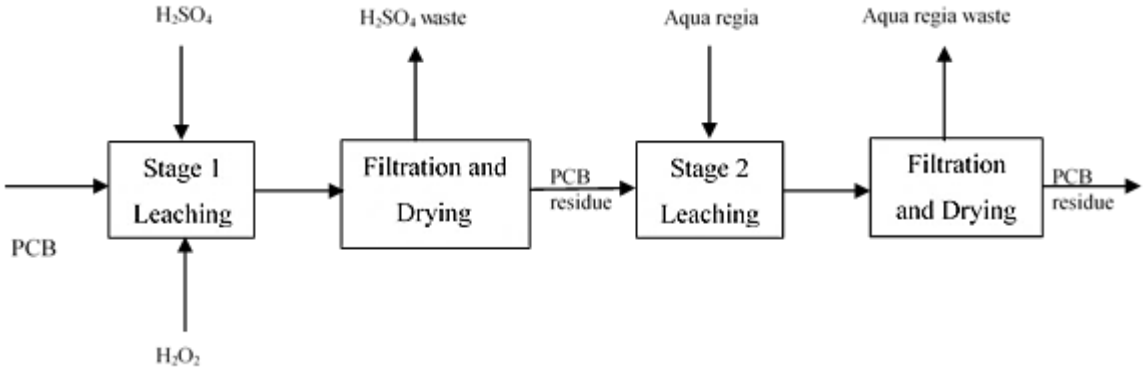

Figure 3.3: Schematic representation of procedure for metal leaching

In the first stage, 400 g of crushed PCBs were leached using 4 litres of 15 wt% H_2SO_4. The leaching was performed for 24 hours at ambient temperature. The product was then filtered and the residue dried in an oven at 60°C. The dried residue was divided using a rotary splitter. Further leaching was performed using aqua regia to completely remove the metals present in the PCB. Aqua regia was prepared by mixing hydrochloric acid (32 wt%) and nitric acid (65 wt%) in a volumetric ratio of 3:1 ($HCl:HNO_3$). The leaching test using aqua regia was performed at a temperature of 60°C. 200 g of H_2SO_4 leach residue was further leached with 2 litres of aqua regia.

Table 3.1: Experimental parameters for leaching

Stage	H_2SO_4, wt%	HNO_3, wt%	HCl, wt%	T, °C	Pulp Density, g/L	Residence Time, h
1	15	-	-	25	100	8
2	-	65	32	60	100	8

3.1.3.1 Equipment

The setup consisted of a 5 litres glass reaction vessel submerged in a water bath holding water. The temperature of the water was set to a specific point which enables the reaction mixture to be cooled or heated to the set point.

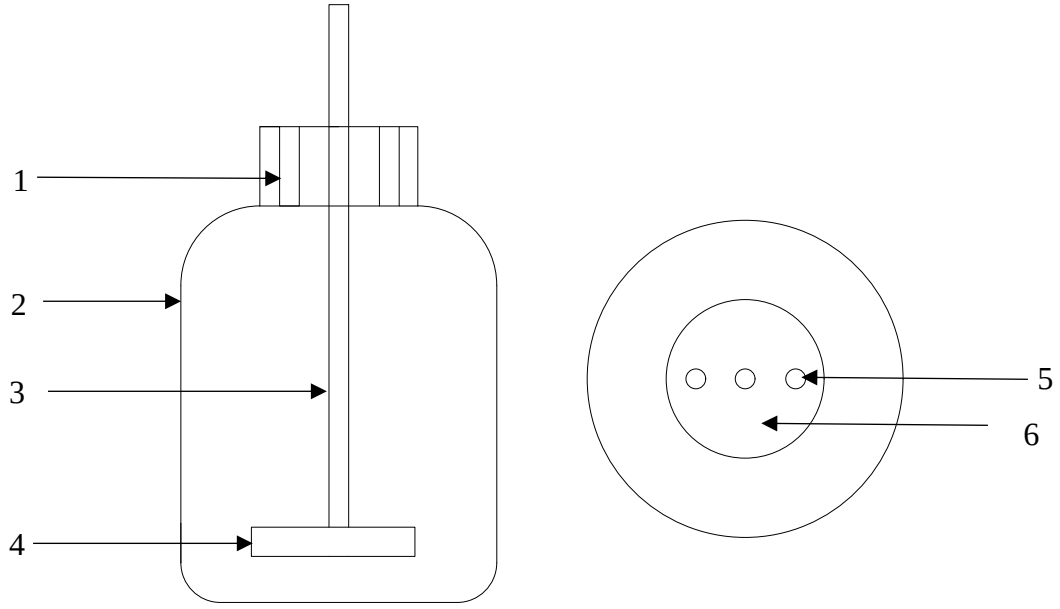

Figure 3.4: Equipment used for leaching

Table 3.2: Components of Leaching set-up

Number	Description
1	Sampling Port
2	5 L glass vessel
3	Teflon impellor
4	Teflon baffles
5	Port for condenser
6	Vessel lid

The reaction vessel was covered with a plastic lid having several ports where the stirrer and the condenser were fitted. There is also a port where the reaction mixture can be sampled during the experiment. The condenser was used to recycle any escaping gasses produced by the leaching processes. Efficient agitation was provided with an overhead stirrer, Teflon impeller and Teflon baffles that were introduced into the reaction vessel. Teflon impellers and baffles were used to ensure that the components do not degrade due to prolonged exposure to lixiviants.

3.1.3.2 Procedure

The temperature of the water in the water bath was set to the desired temperature. 4 litres of H_2SO_4 was prepared and placed in the glass vessel. For the leaching test with aqua regia, 2 litres of the lixiviant was used. The glass vessel containing the lixiviant was placed in the water after it attained the specified temperature, and securely fixed in place.

The setup was left for about 30 minutes to allow the acid attain a similar temperature as the water. The crushed PCBs were then placed in the glass vessel containing the acid. Subsequently, Teflon baffles and impeller were inserted into the vessel. The lid was fitted by pushing the impeller shaft through an aperture. The impeller shaft was connected to an overhead stirrer. The overhead stirrer was switched on and set to 700rpm. Once the lid was in place, the condenser was connected to the lid and the cooling switched on.

At the end of each test, the overhead stirrer and the cooling are switched off. All the connections to the lid were removed and the impeller was unscrewed from the overhead stirrer. The impeller, baffles and the lid were removed afterwards. The contents were decanted to separate the solid from the liquid phase. Water was added several times and decanted after each addition to the residue to wash off the acid. Finally, the product was filtered using a Buchner flask, funnel, filter paper and vacuum pump. The solid residue was dried in an oven at 60°C while the liquid phase was disposed. Each equipment was cleaned subsequently.

3.2 Characterization of the PCB residue

The properties of residue obtained from PCB leaching were characterized using several techniques which were subsequently used as inputs for simulating reduction.

3.2.1 Proximate Analysis

It is a technique where the properties of a substance is determined based on the moisture content, volatile matter, fixed carbon and ash content (Speight, 2005). The proximate analysis was performed on the PCB leach residue using LECO CS 230.

A PCB sample of about 40 mg was placed into an alumina crucible and heated in an inert atmosphere of nitrogen and afterwards in oxygen. The sample was heated from 30°C to 110°C at 50°C/min and maintained at 110°C for 5 minutes under a nitrogen flowrate of 80 mL/min. Subsequently, the temperature was increased to 900°C at a rate of 100°C/min where after the sample was kept isothermally for 5 minutes under nitrogen. Finally, the sample was oxidised for 5 minute using oxygen at the same flow rate as nitrogen.

Drying occurs when the sample is heated to 110℃. The mass loss determined is due to the moisture content. The mass loss during the second stage, where the sample is heated from 110℃ to 900℃, represents loss of the volatile matter. The fixed carbon is the mass lost during the oxidation stage. The mass of residue after the heating is the ash content.

3.2.2 Ultimate Analysis

This is an analysis where the weight percent of carbon, sulphur, hydrogen, nitrogen and oxygen are determined. The weight percent of oxygen is usually calculated by the difference (Speight, 2005). It is also known as elemental analysis. The Vario EL Cube Elemental Analyser from Elementar was used to measure C, H, N and S in the PCB sample. The PCB sample was dried at 110'C to remove water or any absorbed moisture. A clean ball mill was used to homogenize the sample to ensure that a representative sample was analysed. A known weight of dried, homogenous sample was placed in an aluminium foil boat. The sample was introduced into the combustion column at 1050℃. The combustion column was filled with WO_3 and subsequently enriched with oxygen. The C, H, N and S elements bound in the sample burn to form the following gaseous reaction products: CO_2, H_2O, N_2 and NO_X, SO_2 and SO_3 respectively. High purity argon (>99%) carrier gas, flowing at 220 ml/min carries the gaseous products through the reduction tube filled with copper wire. The reduction column reduces the NOx to N_2 and SO_3 to SO_2. All the volatile halogen bound compounds produced during combustion are bound to the silver wool in the reduction column. The pure gasses are then carried to the adsorption columns. The N_2 is not adsorbed and therefore reached the thermal conductivity detector (TCD) first. The CO_2, H_2O and SO_2 each gets adsorbed onto the adsorption columns at room temperature for effective separation. The adsorption columns then get heated sequentially to desorb the different products and are carried through to the TCD. A software computes the percentages of C, H, N and S based on the mass of the sample.

3.2.3 Scanning Electron Microscope

Scanning electron microscope (SEM) is a widely used instrument for analysing the microstructure morphology and the composition of a sample. It systematically scans the surface of interest using focused beam of electrons (primary electrons). The primary electrons interact with the atoms in the sample leading to the generation of various charged particles and photons which contains information about the chemical composition and surface topography of the sample (Stokes, 2008; Zhou et al., 2006).

The PCB residue was characterized using Scanning Electron Microscope (SEM). The sample was mounted in epoxy resin and the surface was polished and coated with a conductive carbon layer. The analysis was conducted by Stellenbosch University Central analytical facility, using a Zeiss MERLIN Field Emission Scanning Electron Microscope, with Energy Dispersive X-Ray Spectrometer (EDS). Beam conditions were 11 nA current, 20 kV accelerating voltage and a distance of 9.5 mm.

3.2.4 X-ray Diffraction

X-ray Diffraction (XRD) supplies information on the phases, structures, and other structural parameters such as average grain size, crystallinity, and crystal defect. XRD provides a way of characterizing crystalline materials, determination of unit cell dimensions, measurement of sample purity. This technique is used for analysing a wide range of materials including pharmaceuticals, plastics, minerals, metals, solar cells, etc. X-rays are created by a cathode ray tube, filtered to produce monochromatic radiation collimated to concentrate and focused toward the material. The incident ray interacts with the material to generate diffracted rays (Bunaciu, Udriştioiu, & Aboul-Enein, 2015).

For the XRD analysis, the PCB sample was pulverized using an agate mortar and pestle. It was then prepared for XRD analysis using a back loading preparation method and analysed with a PANalytical Empyrean diffractometer with PIXcel detector and fixed slits with Fe filtered Co-Kα radiation. The phases were identified using X'Pert Highscore plus software. The relative phase amounts (weight %) were estimated using the Rietveld method. The analysis was conducted by XRD analytical and consulting.

3.2.5 X-ray Fluorescence

It is a technique used to determine the chemical composition of materials. X-rays produced from an x-ray tube or radioactive sources irradiate a material. The atoms of the sample either absorb or scatter the x-ray. The process by which atoms absorb the x-ray by transferring all of its energy to an innermost electron is called "photoelectric effect". During the process, if the x-ray has enough energy to dislodge the inner electrons bound to the nucleus, the atom becomes unstable. Electrons from the outer shell replace the missing inner electrons to stabilize the atom. When this happens, a characteristic x-ray whose energy is the difference between the two binding energies of the corresponding shells is emitted. The emitted x-rays produced from this process are called X-ray fluorescence or XRF. The fluorescent x-ray radiation, which is equivalent to colours of optical light, is characteristic of the element present. It is possible to

determine the elements present in the sample by measuring the energies (determining the colours) (Brouwer, 2010; Schlotz & Uhlig, 2006; Verma, 1956).

The PCB sample was crushed into a fine powder (particle size < 70 µm) with a jaw crusher and milled in a tungsten-carbide Zibb mill prior to the preparation of a fused disc for major and trace elements analysis. The jaw crusher and mill are cleaned with clean uncontaminated quartz between 2 samples to avoid cross contamination. Glass disks were prepared for XRF analysis using 7 g of high purity trace element and Rare Earth Element-free flux ($LiBO_2$ = 32.83%, $Li_2B_4O_7$ = 66.67%, LiI = 0.50%) mixed with 0.7g of the powder sample. Whole-rock major element compositions were determined by XRF spectrometry on a PANalytical Axios Wavelength Dispersive spectrometer at the Central Analytical Facilities, Stellenbosch University. The spectrometer is fitted with an Rh tube and with the following analyzing crystals: LIF200, LIF220, PE 002, Ge 111 and PX1. The instrument is fitted with a gas-flow proportional counter and a scintillation detector. The gas-flow proportional counter uses a 90% argon-10% methane mixture of gas. Major elements were analyzed on a fused glass disk using a 2.4 kW rhodium tube. Matrix effects in the samples were corrected for by applying theoretical alpha factors and measured line overlap factors to the raw intensities measured with the SuperQ PANalytical software. The concentration of the control standards that were used in the calibration procedures for major element analyses fit the range of concentration of the samples. Amongst these standards were NIM-G (Granite from the Council for Mineral Technology, South Africa) and BE-N (Basalt from the International Working Group).

3.2.6 Fourier transform infrared spectroscopy

Fourier Transform Infrared spectroscopy (FTIR) is an analytical method that can be used to detect functional groups and the chemical structure of a liquid, solid or gas. Every bond or functional group has a characteristic frequency at which it vibrates. When infrared (IR) is passed through a sample, some of the radiations are absorbed while others pass through (transmitted). IR radiation at the same frequency is absorbed by the bond and a peak is observed. The radiation absorbed is quantified by calculating absorbance from the incident and emitted radiation intensities (Motang, 2015; Naseska, 2016; Radebe, 2017)

FTIR analysis was performed on the PCB sample to characterize the functional groups of the polymer present in PCB. Thermo Scientific Nicolet iS10 Spectrometer (Thermo Scientific, Waltham, MA) equipped with a Smart iTR diamond ATR accessory was used for the analysis. Spectra were recorded from 4000 to 650 cm^{-1}.

3.3 Thermal Treatment and Analysis

It comprises a variety of measuring methods where the physical properties of a specimen are monitored as a function of temperature as it is subjected to a heating or cooling program. These techniques may include: differential scanning calorimetry (DSC), thermogravimetric analysis (TGA), differential thermal analysis (DTA), etc. (Speyer, 1994).

3.3.1 Differential Scanning Calorimetry

Differential Scanning Calorimetry (DSC) is a technique where the difference in the quantity of heat required to increase the temperature of a sample and reference is measured as a function of temperature. It is an important tool used to study thermodynamic properties such as specific heat capacity, glass transition etc. as well as information regarding reactivity and phase transformation. Both the sample and reference are maintained at nearly the same temperature throughout the experiment. Generally, the temperature program for a DSC analysis is designed such that the sample holder temperature increases linearly as a function of time. The reference sample should have a well-defined heat capacity over the range of temperatures to be scanned (Höhne, Hemminger, & Flammersheim, 2003). The DSC curve may reveal endothermic or exothermic peaks. The area under the peaks describes the enthalpy changes of events occurring. The peaks may be specified based on the size (i.e. the amount of material and energy of the reaction.); position (i.e., start, end, extrapolated onset and peak temperatures) or the shape (which can be related to the kinetics of the process) (Speyer, 1994).

3.3.2 Thermogravimetric Analysis

Thermogravimetric Analysis (TGA) is a technique in which the weight of a sample is measured continuously with respect to temperature or time as the specimen is subjected to a regulated temperature program in a controlled environment. A plot of mass or mass percentage as a function of time is called thermogram or thermal decomposition curve (Skoog, Holler, & Crouch, 1998). It can be used to study chemical decomposition (pyrolysis), oxidation reactions as well as physical processes like vaporization, sublimation, and desorption (Brown, 1989). TGA usually is made up of a sample pan which is supported by a balance. The changes in the mass of the sample as temperature varies are measured with thermobalance or thermogravimetric analysers. The pan is situated in the furnace and is heated or cooled during the test. The mass of the sample is measured and monitored during the experiment. The atmosphere of the sample is purged using inert or reactive gas. A computer system is often used for data acquisition, data processing as well as controlling the flow of purge gas and heating of

furnace. In order to prevent damaging the balance with high temperatures, the balance is thermally isolated from the sample holder situated in the furnace. A sample size between 2 and 50 mg is usually used during TGA experiments. The sample holders used are usually made of platinum, aluminium or alumina with volumes ranging from 40 to 500 µL (Brown, 1989; Gallagher, 2008).

3.3.3 Mass Spectrometry

It is an analytical technique where molecular masses of different species (compounds and atoms) are detected precisely by producing a beam of gas phase ions from the samples. The charged ions are sorted according to their mass-to-charge (m/z) ratios. Mass spectrometers are widely used because they accurately detect and measure molecular masses of samples and also determine the structures of most classes of compounds. The mass spectrometer operates on three main principles: ionization, mass separation and detection. Sample to be analysed is introduced into the system. It is ionized by converting the molecules or atoms into gas-phase ionic species. This is achieved by adding or removing an electron or proton(s) which may break fragment the molecule into pieces. The species are separated based on their m/z (mass to charge) ratios and finally amplified and displayed in the form of mass spectrum.

3.3.4 Reduction Tests

Reduction tests were performed in order to simulate solid state reduction of hematite. This was done in order to understand the behaviour of PCB when used as a reductant. Two set-ups: DSC-TGA and single particle reactor were used for the tests.

3.3.4.1 Materials

The materials used for the reduction tests were high purity chemical grade hematite (Fe_2O_3) and graphite (C) as shown in Table 3.3

Table 3.3: Information of chemicals used for reduction

Substance	Chemical Formula	Purity, wt%	Molar mass, g/mol	Density, g/cm^3
Hematite	Fe_2O_3	> 99	159.69	5.25
Graphite	C	> 99	12.01	2.25

3.3.4.2 Procedure

1 g of hematite and 0.532 g of the graphite (Wang et al., 2016) was used for the reduction process. 1 g of hematite was mixed with 0.532 g of the reductant as shown in Table 3.4. The reagents were weighed using a microbalance.

Table 3.4: Mass of chemicals used in each blend

Sample	Mass in g		
	Hematite	Graphite	PCB
Hematite-Graphite	1.00	0.5320	0.0000
Hematite-20% PCB	1.00	0.4256	0.1064
Hematite-40% PCB	1.00	0.3192	0.2128
Hematite-80% PCB	1.00	0.1064	0.4256
Hematite-100%PCB	1.00	0.0000	0.5320

Hematite and the various blends were placed in a mortar and ground using a pestle to ensure a uniform mixture.

3.3.4.3 DSC-TGA

DSC-TGA was used to investigate the reduction potential of PCB under non-isothermal conditions. The set up used for this study was a Netzsch STA 449 F1 Jupiter differential scanning calorimeter and thermogravimetric (DSC-TGA) instrument with a sensitivity of ±1µg.

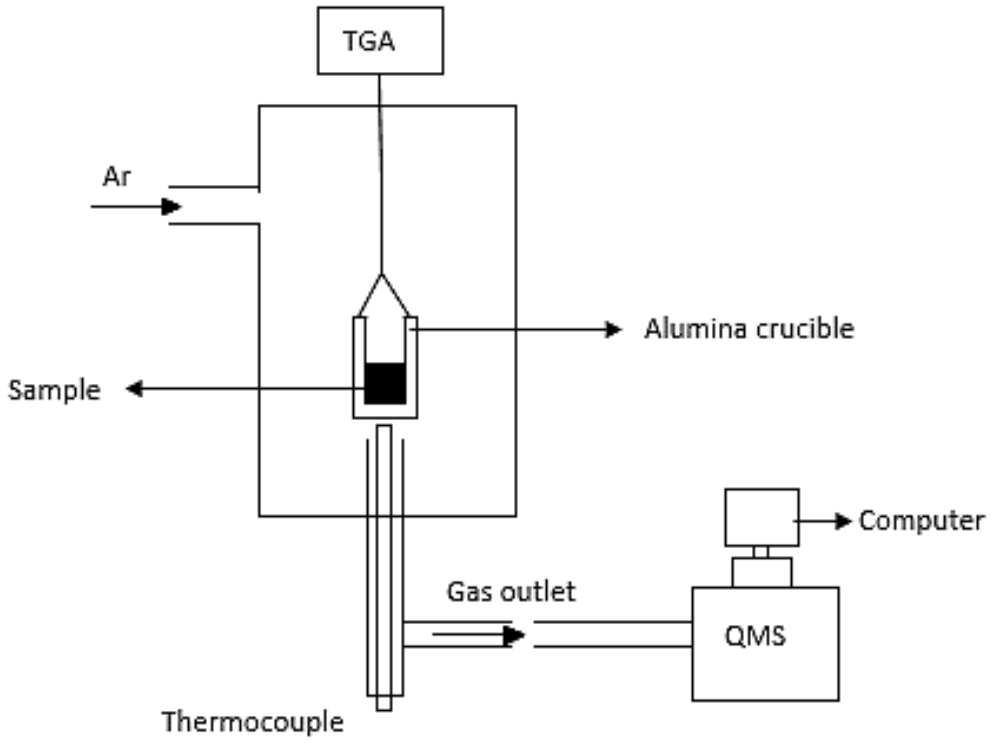

Figure 3.5: Schematic diagram of DSC-TGA coupled with QMS used for the reduction of hematite

The DSC-TGA was coupled with a Pfeiffer Vacuum ThermoStar GSD 301 T3 quadruple mass spectrometer (QMS) to simultaneously analyse the evolved gas to further confirm the reactions occurring. The schematic diagram of the DSC-TGA coupled with QMS is shown in Figure 3.5. The QMS qualitatively detects the presence of a species in the gas. However it does not measure quantitatively the amount or the percentage of species in the evolved gas.

About 20 mg of sample containing the hematite-reductant mixture was weighed in an alumina crucible using a microbalance. The crucible containing the sample was placed on the measuring head of the DSC-TGA, after which the furnace was lowered by pressing the downward lift button on the front display to completely cover the measuring head. The vacuum pump was switched on to remove air and any gas which might interfere with the reduction process. After about 5 min, the vacuum pump was switched off. A constant flow of 70 ml/min high purity (>99%) Ar was used. The species that were expected to be detected were fed into QMS by typing the number representing mass/charge ratio (m/z) into the computer system. For instance, 18 is an input for H_2O. The samples were heated from ambient temperature to 1200℃ at a heating rate of 10℃/min. The QMS detected the presence of CO, CO_2 and other gases predicted by FactSage© in the off gas. The various compounds in the off-gas are ionized and separated based on mass/charge (m/z) ratio in the QMS. TGA measured the change in mass that occurs as a result of the reaction taking place and the DSC shows whether it is exothermic or endothermic. The QMS analysed the off-gas as the test progresses to confirm the reactions occurring.

At the end of each test, the mass spectrometer was switched off and the furnace was allowed to cool. Afterwards, the furnace was lifted up by pressing the upward lift button on the front display and the crucible was taken out of the measuring head. The crucible containing the product was weighed and the product was kept for analysis.

3.3.4.4 Single Particle Reactor

Further reduction tests were carried out in a single particle reactor (SPR) to study reduction tests occurring under isothermal conditions. It consists of a quartz glass reactor which is heated to the desired temperature, a nitrogen purge system, video camera and off-gas analyser as shown in Figure 3.6.

The flow controller regulates the flowrate of the nitrogen gas in the reactor. Three analysers, Chemiluminescence NOx Analyser model 200EM, Servomex xentra 4900 Continuous Emissions Analyser and ABB AO20202, were used to detect and measure the presence of NO, O_2/SO_2 and CO/CO_2 respectively. The analysers are connected to a data logging computer. The video camera may be used to record the images of a sample as reaction progresses.

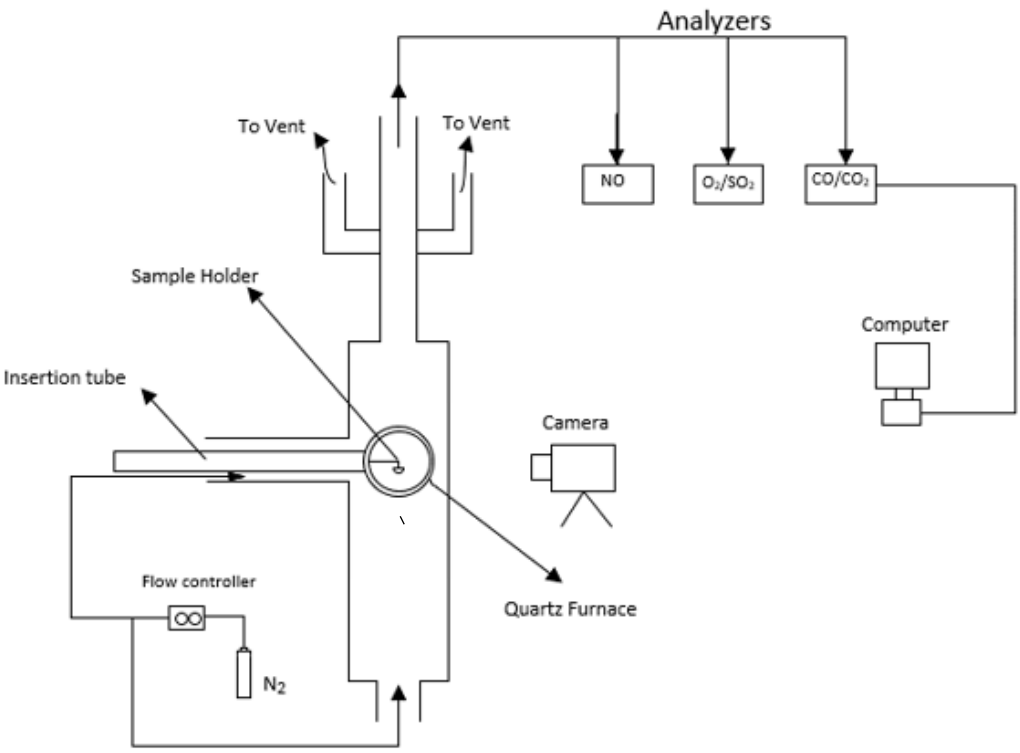

Figure 3.6: Schematic diagram of SPR used for the reduction of hematite

About 0.5 g of hematite-reductant sample was pelletized using a hydraulic press under a pressure of 100 bar for 1 min with distilled water added to ensure complete compactness. The pellets were air dried in an oven at 120℃ to ensure they are totally dried before the reduction tests. The pellet was then place on a sample holder after its weight is recorded. The sample holder containing the pellet was hanged in the insertion tube. The gas analysers were calibrated by flowing known concentration of gases through them. A flow rate of 1 litre per minute nitrogen was set using the flow controller to purge the reactor. The furnace was heated up to the desired temperature at which the reaction would occur. When the reactor attained the desired temperature, the insertion tube was pushed into the hot zone. The video camera was switched on to record the images of the sample as reaction progressed. The reduction tests were carried out at 900℃ and 1000℃. The gas analyser measured the volume percent of CO and CO_2 in the evolved gas.

The SPR is shut down when it was observed that no CO or CO_2 was detected by the analysers. The analysers were first switched off. The insertion tube was pulled out of the hot zone and allowed to cool for about 5 minutes after which it was pulled out completely. The sample holder was removed. The furnace was switched off afterwards.

3.4 Thermodynamic Simulations

FactSage© and EMSIM simulator (Ex Mente Technologies, 2018) were used for the thermodynamic simulations. The characteristics of the leach residue of PCB together with properties of chromite ore (Table 3.5), iron ore (Table 3.6) and coal (Table 3.7) reported in literature were used as input in FactSage© software package and EMSIM.

Table 3.5: Composition of Chromite ore used for smelting (Ex Mente, 2018)

Phase	Mass fraction, %
$FeCr_2O_4$	60.190
$MgAl_2O_4$	15.000
Fe_2O_3	9.936
Mg_2SiO_4	6.594
$CaMg_2Al_{16}O_{27}$	3.352
$Mg_4Al_{10}Si_2O_{23}$	3.289
$MgTiO_3$	0.997
$MnTiO_3$	0.500
Cr_2O_3	0.116
$CaSO_4$	0.013
$Ca_3P_2O_8$	0.013

Table 3.6: Composition of Iron ore used for smelting (Sohn & Fruehan, 2005)

Phase	Mass fraction, %
Fe_2O_3	90.08
SiO_2	7.17
Al_2O_3	1.02
CaO	0.96
MgO	0.51
P_2O_5	0.09
MnO	0.07
Na_2O	0.07

Table 3.7: Properties of Coal (Kleynhans et al., 2017)

Carbon	Hydrogen	Nitrogen	Oxygen	Calorific Value
80.10%	2.29%	1.45%	2.12%	30.49 MJ/kg
Moisture	**Ash**	**Volatiles**	**Fixed Carbon**	**Sulphur**
1.6%	11.7%	5.1%	81.6%	0.74%

3.4.1 EMSIM

EMSIM (Ex Mente Technologies, 2018) is a web-based modelling and simulation software that users interact with through a web browser. It estimates process behaviour and performance based on typical operational inputs, comparable to how the actual plant is operated. When feed rates and ratios for the input streams are specified, the model would calculate the flow rates and

compositions of the output streams, as well as parameters such as yields, recoveries, specific raw material consumptions, and specific energy consumption at equilibrium. EMSIM uses FactSage thermochemical data. The FactSage data makes it possible to estimate the enthalpies of input and output streams accurately, and therefore do accurate energy balance calculations. The same data supports complex equilibrium calculations that are used to estimate the phase composition of product streams and calculate properties such as liquidus temperatures and viscosities (Zietsman, Steyn, & Pretorius, 2018).

Industrial flowsheet modelling was performed using EMSIM. Appendix A.1 shows the steps used in creating the models. Chromite smelting operation carried out in an electric arc furnace at 1700℃ was simulated using EMSIM. At temperatures 900℃, 1000℃, 1100℃, 1200℃ and 1700℃, iron smelting in a blast furnace were simulated using EMSIM. The inputs were repeated in each case varying the blend and the organic content of the PCB. The off-gas composition, degree of metallization and the energy required by each of the blends were compared to coal under the same conditions.

3.4.2 FactSage

Since there is an infinite number of products and arrangements that can be produced from certain reactants, it is vital to ascertain which products are favoured given chemical composition, temperature and pressure. The final products formed during the reduction of ore will be the species with the lowest Gibbs energy from the reactants. FactSage equilib module makes use of the Gibbs energy minimization algorithm for determining the products of complex heterogeneous equilibrium using compound and solution databases. The thermodynamic calculations do not consider the kinetics of the reaction as well as the physical properties of the products such as viscosity of slag, entrainment of alloy etc. (Bale et al., 2008; Malan, 2014).

Thermodynamic calculations were performed using equilib module of FactSage 6.2 to predict the outcome of the reduction of hematite. After a new equilibrium calculation was created, the appropriate units were selected. The ‘initial conditions’ was deactivated and new reactants added. 1 g of hematite was reduced with 0.532 g of reductant as used in the reduction tests. Table 3.4 show the masses used in each calculation. The properties of the PCB residue previously saved as mixtures were imported and added as a mixture. The FACT, ELEM, STGE and FToxid databases were selected for the calculations.

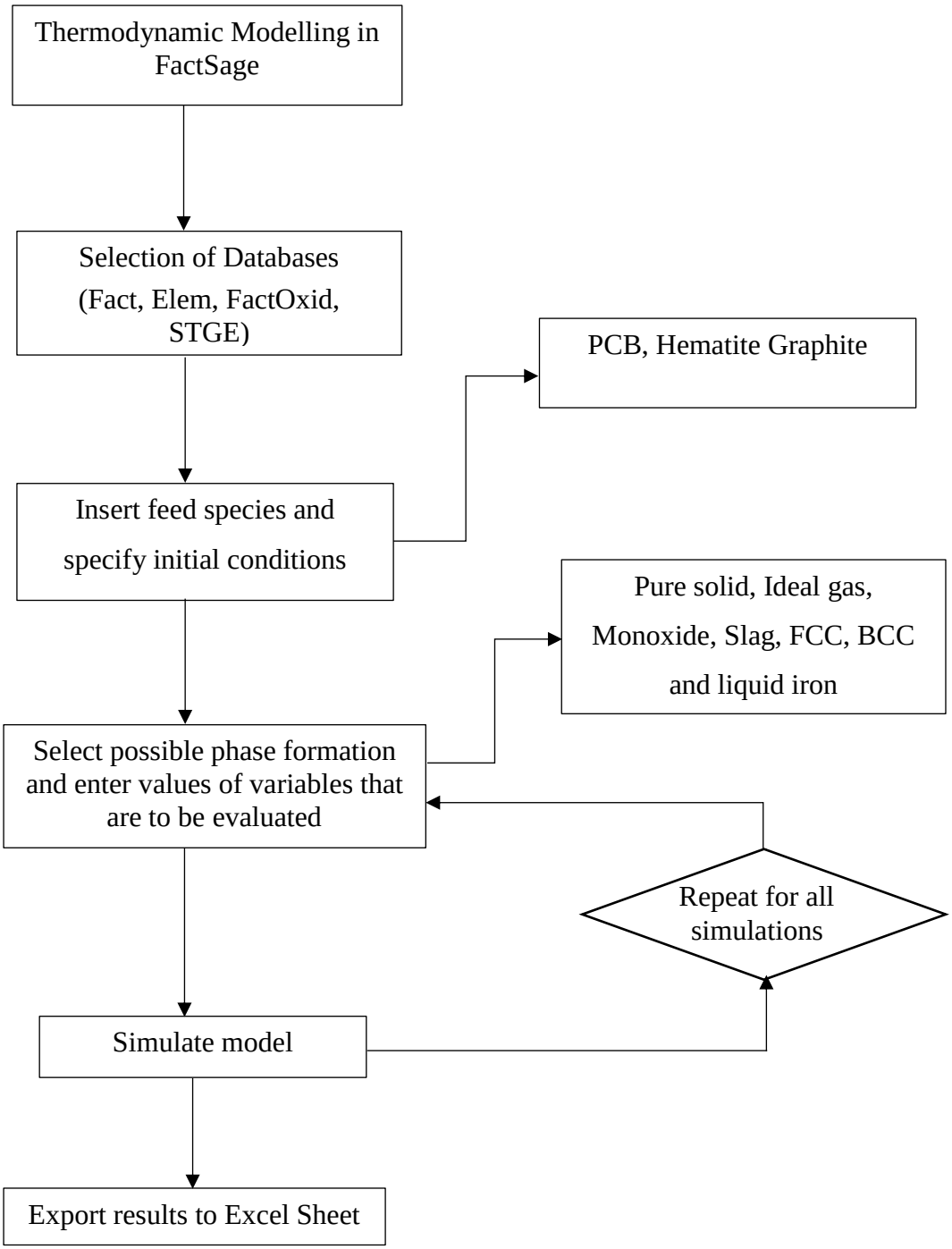

Figure 3.7: 6 basic steps for setting up and simulating a thermodynamic model in FactSage

Thermodynamic calculations were performed from 25℃ to 1500℃ with 25℃ interval. The compound species and the solution phases selected were, ideal gas, pure solids, Monoxide, Slag, Spinel, Liquid iron, BCC and, FCC. The 'normal' equilibrium was activated before the calculations were performed at 1 atm.

4 Results and Discussion

4.1 PCB Leach Residue Characterization

The residue obtained after leaching PCB was characterized using different techniques.

The ultimate analysis or elemental analysis shows that PCB contains carbon and hydrogen content of 30.43% and 3.10% respectively (Table 4.1). The carbon content is significantly less than that of coal (80%), while hydrogen composition is slightly greater than coal (1.60%) as shown in Table 3.7. Both elements give an indication of the reduction potential of PCB although hydrogen has a higher reduction potential. The presence of both carbon and hydrogen indicates the existence of hydrocarbons in the PCB. Carpenter, (2010) stated that the hydrogen bearing materials improves indirect reduction because the generation of H_2 as seen in Equation B.14 is less endothermic and proceeds faster than CO regeneration (Equation B.15).

The weight percent of nitrogen and sulphur in the PCB is 1.42% and 0.63% respectively. These values are similar to the amount present in coal (Table 3.7). The presence of nitrogen and sulphur may be attributed to nitrogen and sulphur containing compounds in the flame-retardants or plastics of the PCB. Polyurethane (PU) is a nitrogen-containing polymer which is made of recurrent units of urethane (–NH–COO–). Its presence in PCB may be the source of nitrogen.

The analysis also revealed oxygen percentage of 20.72%. This value is greater than the oxygen in coal (2.12%) in Table 3.7. Dankwah et al. (2015) investigated the use of mixed plastics as a reductant in iron making. They observed a high CO_2 emission when PET was used as a reductant and attributed it to a high oxygen content. It can be inferred from their observation that the high amount of oxygen present in PCB will lead to increase in the amount of CO_2 during reduction.

Table 4.1: Ultimate analysis of PCB leach residue (wt%)

Carbon	Hydrogen	Nitrogen	Sulphur	Oxygen
30.43	3.10	1.42	0.63	20.72

Table 4.2: Proximate analysis of PCB leach residue (wt%)

Moisture Content	Volatile Matter	Fixed Carbon	Ash Content
3.60	44.80	11.50	40.10

The proximate analysis (Table 4.2) reveals that PCB decomposes with a significantly higher amount of volatile matter compared to coal as shown in Table 3.7. PCB contains epoxy resin,

different kinds of plastics, flame retardants, and fillers. These materials decompose at high temperature thus increasing the percentage of the volatile matter in the PCB. Moreover, plastics are made of long polymeric chains of carbon and hydrogen. It has been reported that the use of plastics in blast furnaces leads to production of C1 to C4 hydrocarbons, H_2 and CO which are known to have reduction potential (Sahajwalla et al., 2010).

The moisture content of PCB (3.6%), representing the amount of water present in the PCB, is slightly higher than that of coal (1.6%) in Table 3.7. The moisture present is likely to be the water left after drying since the PCB may not have been completely dried after the leaching test. The water content may contribute to the formation of CO and H_2 by reacting with carbon as shown in Equation B.13. Both CO and H_2 formed take part in the reduction process. Thus, the moisture content indirectly enhances the reduction process. However, Carpenter (2010) reported that high moisture contents affect handleability of the reducing agent since it causes blockage during transport to injection lances of blast furnace. Moreover, energy is consumed in driving off the water content.

The fixed carbon of PCB (11.5%) represents the carbon content present in the char after decomposition of the PCB. This value is lower than that of the coal (81.6%). The fixed carbon also takes part in the reduction process.

The ash composition represents the inorganic content present in the PCB which remains unchanged after combustion (Evangelopoulos et al., 2015). PCB has ash content of about 40.1%, which is notably higher than coal (11.7%) in Table 3.7. This is attributed to the presence of glass fibre and ceramics as well as metals used for the PCB. The glass fibre and ceramics is mainly composed of SiO_2, Al_2O_3 and CaO.

The ash analysis and the XRF reveals that about 83% of the ash, representing about 30% of the PCB, is SiO_2. This is the highest percentage of the PCB. Carpenter, (2010) stated that SiO_2 in reductant may lead to the presence of Si in hot liquid metal. He also reported that most of the silicon ended up in the slag (94%) with 4% in the hot metal and 2% in the dust. Some of the SiO_2 is reduced under the reducing conditions and at high temperatures enters the molten iron as shown in Equation 4.1

$$SiO_2 + 2C(s) = Si(\text{in liq. Fe}) + 2CO(g) \qquad \textbf{Equation 4.1}$$

Alkaline oxides such as CaO, MgO, Fe_2O_3 were present in the PCB. It is believed that the presence of the alkaline oxides acts as fluxes which lowers the melting temperatures,

particularly in the presence of excess SiO_2. Table 4.5 and Appendix C show the results of XRF scan of PCB residue.

Even though the PCB was leached to ensure that all the metals completely dissolved in the acid, traces of metals like Cu, Ba, Ni etc. as shown in Table 4.3 were present in the ash. These metals mainly came from the soldering tin, copper foil and other electronic components of the PCB. The presence of Cu is undesirable in iron making process because it makes steel brittle (Fink, 1999; Lotfian et al., 2016).

Table 4.3: Ash content of PCB leach residue using ICP-OES (wt%)

SiO_2	Al_2O_3	Fe_2O_3	TiO_2	CaO	MgO	K_2O	MnO	P
84.00	6.28	0.73	0.73	6.00	0.70	0.07	0.01	0.02
83.90	6.39	0.74	0.74	6.05	0.70	0.08	0.01	0.02
Ba	**Cr**	**Cu**	**Ni**	**Sn**	**Sr**	**V**	**Zn**	**Zr**
0.49	0.01	0.11	0.03	0.07	0.04	< 0.01	0.03	0.01
0.49	0.01	0.11	0.03	0.07	0.04	< 0.01	0.03	0.01

Table 4.4: Halide Content and calorific value of PCB leach residue

F, mg/kg	Cl, mg/kg	Calorific value, MJ/kg
2500	4174	12.08
2602	4162	

The presence of halides (F and Cl) shown in Table 4.4 is due to the halogenated flame retardant of the PCB. The chlorine present may also be attributed to PVC plastic in the PCB. As reported previously in 2.5, the presence of chlorine may lead to the formation of chlorine containing gas such as HCl when PCB is used as a reductant. Several studies on recycling plastics have reported that addition of CaO or limestone aids in dehalogenation of plastics by neutralizing the HBr or HCl formed (Shen et al., 2016; Vasile et al, 2006). It can be inferred from this that the CaO present in the ash helps in dehalogenation of PCB.

The calorific value of PCB is less than that of coal. The low calorific value is ascribed to the high ash content of the PCB. The calorific value represents the energy value of the PCB. According to Hadi et al. (2015), the glass fibers of PCB are converted to a glassy slag resulting in a drastic reduction in the combustion efficiency.

XRD analysis (Figure 4.1) revealed that PCB is highly amorphous. Trace amounts of lithium titanium oxide and quartz were also seen.

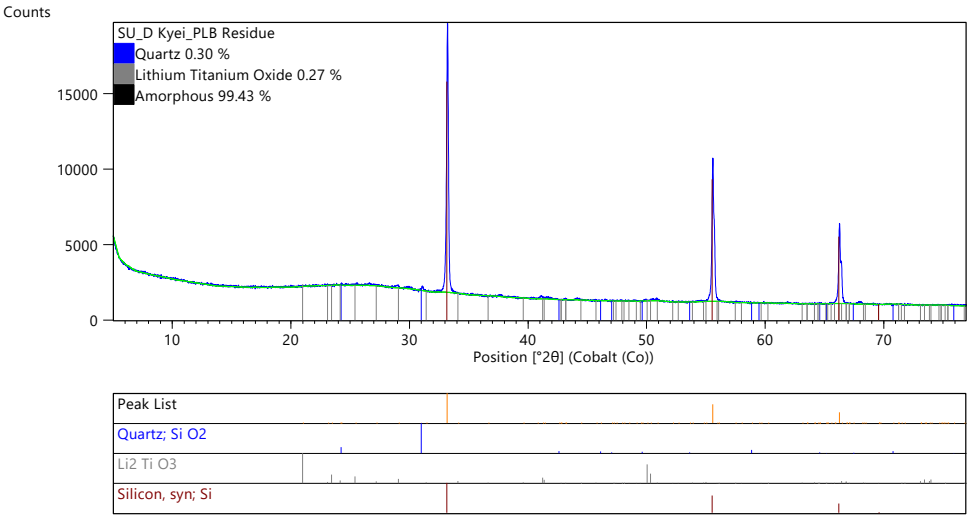

Figure 4.1: XRD pattern of PCB leach residue

Table 4.5: XRF results of PCB leach residue (wt%)

Al_2O_3	CaO	Cr_2O_3	Fe_2O_3	K_2O	MgO
2.62	2.66	bdl	0.31	0.02	0.25
MnO	**Na_2O**	**P_2O_5**	**SiO_2**	**TiO_2**	**L.O.I.**
bdl	0.03	0.02	31.86	0.31	59.85

bdl = below detection limit; LOI = loss on ignition

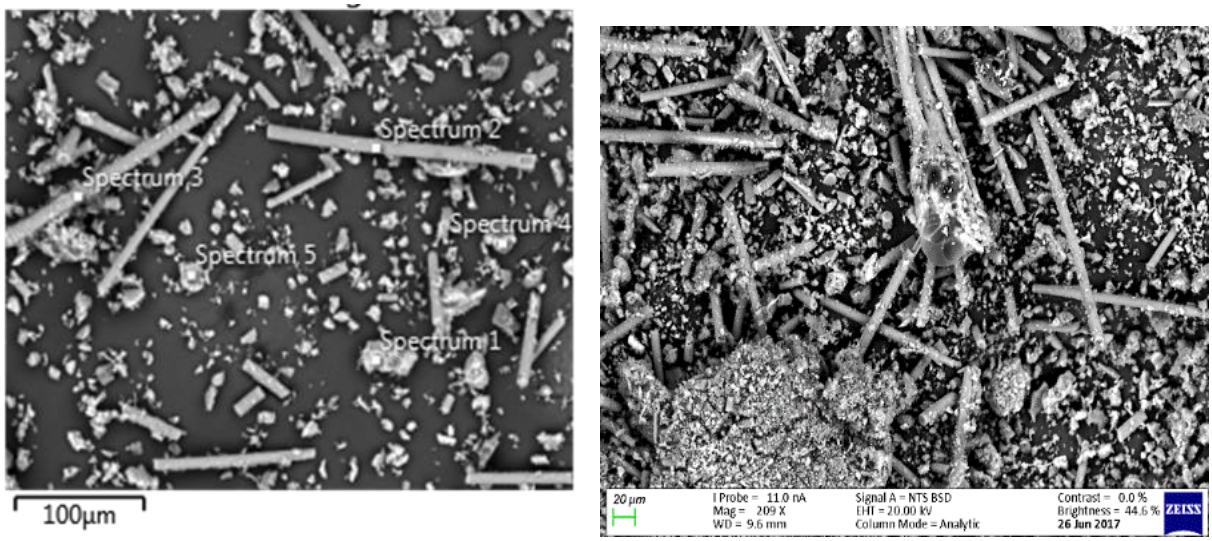

(a) (b)

Figure 4.2: SEM images of PCB leach residue (a) with spectrum labels; (b) without spectrum label

Figure 4.2 shows two SEM images of the PCB sample. The results revealed that the residue contained carbon which ranged from 17 wt% to 60 wt% among different particles. Oxygen content among the particles was varying from 26 wt% to 60 wt%. Silicon content ranged from 0.65 wt% to 30 wt%. Aluminium also fluctuated from particle to particle from 0.69 wt% to 6.85

wt%. Other elements like chlorine, iron, copper and titanium were detected by the SEM (Table 4.6**)**

Table 4.6: Composition and weight percent of elements in the PCB grains

Spectrum Label	Spectrum				
	1	**2**	**3**	**4**	**5**
C	46.92	18.4	17.29	54.15	60.42
O	26.53	46.01	60.5	36.05	29.98
S	0.00	0.50	0.00	0.00	0.00
Al	1.08	0.65	0.96	5.75	6.85
Si	15.99	30.3	19.53	2.27	0.54
Cl	7.94	1.50	0.51	1.77	2.20
Ca	0.00	0.31	0.81	0.00	0.00
Ti	0.00	0.33	0.40	0.00	0.00
Fe	0.61	0.00	0.00	0.00	0.00
Cu	0.93	0.00	0.00	0.00	0.00
Total	**100**	**100**	**100**	**100**	**100**

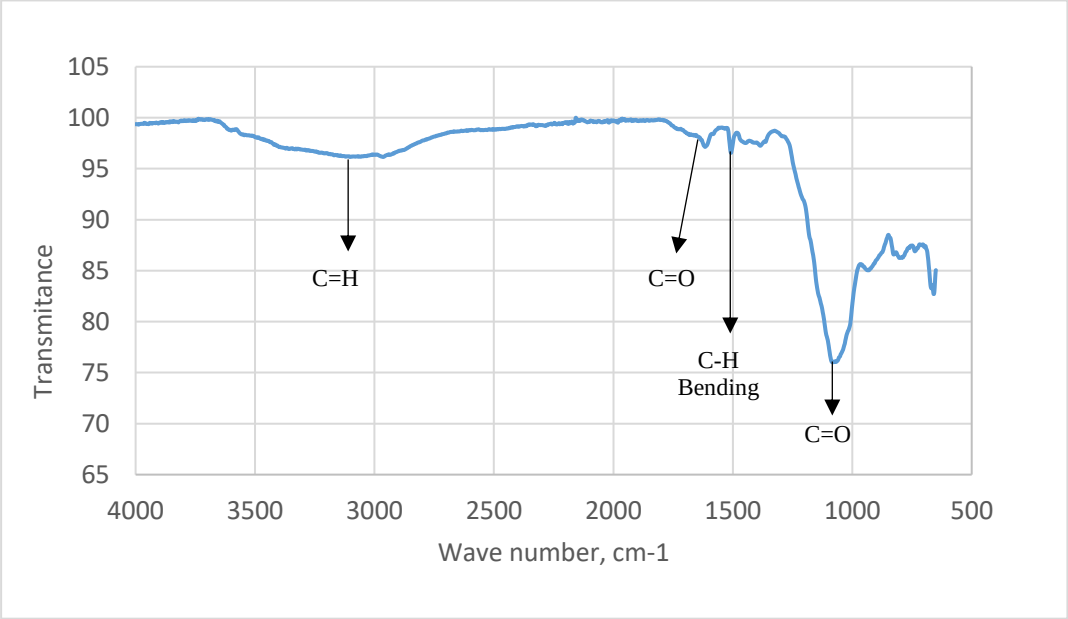

Figure 4.3: FTIR of PCB leach residue

FTIR analysis was performed on the PCB leach residue to determine the functional groups of the organic content present and establish the type of polymeric content in PCB. Figure 4.3 shows the peaks and the corresponding functional groups. Rajagopal et al. (2017) observed a similar pattern in the investigation on sustainable composite panels from non-metallic waste printed circuit boards and automotive plastics.

4.2 Thermal Behaviour of Reagents

Hematite, graphite and PCB were placed individually in the DSC and heated to 1200℃ at 10℃/min in argon atmosphere. Figure 4.4 to Figure 4.6 shows the thermal behaviour of hematite, graphite and PCB respectively under inert conditions.

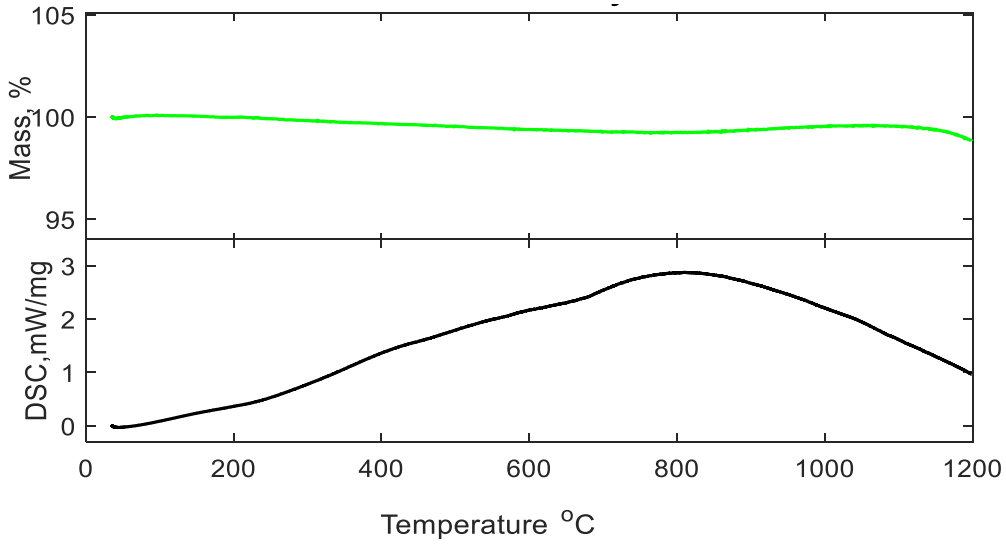

Figure 4.4: Thermal analysis Hematite only

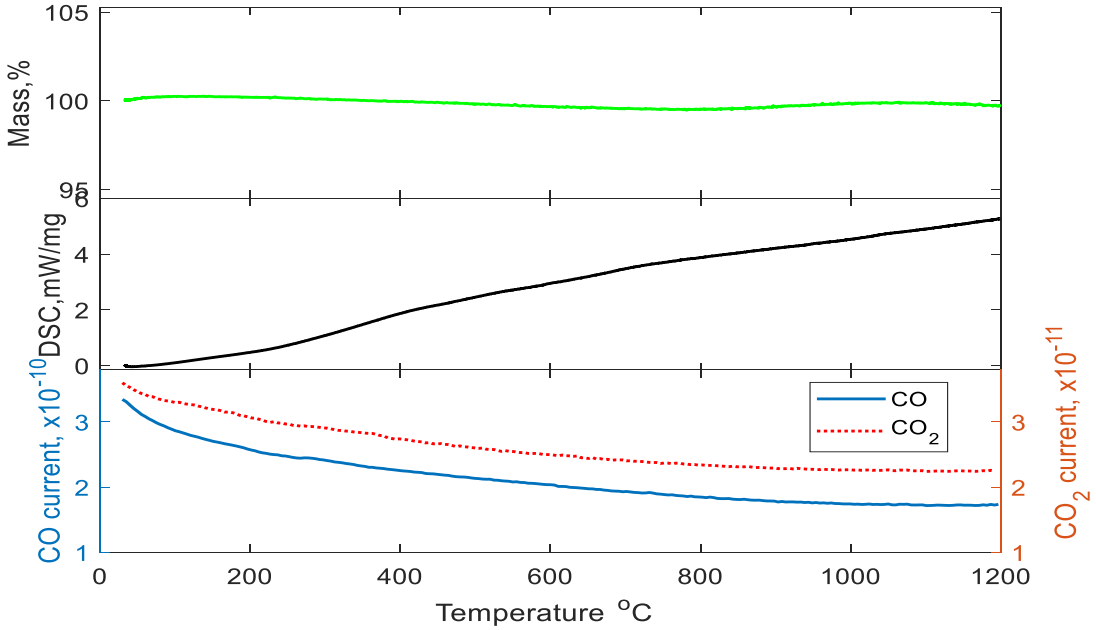

Figure 4.5: Thermal analysis of graphite only

The test with hematite alone Figure 4.4 reveals a slight exothermic peak at about 800℃. This is due to the formation of magnetite. According to Cao et al. (1999), hematite is converted to magnetite when it is heated under inert atmosphere above 420℃ as shown in Equation 4.2.

$3Fe_2O_3 = 2Fe_3O_4 + {}^1/_2\,O_2$ **Equation 4.2**

There was no significant change in mass when hematite only and graphite only were heated to 1200℃. However, there was a notable loss of mass during the run with PCB only (Figure 4.6). About 30% of the PCB mass was lost between temperatures 275℃ and 325℃. This was also observed by Li et al. (2010) during low-temperature pyrolysis of PCB as well as Rajagopal et al. (2016) in kinetic studies of high-temperature transformations of waste printed circuit boards from computer monitor and CPU. The mass loss is attributed to the pyrolysis of PCB. Epoxy resin, the flame retardants and polymer content in the PCB decompose and are released in gaseous form. The mass spectrometer detected the presence of CO, CO_2, HBr, S_2 and hydrocarbons like CH_4 and C_2H_6 in the off-gas as shown in Figure 4.7 and Figure 4.8

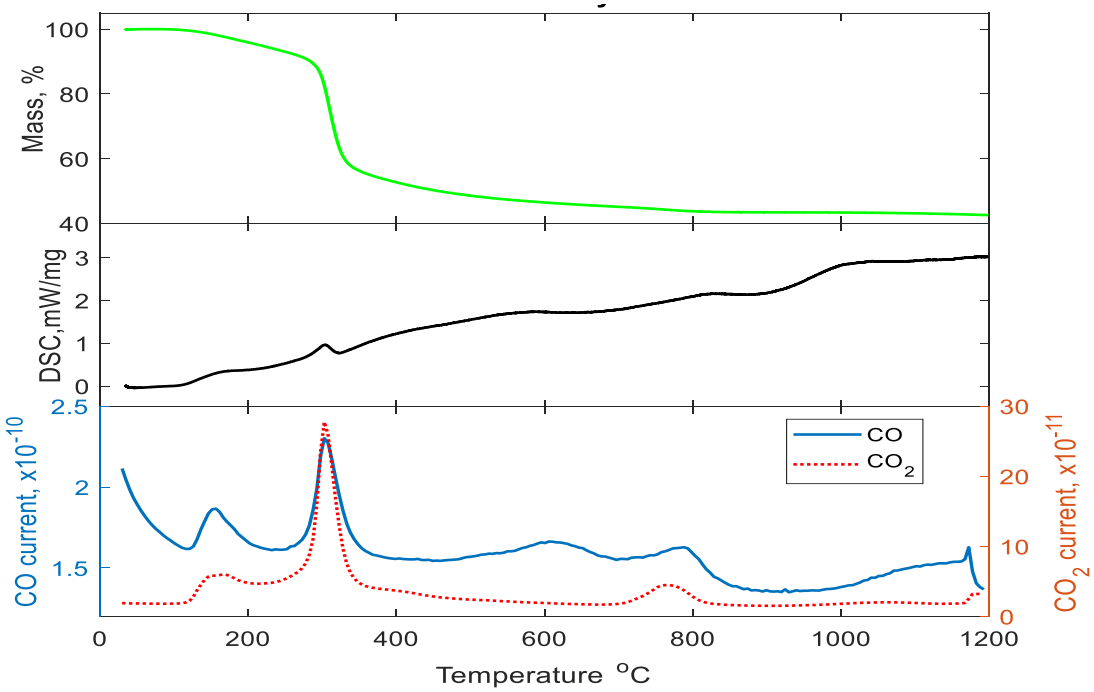

Figure 4.6: Thermal analysis of PCB only

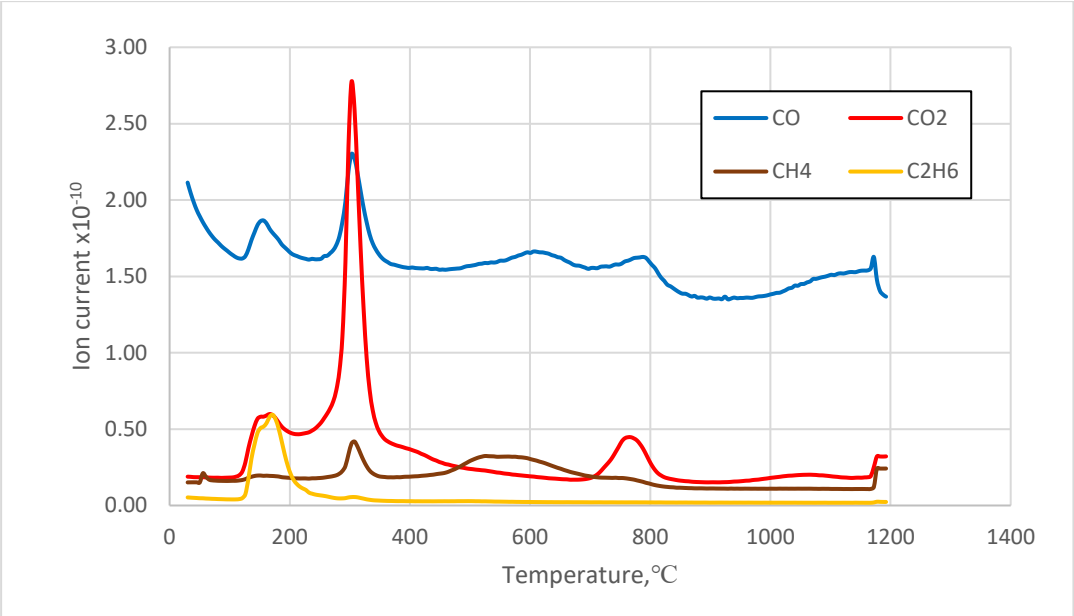

Figure 4.7: Composition of off-gas during thermal analysis of PCB

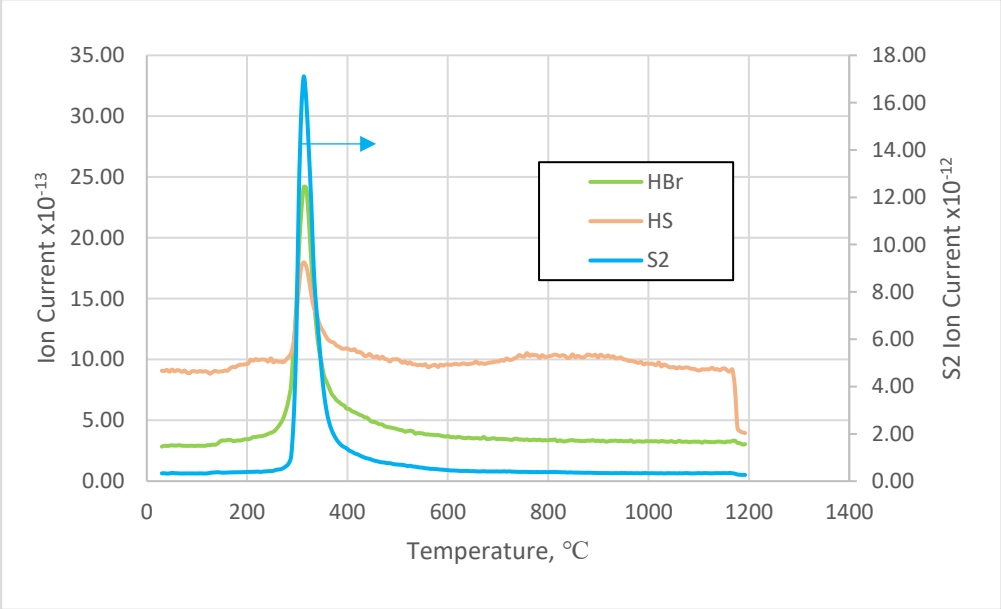

Figure 4.8: Off-gases produced with lower ion current

PCB and graphite were mixed in the same ratio as 20%PCB blend (Table 3.4) and heated from ambient temperature to 1200℃ in argon atmosphere. This was done to ascertain the interaction of PCB and graphite in the blend. Figure 4.9 reveals no distinct DSC peaks. However, mass loss (10%) occurred around 300℃ and a slight mass loss (about 3%) afterwards. Mass loss at 300℃ is attributed to the pyrolysis of PCB. The mass loss seen after 300℃ indicates that PCB partially interacts with graphite in blend. Moreover, CO peak seen at 600℃ may also be attributed to PCB-graphite interaction.

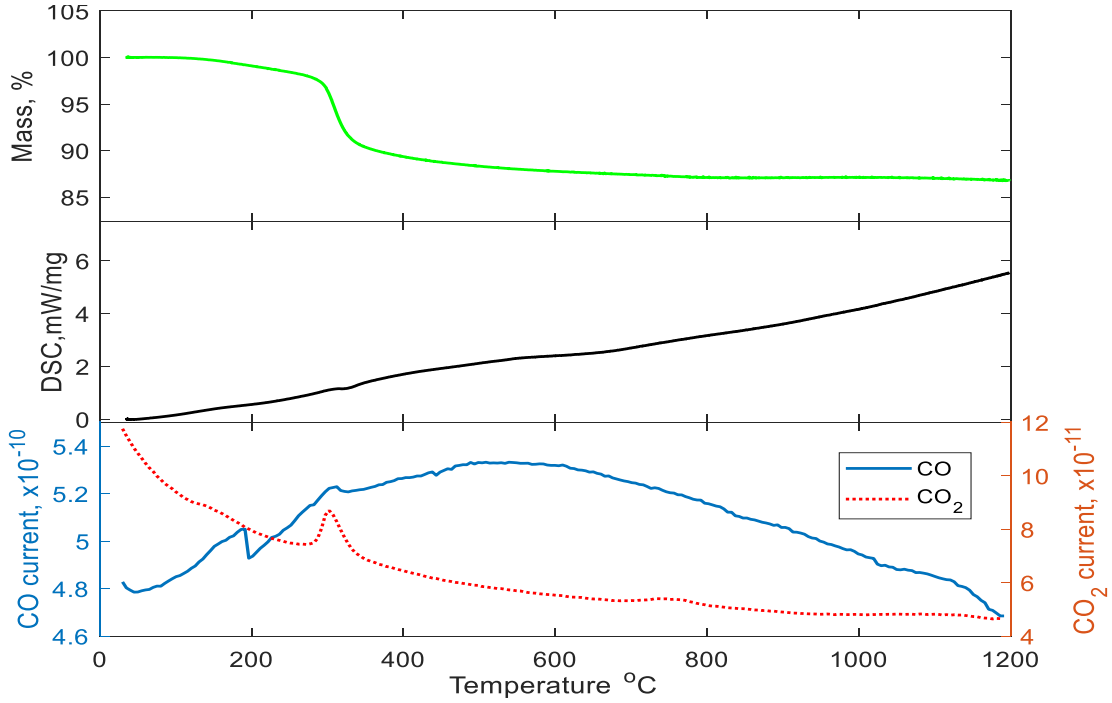

Figure 4.9: Thermal analysis of graphite and 20%PCB

4.3 Hematite reduction in DSC-TGA under Non-Isothermal Conditions

4.3.1 Hematite Reduction with Graphite

During the hematite-graphite reduction, the mass of the sample (Figure 4.10) starts to decrease around 900℃. This indicates the onset of the reduction of hematite. It is believed that hematite is converted to magnetite at 900℃, due to the change in mass and the release of CO_2. Jung & Yi (2013) attributed the initial formation of CO_2 as a combination of Equation 4.3 and Equation 4.4. They stated that the gas-solid reaction (Equation 4.4) is faster than the solid-solid reaction (Equation 4.3). CO produced quickly reacts with hematite and produces CO_2. Thus only CO_2 is observed by the mass spectrometer.

Two endothermic peaks were observed during the reduction of hematite using graphite at 1120℃ and 1150℃ respectively as shown in Figure 4.10. It is believed that iron is formed at 1120℃. This is because at that temperature, there is a steep mass change which corresponds with a CO peak. The mass change is also attributed to gasification of carbon or a dominant Boudouard reaction (Equation 4.5). It can be seen by the sudden increase in the partial pressure of CO. The increase in the CO is believed to accelerate the formation of iron. The endothermic peak at 1150℃ may be ascribed to the melting of the graphite in the iron since the peak did not have a corresponding change in mass. This serves as a confirmation of the formation of iron at 1120℃. The mechanism for solid state reduction of hematite is described in Appendix B.1.

$3Fe_2O_{3(s)} + C_{(s)} = 2Fe_3O_{4(s)} + CO_{(g)}$ **Equation 4.3**

$CO_{(g)} + 3Fe_2O_{3(s)} = 2Fe_3O_{4(s)} + CO_{2(g)}$ **Equation 4.4**

$C_{(s)} + CO_{2(g)} = 2CO_{(g)}$ **Equation 4.5**

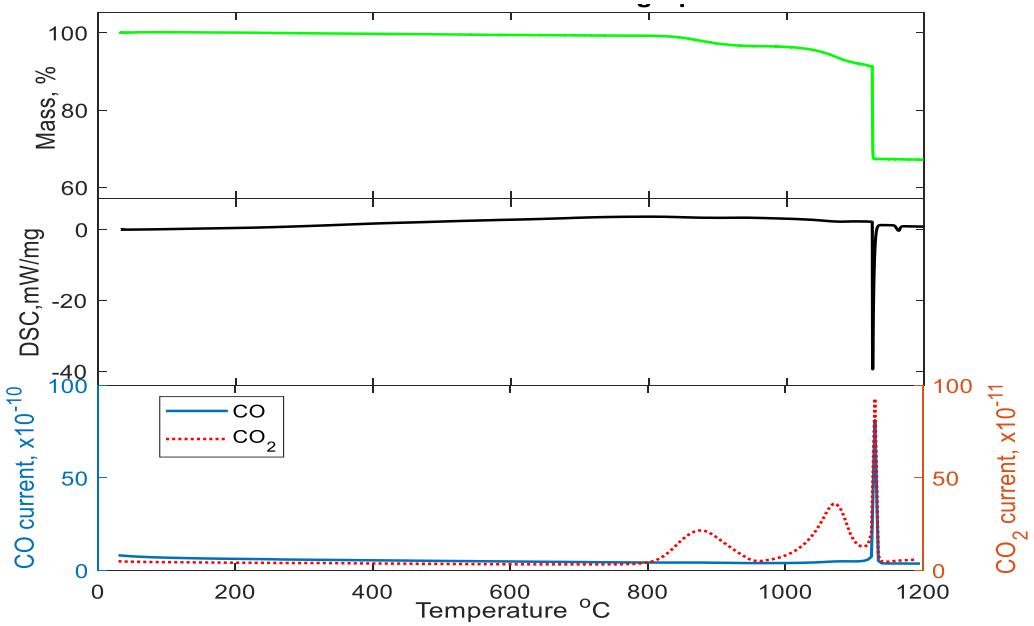

Figure 4.10: Reduction of Hematite with Graphite

4.3.2 Hematite Reduction with PCB only

In the reduction test of hematite with 100%PCB (Figure 4.11), the mass change observed around 300°C is due to the pyrolysis of the PCB.

It can be inferred that the reduction of hematite with PCB has faster kinetics than reduction with graphite. This is due to the steady mass loss at temperatures between 500°C and 900°C as well as the release of CO and CO_2. PCB releases volatiles which contain hydrocarbons capable of reducing hematite at lower temperatures than pure carbon. Chongmin et al. (2009), in their study on the use of plastics in iron oxide reduction stated that the high percentage of volatile matter in plastics increases porosity. The increase in porosity facilitates the mass transfer conditions in the gas-solid reaction system and enlarges the reaction interfacial area for reduction which improves reduction of iron oxide.

Sohn & Fruehan (2005) found that up to 900°C, reduction by H_2 is considerably faster than by carbon in pellet or by CO. Equation B.2 shows that during the decomposition of hydrocarbons in the PCB, H_2 is released and it takes part in the reduction process as shown in Equation B.8. Moreover, it is believed that the plastics content present in the PCB forms a liquid phase which allows it to have more contact with the hematite during reduction experiments.

FactSage© predicts the formation of fayalite (Fe_2SiO_4) between 200°C and 800°C when PCB is used as a reducing agent for hematite. The exothermic peak observed at 750°C is attributed to the formation of Fe_2SiO_4 (Equation 4.8).

$$Fe_2O_3 + 3CH_4 = 2Fe + 6H_2 + 3CO \quad \textbf{Equation 4.6}$$

$$Fe_2O_3 + 3C_2H_6 = 2Fe + 9H_2 + 3CO \quad \textbf{Equation 4.7}$$

$$Fe_2O_3 + SiO_2 = Fe_2SiO_4 + {}^1/_2O_2 \quad \textbf{Equation 4.8}$$

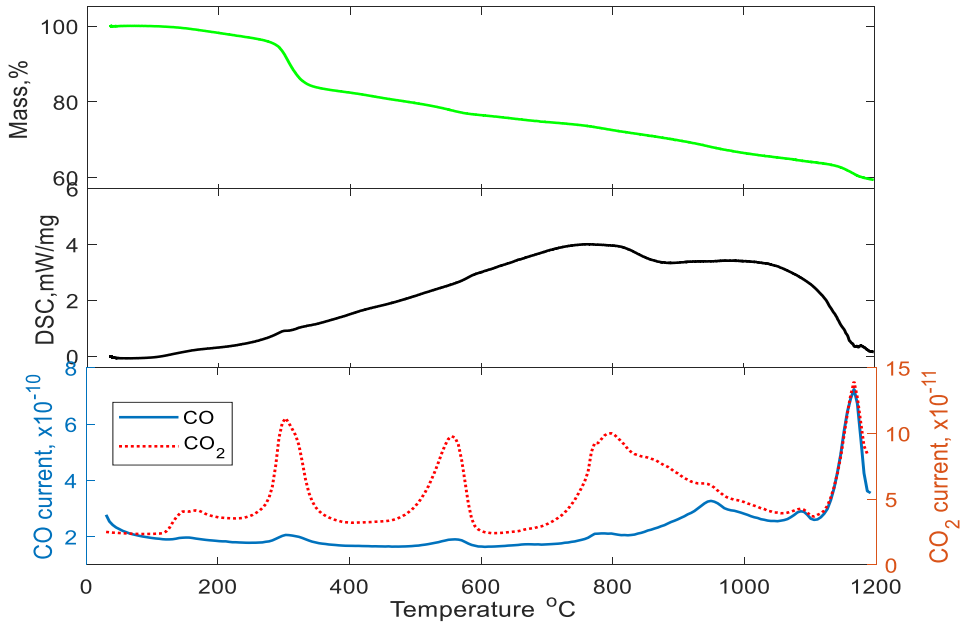

Figure 4.11: Reduction of Hematite with 100%PCB

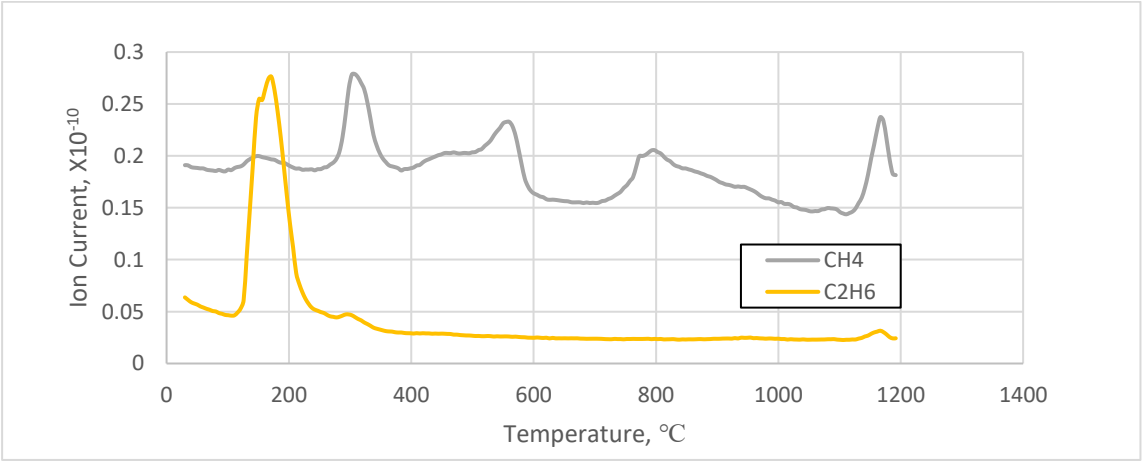

Figure 4.12: Hydrocarbons present in off-gas during hematite reduction with 100%PCB

Figure 4.12 shows the peaks of CH_4 and C_2H_6 that was detected during hematite-100%PCB reduction. The peaks identified at temperatures less than 500°C is due to the pyrolysis of PCB.

The other peaks detected indicates that hydrocarbons are released during the reduction of hematite with PCB or PCB blends which take part in the reduction process as seen in Equation 4.6 and Equation 4.7.

4.3.3 Hematite Reduction with PCB-Graphite Blends

When PCB-graphite blends were used in the reduction of hematite, each test showed the behaviour of both hematite-PCB and hematite-graphite reductions. Also, it is observed that, as the PCB in the blend used as a reductant increases, the endothermic peak at 1120°C decreases. This indicates that a lower amount of energy is required for the formation of iron. The decreasing endothermic peak can also be ascribed to the decreasing weight percentage of carbon and increasing volatile content in the blend. This observation confirms the results obtained in the mass and energy balance simulations with EMSIM.

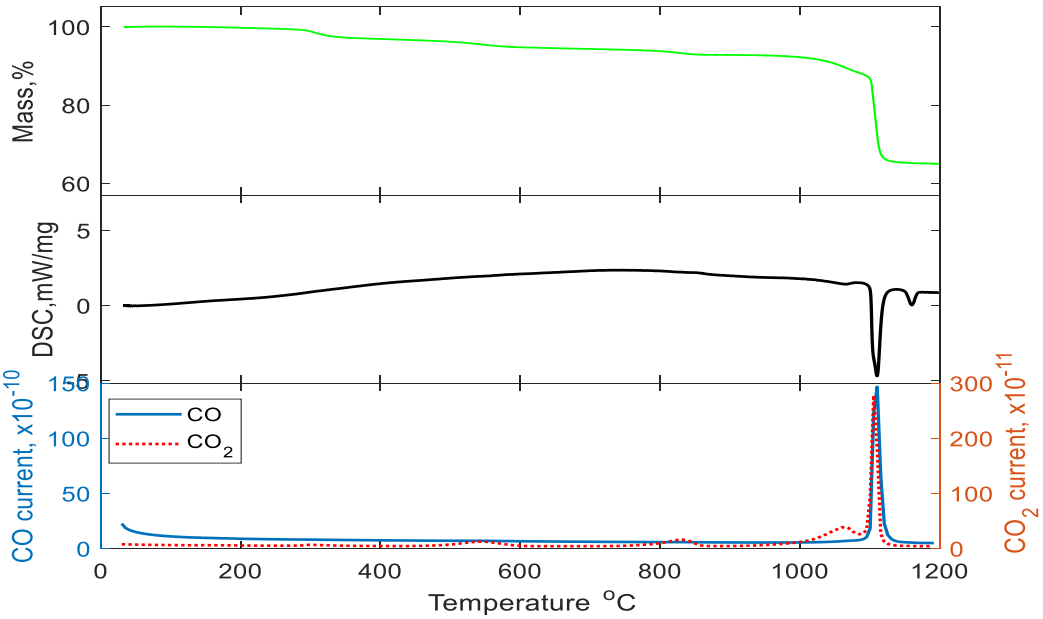

Figure 4.13: Reduction of Hematite with 20% PCB

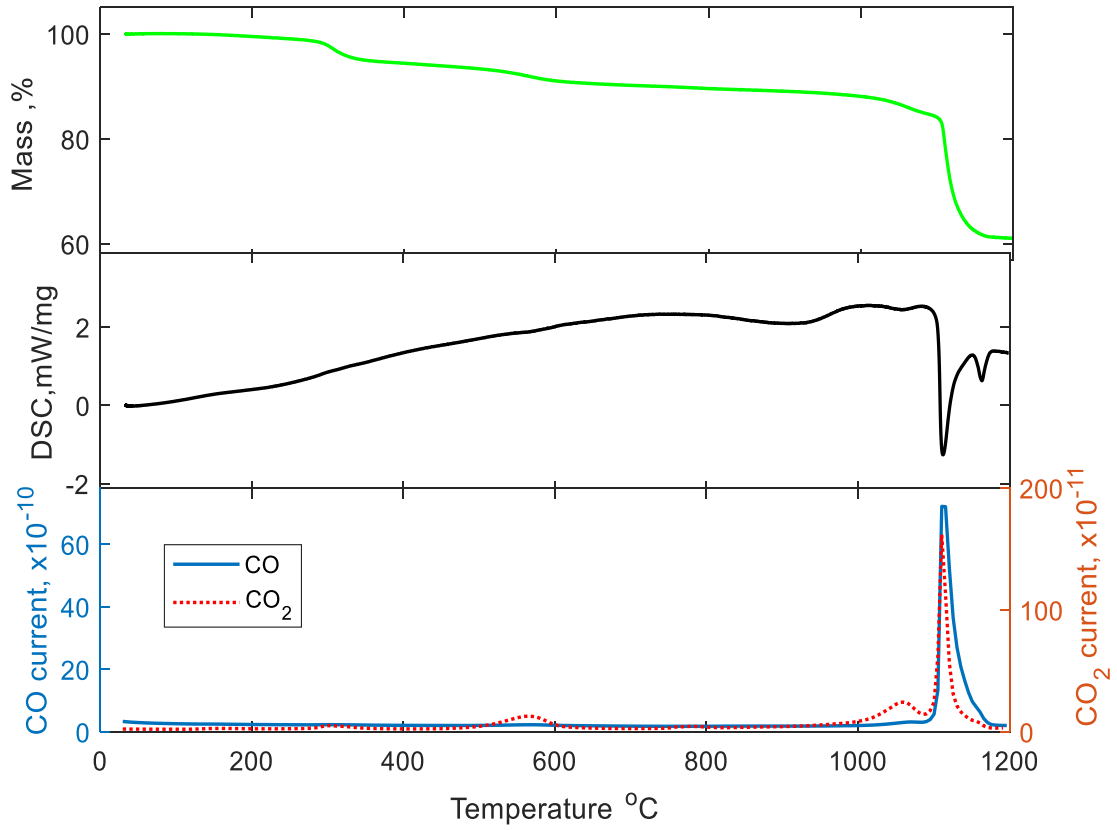

Figure 4.14: Reduction of Hematite with 40% PCB

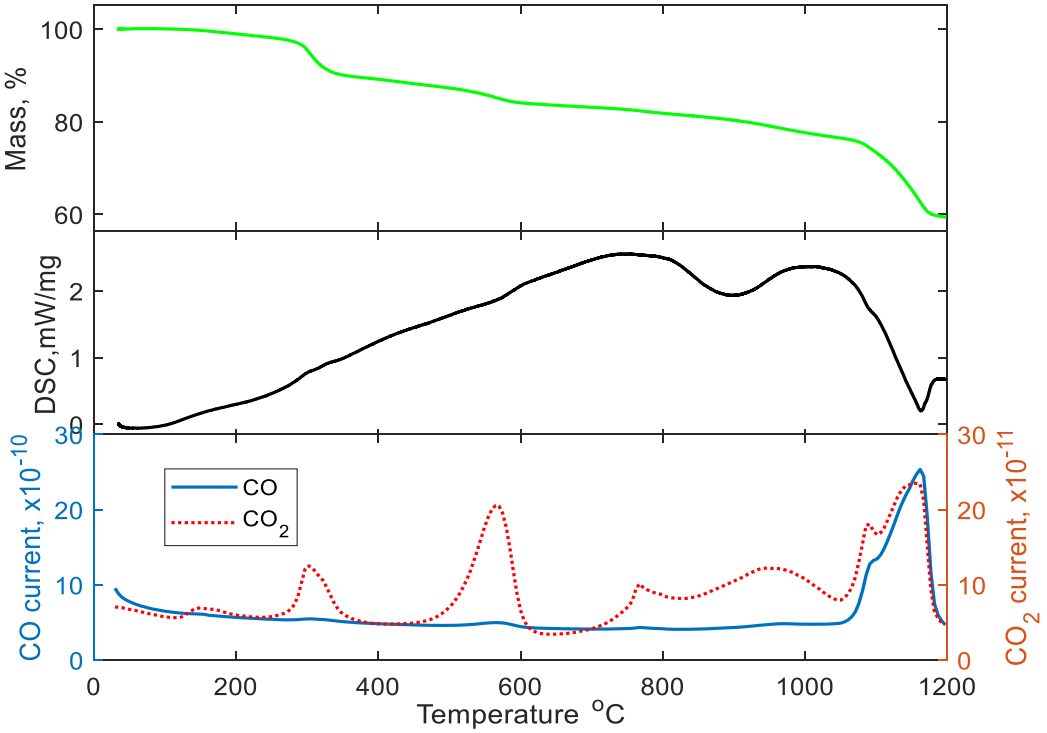

Figure 4.15: Reduction of Hematite with 80% PCB

4.3.4 Reduction Degree

The reduction degree is an indication of how much oxygen has been removed from the hematite. It was calculated using Equation 4.10 based on the mass lost during the reduction in the DSC-TGA (Jung & Yi, 2013). Appendix B.3 shows the procedure for reduction degree calculation.

The overall reduction may be expressed by the reaction

$$Fe_2O_3\ (s) + 3C = 2Fe + 3CO \qquad \textbf{Equation 4.9}$$

$$\text{Reduction Degree} = \frac{{}^{\Delta W}/_{W}}{{}^{3MW_{CO}}/_{(MW_{Fe2O3}+3MW_{C})}} \qquad \textbf{Equation 4.10}$$

ΔW = Mass lost; W = initial mass; MW_{CO} = Molecular weight of CO; MW_{Fe2O3} = Molecular weight of Fe_2O_3 and MW_C = Molecular weight of C

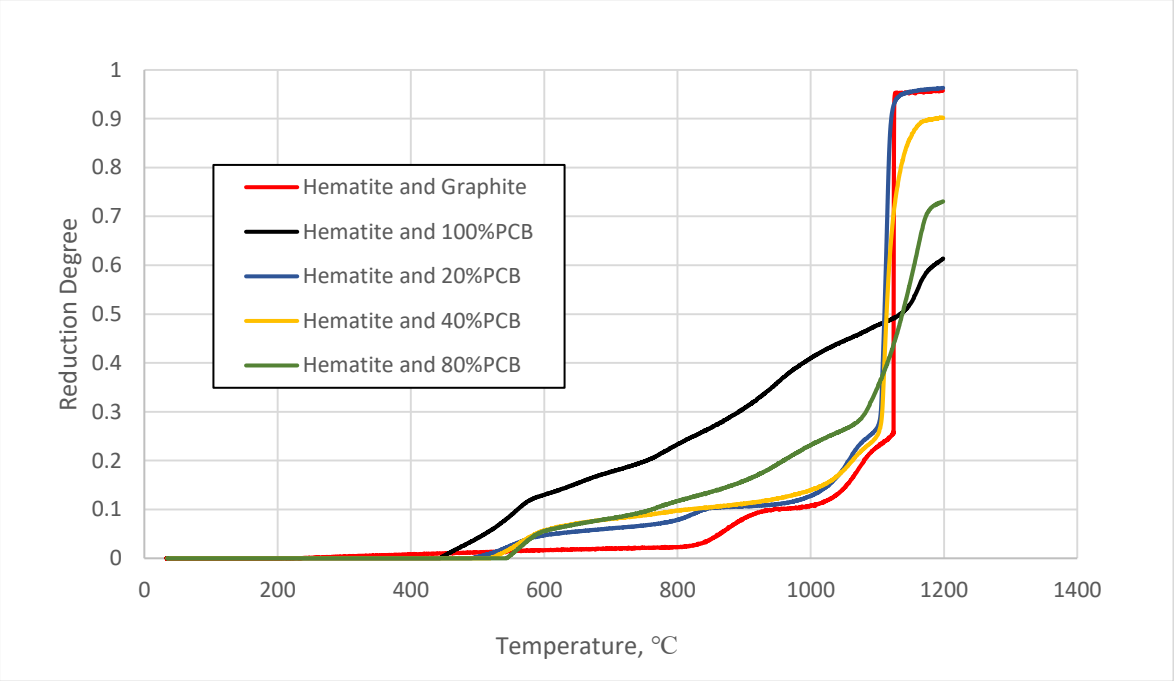

Figure 4.16: Reduction degree

The reduction degree calculated revealed that PCB reduces hematite better at temperatures lower than 1000℃. However, at temperatures greater than 1100℃, graphite acts as a better reductant. At the end of the reduction test, the use of graphite and 20%PCB gave the highest reduction degree of about 97%. Moreover, it is observed that increasing the mass percent of PCB in the reductant leads to an overall decrease in the reduction degree.

Hematite reduction test in DSC-TGA were repeated. Figure B2 to B6 shows the mass loss of the occurred during each test and their respective repeats. The standard deviation at each of the

temperatures were calculated. Table B1 to B5 shows the mass and the standard deviation at selected temperatures during reduction of hematite. Since each of the reduction tests has over 11600 data points, the temperatures 50℃ to 1200℃ with intervals 50℃ were selected. The average value for the standard deviation for all the data point is shown in Table B6

4.3.5 SEM Analysis on the Products

The products obtained from each of the reduction test was analysed using back scattered SEM analysis. The images reveal very bright spots when PCB or blends of PCB are used as reducing agent. SEM produces brighter spots to indicate the presence of elements with higher atomic mass. The analysis of the bright spots in the products of the reduction test with PCB reveal the presence of iron, barium and silicon. The presence of iron and silicon may be attributed to the fayalite that was formed. SEM analysis of hematite-graphite reduction shows the presence of only iron and carbon. The image show tiny bright spots which is almost evenly distributed in the sample. This is an indication that the excess carbon melts into the iron that was formed.

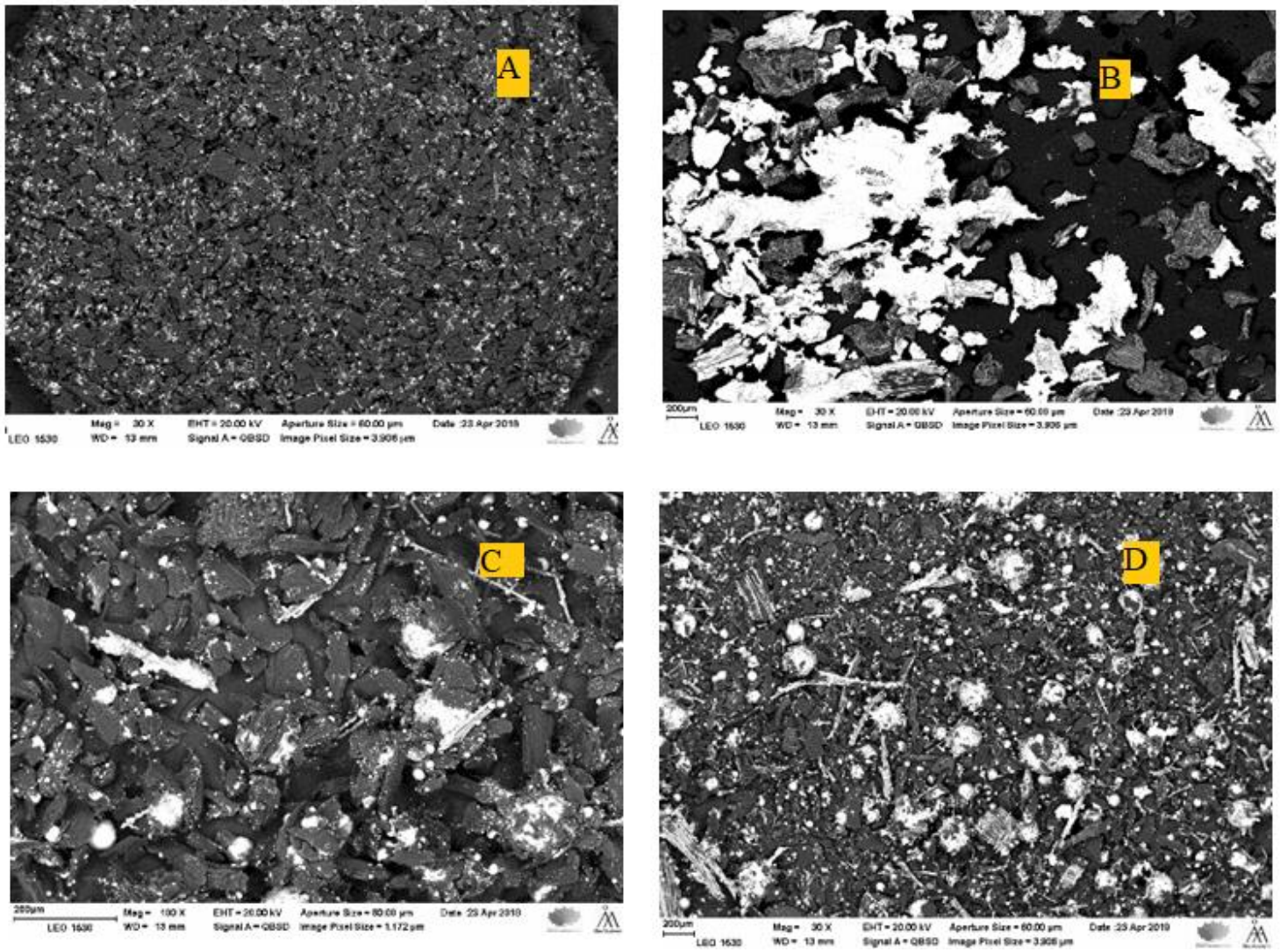

Figure 4.17: SEM images of (A) Hematite-Graphite; (B):Hematite-100%PCB; (C) Hematite-20PCB; (D) Hematite-40PCB

4.4 Hematite Reduction under Isothermal Conditions

4.4.1 Reduction in DSC-TGA

In order to simulate isothermal reduction of hematite, mixtures of hematite and PCB, as well as hematite with graphite, were placed in DSC-TGA, heated at 10℃/min to 900℃ and 1000℃ and allowed to stay at that temperature for 30 minutes in argon atmosphere. Figure 4.18 and Figure 4.19 shows graphs during isothermal conditions at 900℃ while Figure 4.20 and Figure 4.21 show the graphs at 1000℃.

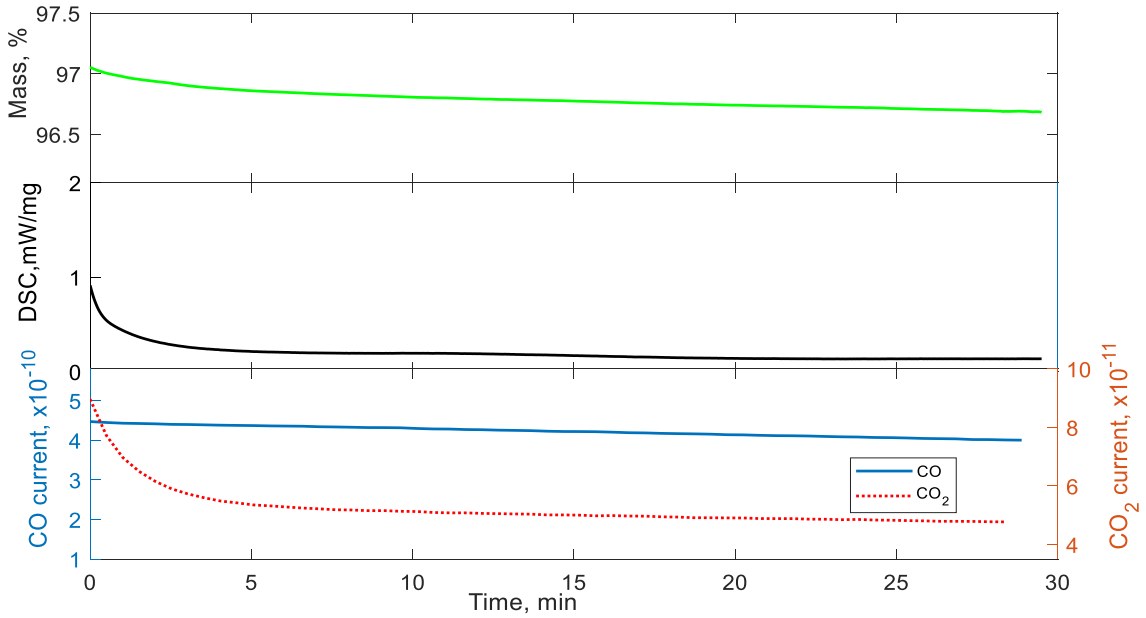

Figure 4.18: Reduction of hematite with graphite under isothermal conditions at 900℃

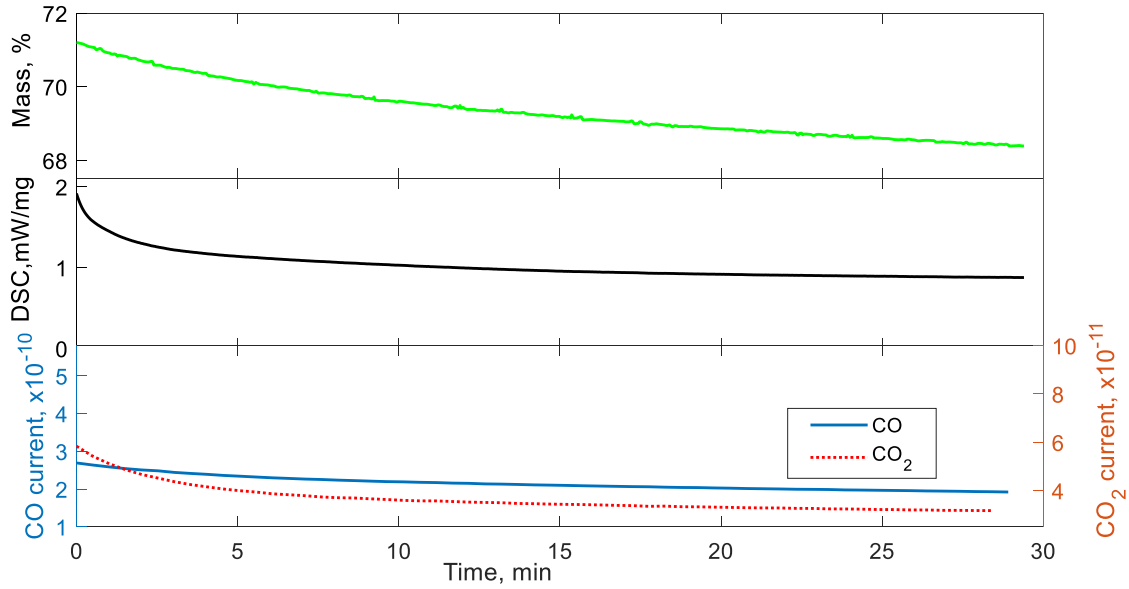

Figure 4.19: Reduction of hematite with 100%PCB with isothermal conditions at 900℃

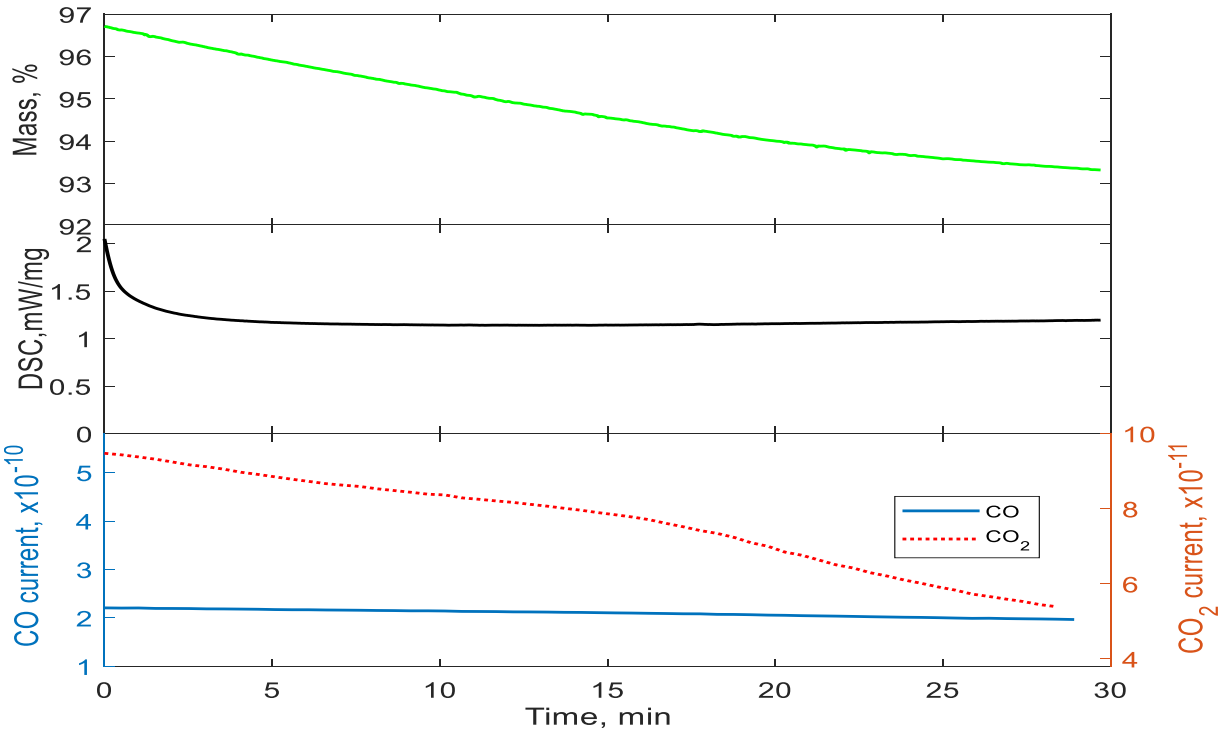

Figure 4.20: Reduction of hematite with graphite with isothermal conditions at 1000°C

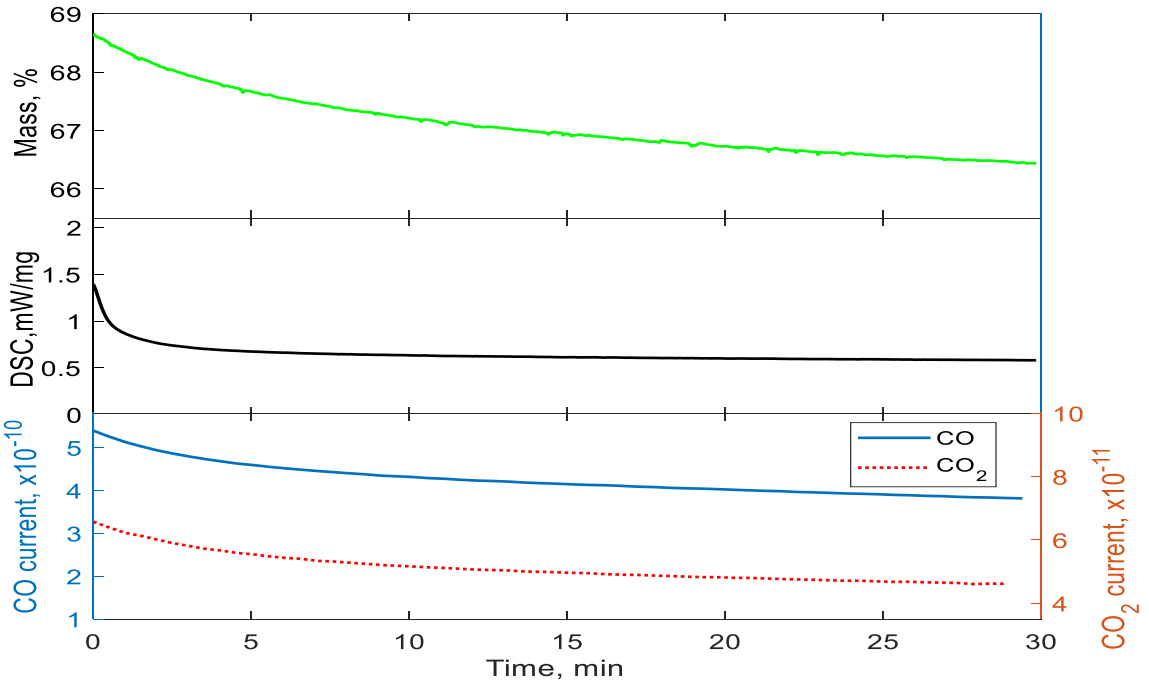

Figure 4.21: Reduction of hematite with 100%PCB with isothermal conditions at 1000°C

The test with 100%PCB (Figure 4.19 and Figure 4.21) as reductants showed a mass change less than 4% of the initial mass during isothermal condition at both temperatures. There was no observable change when hematite was reduced with graphite at 900°C (Figure 4.18). However, a mass change of about 3% was seen at 1000°C (Figure 4.20) during the test with graphite as

the reductant. There were no distinguishable peaks of CO and CO_2 observed during each of the isothermal reduction test.

4.4.2 Reduction Tests in SPR

Isothermal reduction tests were carried out in SPR at 900°C and 1000°C under inert conditions using 1 litre per minute nitrogen. The volume percent of CO and CO_2 were measured and recorded.

4.4.2.1 Reduction in SPR at 900°C

Figure 4.22 to Figure 4.26 shows the volume percent of CO and CO_2 in the off-gas during the reduction tests at 900°C. It can be observed in the hematite-graphite reduction that a peak of about 0.8 vol% of CO_2 was seen with no CO peaks. This corresponds with the results obtained during DSC tests as discussed previously (4.3.1).

Moreover, the XRD analysis on the hematite-graphite test showed the presence of wustite. This indicates that part of the magnetite reacts with CO and is converted to wustite as shown in Equation 4.11.

$$Fe_3O_4 + CO_{(g)} = FeO + CO \qquad \textbf{Equation 4.11}$$

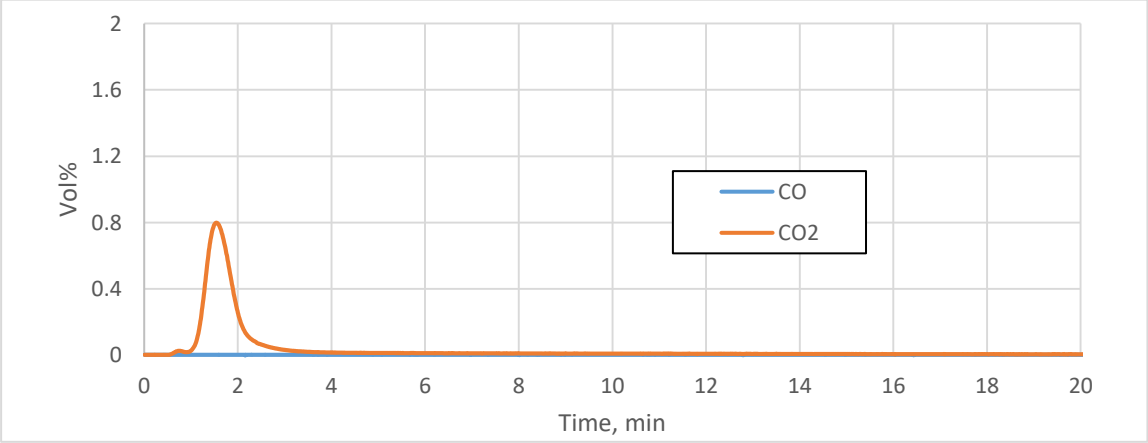

Figure 4.22: Volume percent of CO and CO_2 in off-gas during reduction of hematite with Graphite at 900°C

It is observed that when PCB or blends of PCB-graphite were used as reducing agent at 900°C, both CO and CO_2 are produced in the evolved gas. This may be ascribed to the presence of hydrocarbons in PCB. Monazam et al. (2012) studied the kinetics of the reduction of hematite with CH_4 in a TGA. They summarized the reduction of hematite to magnetite as Equation 4.12

and subsequent formation of wustite from magnetite as Equation 4.13. Both equations reveal the presence of CO and CO_2 in the product gas. As previously seen in the DSC-TGA reduction test of hematite-100%PCB, hydrocarbons such as CH_4 and C_2H_6 take part in the reduction of hematite to form metallic iron as shown in Equation 4.6 and Equation 4.7. Moreover, CO formed may be attributed to oxygen in the PCB reacting with the hydrocarbons as shown in Equation 4.14.

$$4CH_4 + 27Fe_2O_3 = 18Fe_3O_4 + 2CO_2 + 2CO + 3H_2O + 5H_2 \quad \textbf{Equation 4.12}$$

$$3CH_4 + 8Fe_3O_4 = 24FeO + 2CO_2 + CO + 3H_2O + 3H_2 \quad \textbf{Equation 4.13}$$

$$C_nH_m + {}^{n}/_{2}O_2 = nCO + {}^{m}/_{2}H_2 \quad \textbf{Equation 4.14}$$

Rao (1971) reported that the CO available governs the hematite reduction process. The presence of CO peak during the reduction of hematite with PCB and blends of PCB at 900°C further shows that PCB acts as a better reductant at lower temperatures compared to graphite. Additionally, Carpenter (2010) stated that H_2 and H_2O has higher ability to diffuse into and out of individual pellets and sinter is significantly higher than CO and CO_2. Higher diffusibility promotes faster reduction rates, particularly at lower temperatures. Equation 4.12 to Equation 4.14 show that H_2 gas is released during the reduction of hematite using PCB or PCB-graphite blends. The gas analysers, however, are limited to detect only CO and CO_2 but not H_2 which takes part in the reduction process. XRD results show the formation of iron and lower forms of iron oxide when PCB and blends of PCB were used to reduce hematite at 900°C. This confirms that the hydrocarbons in the PCB take part in the reduction of hematite resulting in PCB being a better reductant at lower temperatures. XRD patterns can be seen in Appendix D.

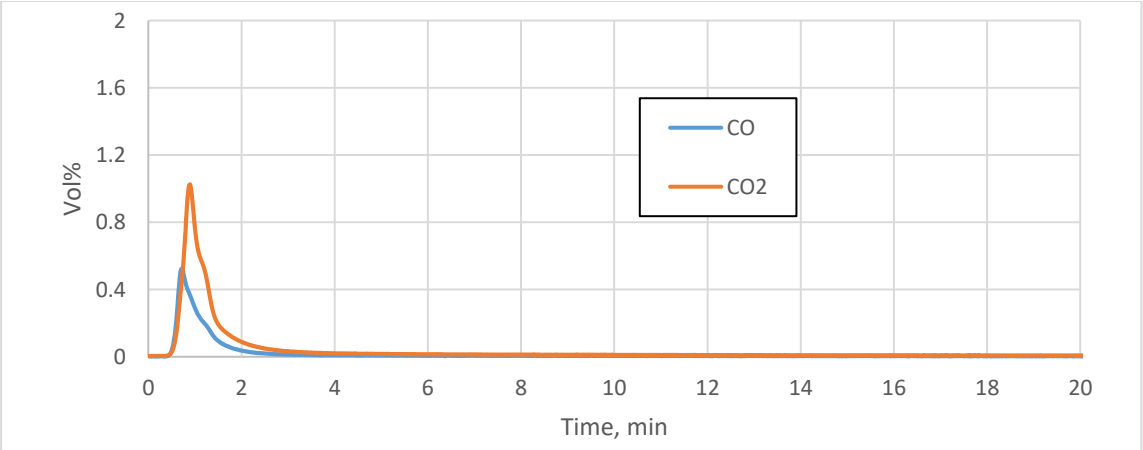

Figure 4.23: Volume percent of CO and CO_2 in off-gas during reduction of hematite with 20% PCB at 900°C

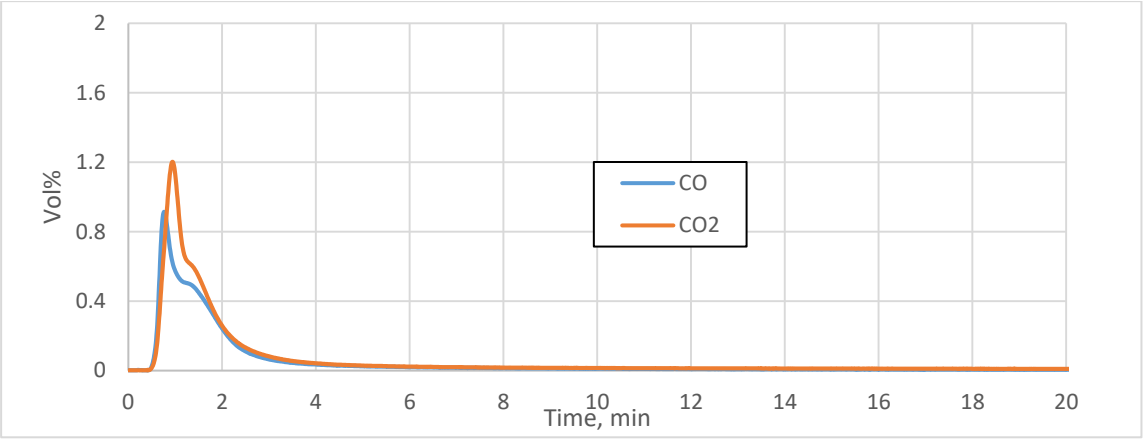

Figure 4.24: Volume percent of CO and CO_2 in off-gas during reduction of hematite with 40% PCB at 900°C

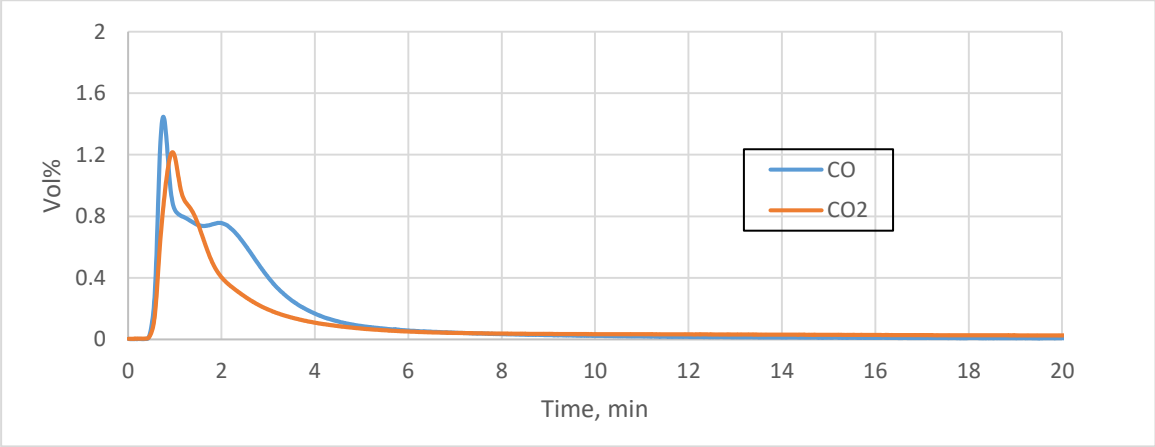

Figure 4.25: Volume percent of CO and CO_2 in off-gas during reduction of hematite with 80% PCB at 900°C

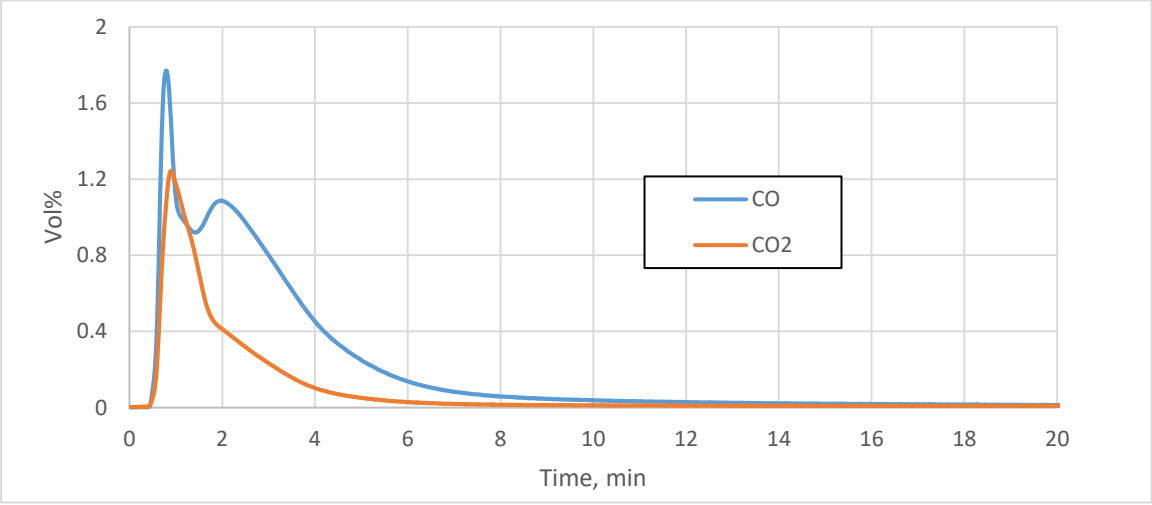

Figure 4.26: Volume percent of CO and CO_2 in off-gas during reduction of hematite with 100%PCB at 900°C

Table 4.7: XRD results of products from reduction of hematite in SPR at 900℃

Phase	Graphite	Reduction of Hematite with 40%PCB	80%PCB	100%PCB
C	80%	51%	46%	17%
Fe_3O_4	14%	-	-	-
FeO	6%	49%	19%	-
Fe	-	-	-	7%
Fe_2SiO_4	-	-	35%	30%
SiO_2	-	-	-	46%

4.4.2.2 Reduction in SPR at 1000℃

Reduction of hematite tests were carried out at 1000℃. Figure 4.27 to Figure 4.31 shows the volume percent of CO and CO_2 in the evolved gas during the reduction. Two peaks of CO_2 were observed when pure graphite was used as a reducing agent. The first CO_2 peak observed about 1 minute from the start of the experiment may be attributed to the conversion of hematite to magnetite as discussed in 4.3.1. The second peak may be due to the conversion of magnetite to wustite and subsequently to iron. The formation of metallic iron is accompanied by the CO peak around 8 minutes. Jung & Yi (2013) performed isothermal reduction of hematite using graphite at 1000℃ and observed a similar pattern. They reported that when pure carbon is used in reducing hematite, magnetite to wustite takes relatively longer than that of wustite to metallic iron. Moreover, Rao (1971) found that formation of iron phase from the reduction of wustite acts as a catalyst for carbon gasification. Additionally, the CO peak may be ascribed to a dominant Boudouard reaction (Equation 4.5).

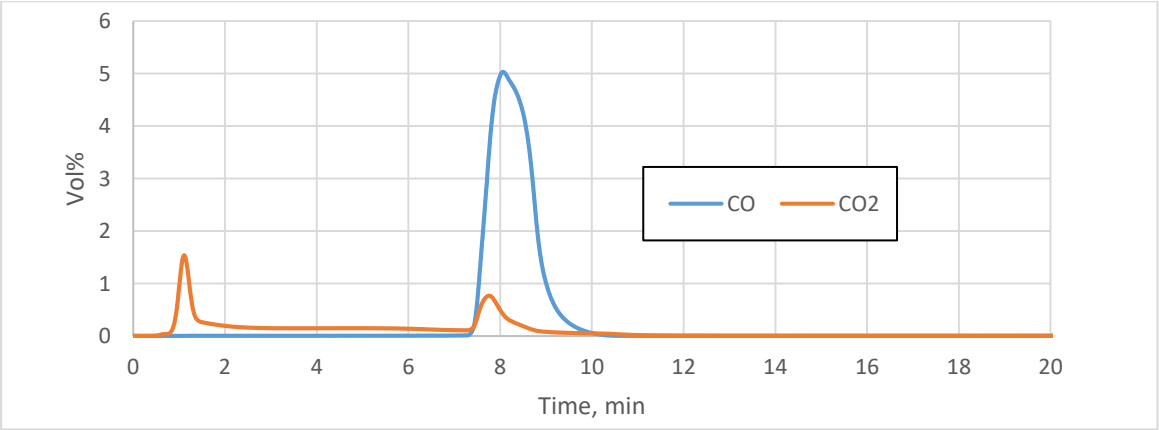

Figure 4.27: Volume percent of CO and CO_2 in off-gas during reduction of hematite with Graphite at 1000℃

In the reduction of hematite using 20% PCB and 40%PCB, two distinct CO peaks were observed (Figure 4.28 and Figure 4.29). The first peak that occurred in less than a minute is due

to the reduction of hematite by PCB while the second peak is as a result of the reduction by graphite. In the hematite-20%PCB reduction test, the second CO occurred between 15 and 20 minutes. That of hematite-40%PCB reduction test occurred around 10 minutes. As discussed earlier (4.4.2.2), when graphite is used during the reduction of hematite, conversion of magnetite to wustite takes relatively longer than that of wustite to metallic iron. The length of time between the two CO peaks suggests that during hematite-20%PCB and hematite-40%PCB reduction test, PCB reduces hematite to magnetite, while wustite and metallic iron is formed due to the reduction of magnetite by graphite.

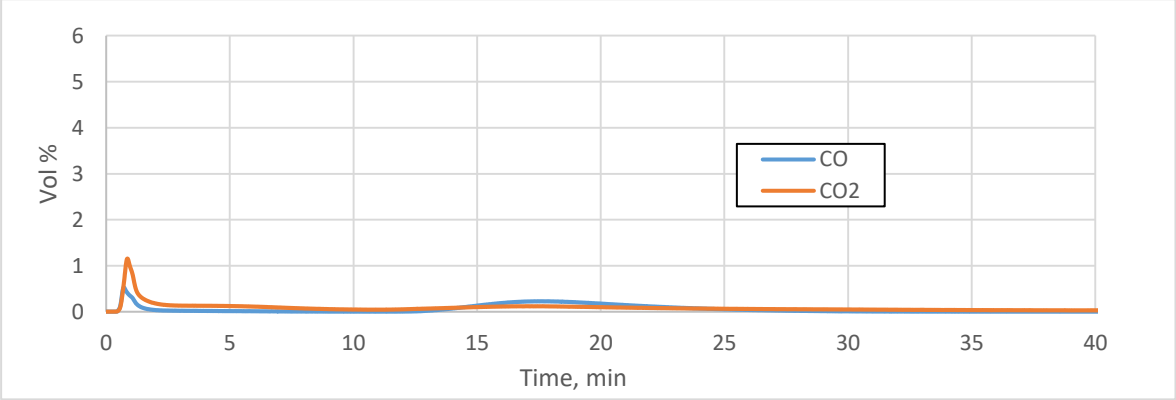

Figure 4.28: Volume percent of CO and CO_2 in off-gas during reduction of hematite with 20%PCB at 1000°C

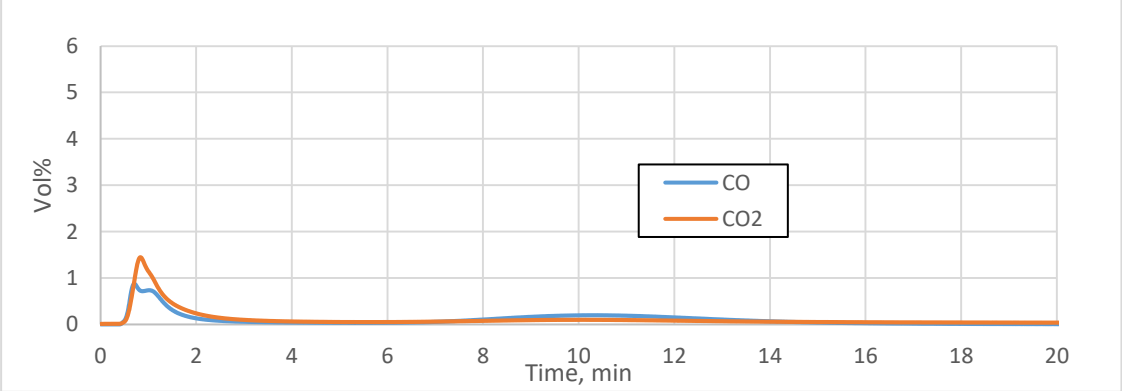

Figure 4.29: Volume percent of CO and CO_2 in off-gas during reduction of hematite with 40%PCB at 1000°C

During the reduction of hematite with 80% PCB and 100%PCB, two CO peaks were observed in less than 6 minutes of the reduction test. The two CO peaks appear to overlap. The first CO peak may be ascribed to Equation 4.14 while the second peak may be an indication of the reduction of hematite. XRD results show the presence of metallic iron for all the reduction test.

Metallic iron present in the product of hematite-80%PCB and hematite-100%PCB shows that H_2 is released from PCB and takes part in the reduction of hematite to iron.

XRD also shows that fayalite is produced when PCB is used as a reducing agent.

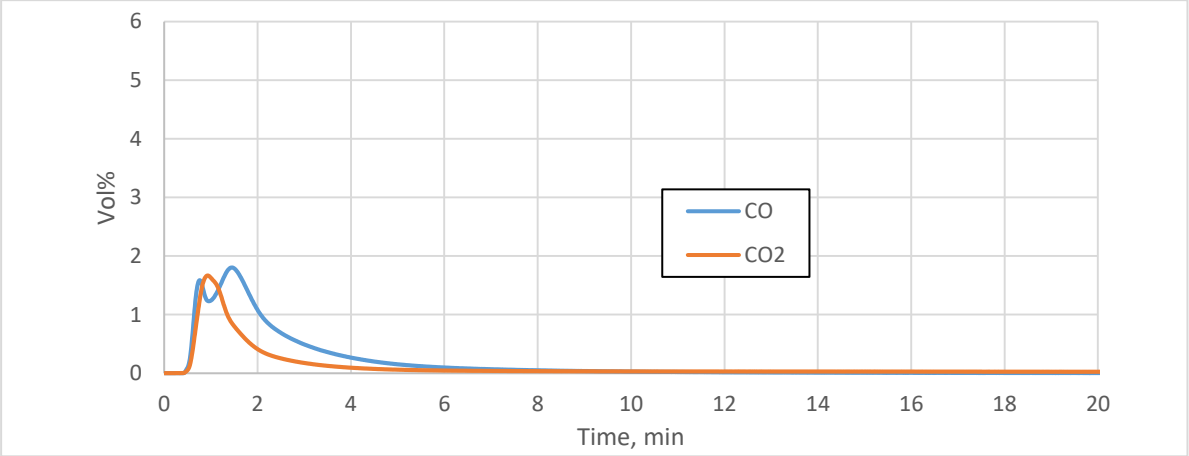

Figure 4.30: Volume percent of CO and CO_2 in off-gas during reduction of hematite with 80%PCB at 1000°C

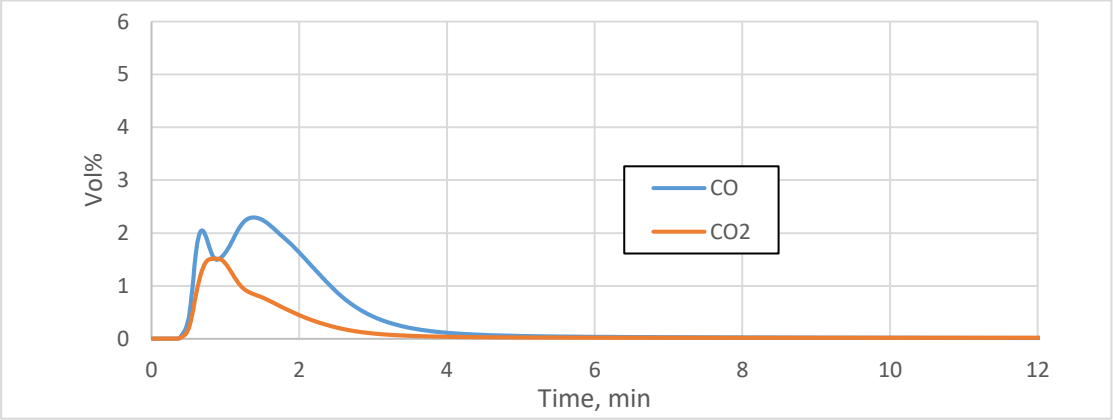

Figure 4.31: Volume percent of CO and CO_2 in off-gas during reduction of hematite with 100%PCB at 1000°C

Table 4.8: XRD results of products from reduction of hematite in SPR at 1000°C

	Reduction of Hematite with			
	Graphite	**40%PCB**	**80%PCB**	**100%PCB**
C	90%	90%	56%	31%
Fe_3O_4	-	-	-	-
FeO	-	4%	-	-
Fe	10%	5%	13%	17%
Fe_2SiO_4	-	-	31%	51%
SiO_2	-	-	-	-

4.5 FactSage Simulations of Hematite Reduction

Reduction of pure hematite (Fe_2O_3) using pure carbon (graphite) as well as blends of PCB and graphite were simulated using FactSage. This was done to predict and compare the products expected during the reduction test in DSC-TGA. The masses used for the preparation of each sample (Table 3.4) were used as input in FactSage and calculations were performed from 25°C to 1500°C with an interval of 25°C (as described in Figure 3.7). Figure 4.32 to Figure 4.35 show the mass fraction of the products that were predicted by FactSage.

It can be seen that the formation of solid iron starts around 700°C for all the reduction tests. Apart from the hematite-100%PCB and hematite-80%PCB reductions, liquid iron [Fe(liq)] forms at temperatures above 1150°C for all the reduction tests. When PCB or blends of PCB are used as reductants, FactSage predicts the formation of fayalite (Fe_2SiO_4) between temperatures 200°C and 800°C. This is due to the presence of SiO_2 in the PCB (Equation 4.8).

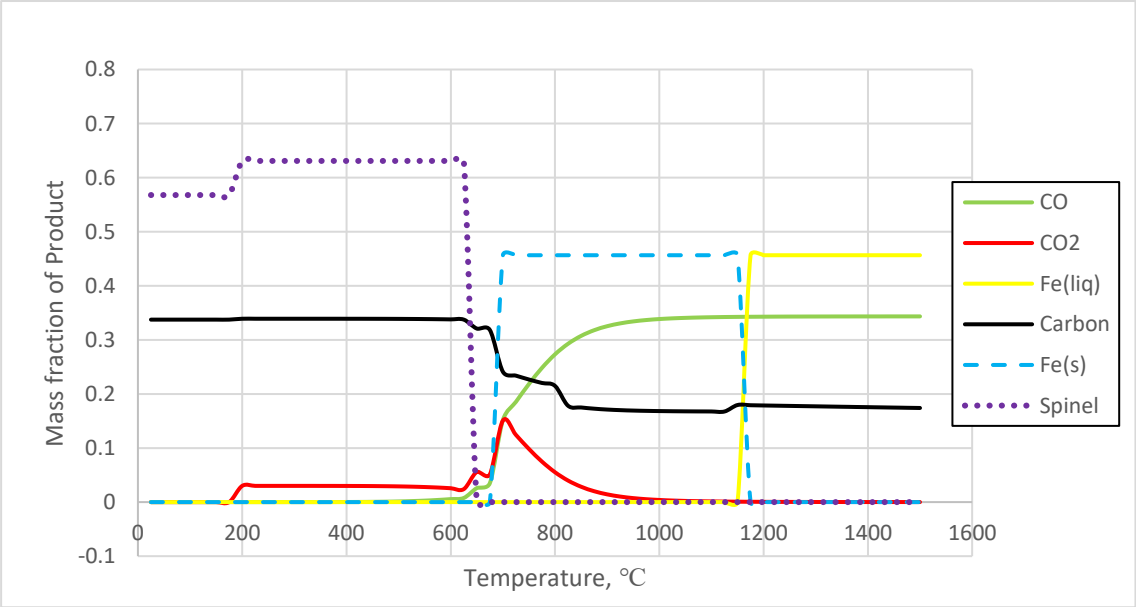

Figure 4.32: Mass fraction of products obtained from FactSage calculation during the reduction of hematite with graphite.

Fe(s) = solid iron; Fe(liq) = liquid iron

At a temperature close to 700°C, there is a sharp increase in the mass of CO and a decrease in the CO_2 produced. This indicates the gasification of carbon.

Figure 4.36 and Figure 4.35 indicate that all the carbon present in the reductant is used up for hematite-100%PCB and hematite-80%PCB reduction tests.

At temperatures less than 650°C, FactSage predicts the formation of spinel for all the reduction tests. The spinel consists of $Fe_3O_4[2-]$, $Fe_3O_4[1-]$, $Fe_3O_4[1+]$, Fe_3O_4, $FeO_4[6-]$. Very small quantities of $AlFe_2O_4$, $AlFe_2O_4[1+]$, $AlFe_2O_4[1-]$, $AlO_4[5-]$, $Al_3O_4[1+]$ and $AlO_4[5-]$ were present when PCB and blends of PCB were used as reducing agents.

The slag predicted by FactSage consists mainly of SiO_2, CaO, Al_2O_3.

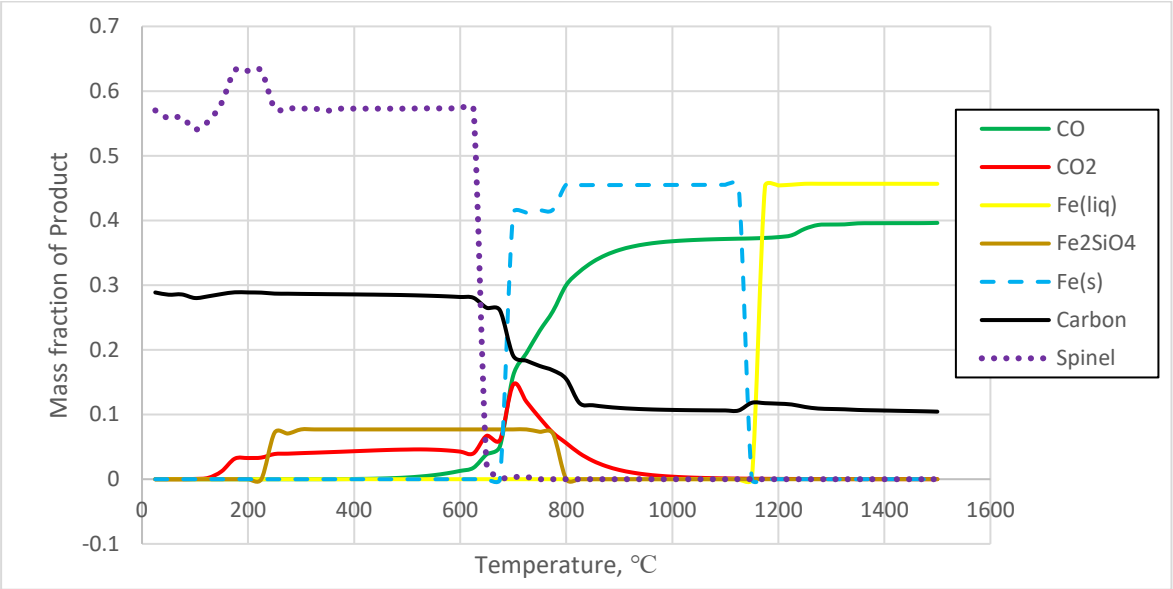

Figure 4.33: Mass fraction of products obtained from FactSage calculation during the reduction of hematite with 20%PCB

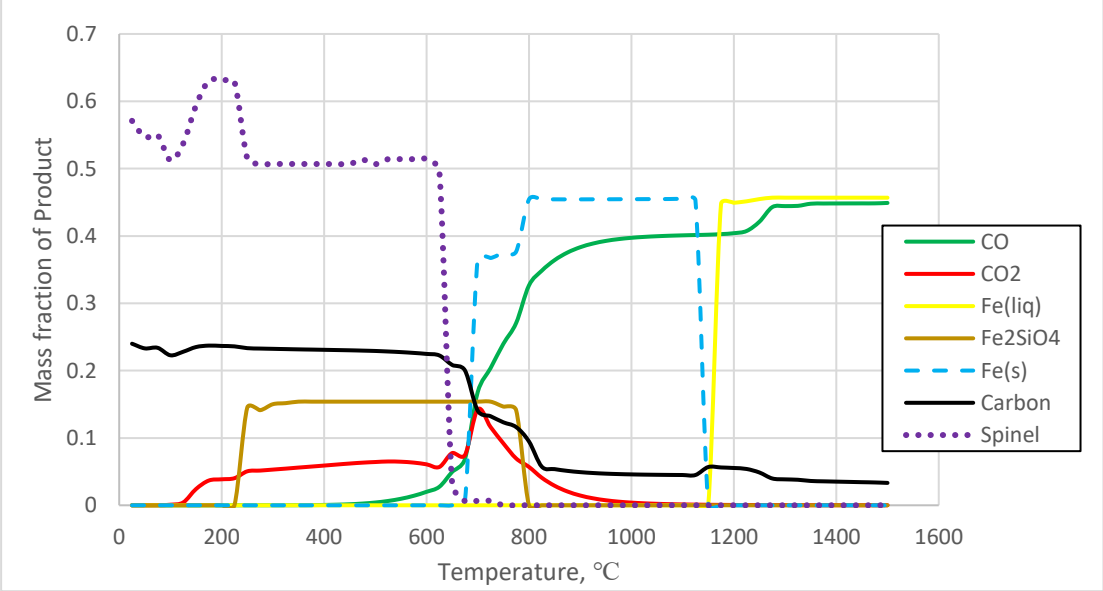

Figure 4.34: Mass fraction of products obtained from FactSage calculation during the reduction of hematite with 40%PCB

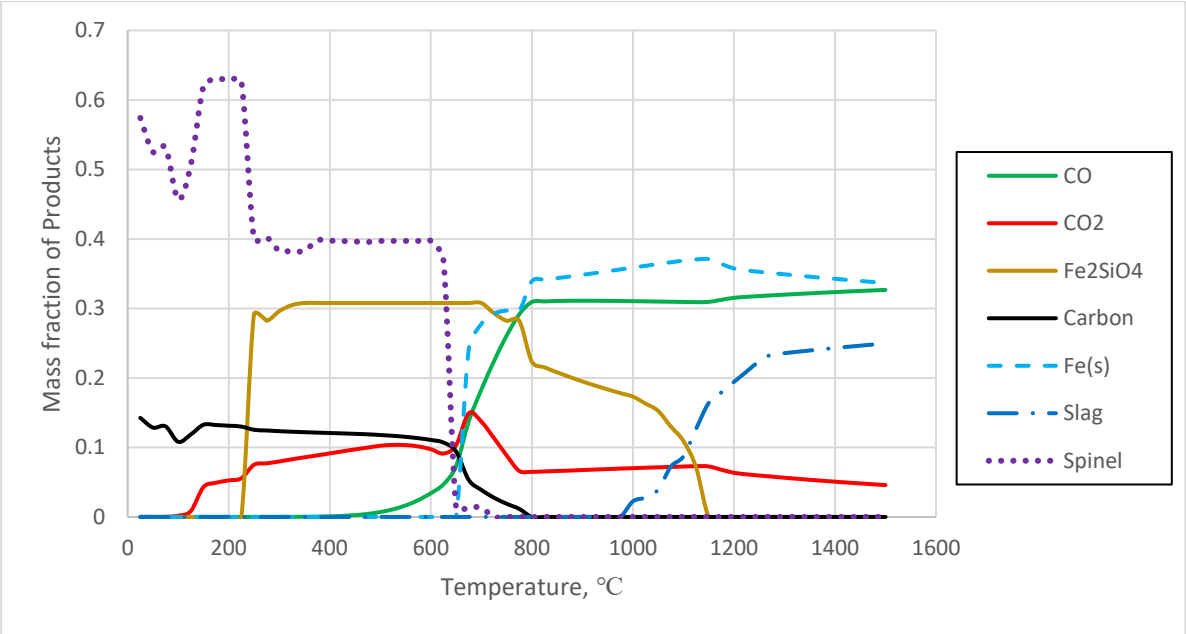

Figure 4.35: Mass fraction of products obtained from FactSage calculation during the reduction of hematite with 80%PCB

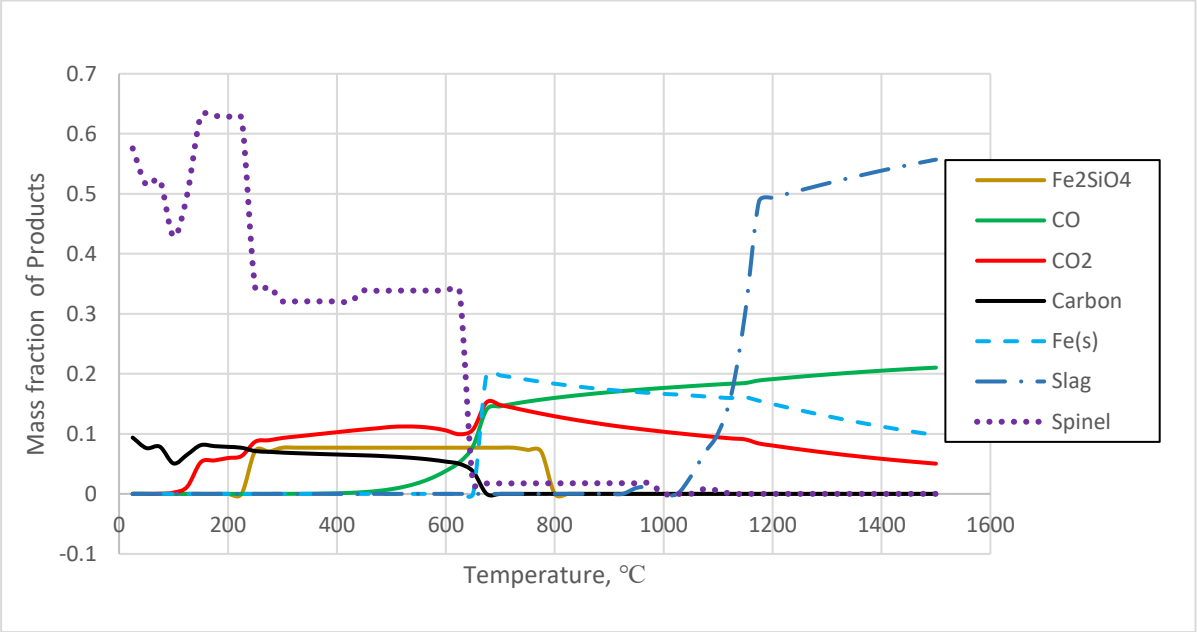

Figure 4.36: Mass fraction of products obtained from FactSage calculation during the reduction of hematite with 100%PCB

4.6 EMSIM Simulations

EMSIM was used to study smelting of 1 ton of chromite (Table 3.5) and iron ore (Table 3.6). Two scenarios were applied to understand how PCB behaves when used as a reductant. In the first case, 1 ton/h ore was reduced using 300 kg/h reducing agent at 1700°C. PCB-coal blends with varying blending ratios were used as reductant. The blends were varied by their mass percent. In the second scenario, however, the reductant used in the smelting operation contains 300 kg/h of carbon.

4.6.1 Chromite Smelting

As shown in Figure 4.37, the metal recovery as well as the energy required for the smelting process reduces as the percentage of PCB in the blend increases. It is observed that up to about 20% PCB in the blend, the percentage metallization remains at about 97% with energy savings of about 200 kWh. The decrease in the energy required is attributed to the high percentage of volatile matter present in PCB. In addition, the results confirm the investigation by Hattori (2005) where the use of plastics as reducing agent showed a reduced electrical power consumption. Chongmin et al. (2009) stated that the high volatile matter leads to energy saving and improved efficiency. Moreover, the decrease in metal recovery is ascribed to the lower carbon percentage present in PCB since carbon content is responsible for the reduction of the ore to metal.

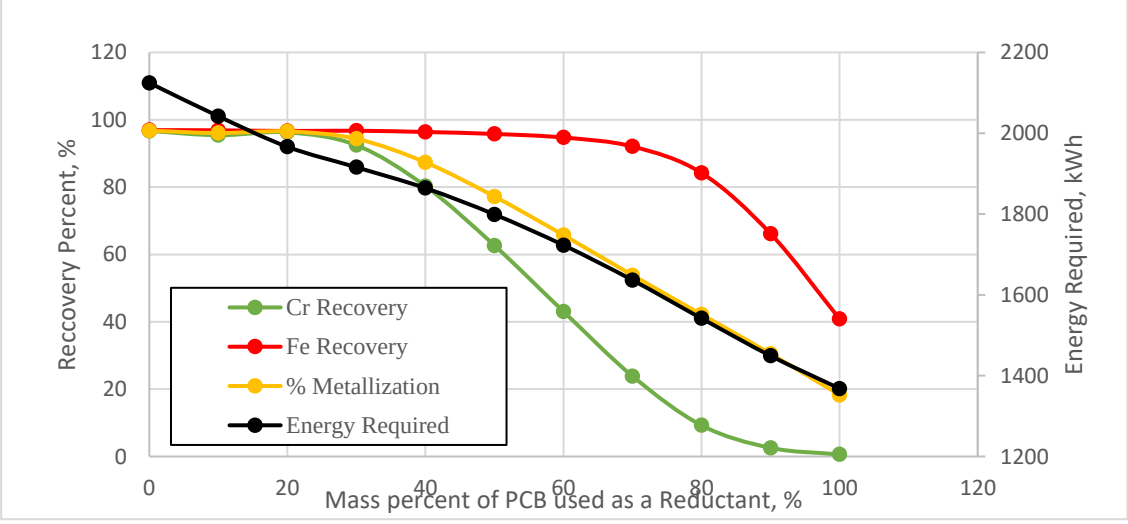

Figure 4.37: Metal recovery and energy required for chromite smelting

During the smelting of chromite ore, alloy, gas, slag and spinel were obtained as products (Figure 4.38). It is observed that the alloy content reduces as the mass percent of PCB increases in the blend. This is also ascribed to the low percentage of carbon in PCB relative to the coal.

Sahajwalla et al. (2012) stated that blend of end-of-life polymers and coke can be used to efficiently increase slag foaming in electric arc furnace steelmaking. The results obtained from chromite smelting simulation confirmed it because as PCB increases in the blend, the slag formed also increases. This is due to the presence of alkaline oxides such as CaO, MgO, Fe_2O_3 and the high percentage of SiO_2 present in the PCB. The slag mainly contains SiO_2, Al_2O_3, CrO and MgO. The solid spinel consists of $MgCr_2O_4$, $MgAl_2O_4$, $AlCr_2O_4$[1+] $CrAl_2O_4$, $FeAl_2O_4$, etc.

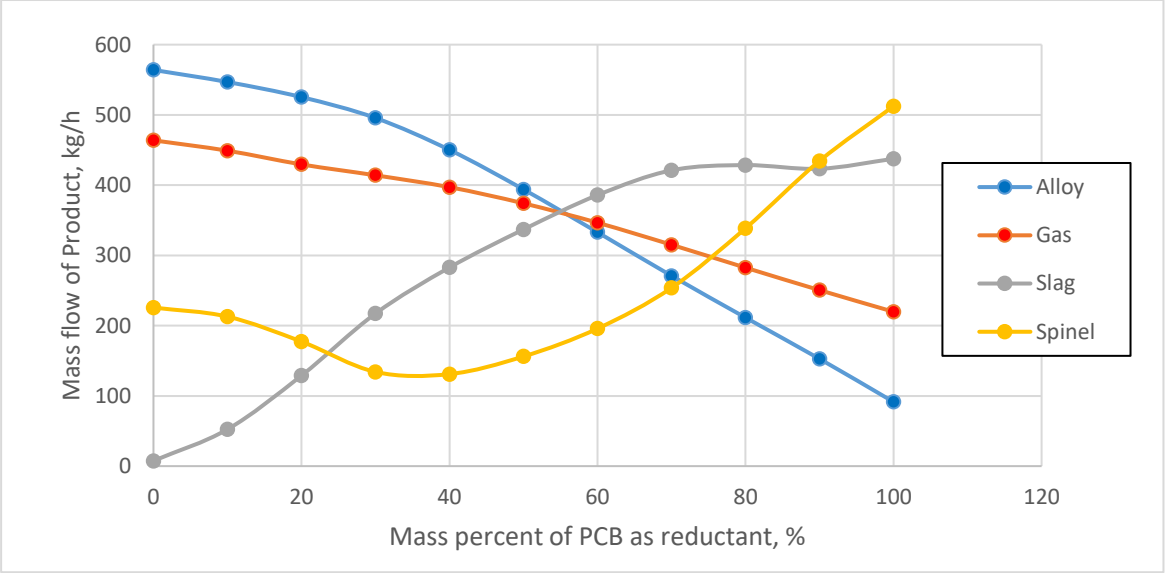

Figure 4.38: Products of chromite smelting

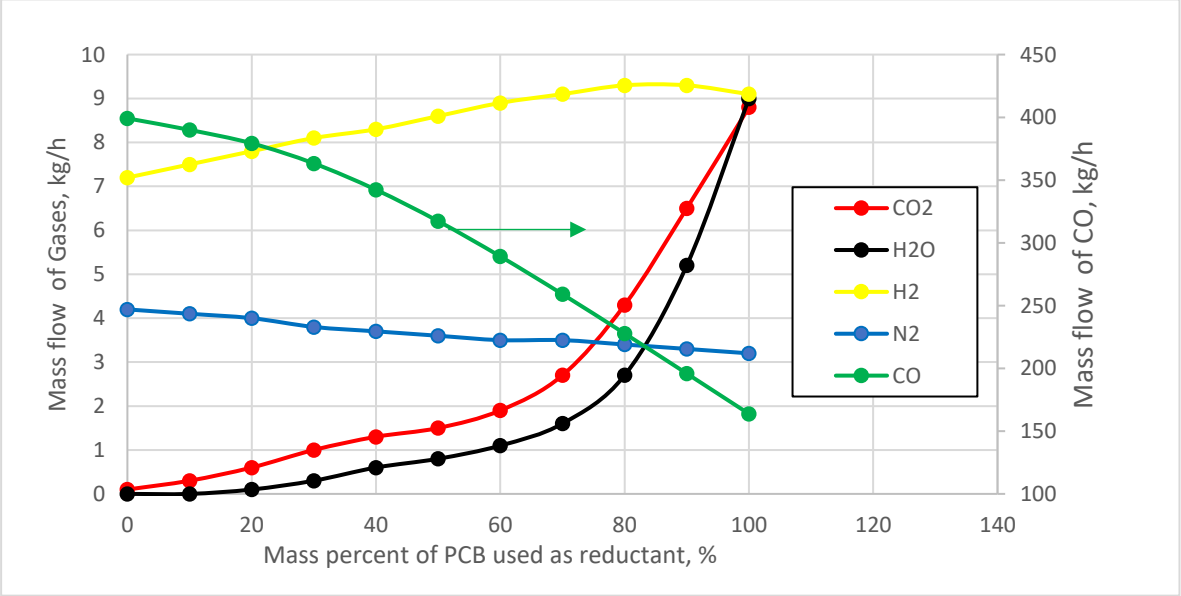

Figure 4.39: Mass flowrate of gases during chromite smelting

Since the PCB contains more volatiles, it was expected that the total gas released would be higher during reduction with blends containing higher mass percent of PCB. However, this is not the observation. It can be seen in Figure 4.38 that the total gas released decreases as the mass percent of PCB increases in the blend. This is because the volatiles in the PCB contains hydrocarbons which take part in the reduction process.

Figure 4.39 shows the mass flowrate of gases that were produced during the smelting of chromite. EMSIM predicted that at equilibrium, the composition of the gas include SiO, CH_4, C_2H_2, SiS, etc. These gases were not included in the plot because the individual mass flowrates were less than 0.1kg/h. It is observed that, in each of the blends, over 80% of the off-gas produced during smelting is CO. Moreover, the flowrate of CO decreases steadily with increase of PCB in the blend. This is an indication of lower carbon unit in the PCB. In addition, the CO_2 flowrate increases as PCB in the blend increases. As stated earlier (4.1), Dankwah et al. (2015) reported that the use of PET as reducing agent increases the CO_2 produced. The observation in Figure 4.39 agrees with their investigation since CO_2 release increased as the mass percent of PCB increases in the blend probably due to the fact that overall CO decreases as reduction decrease leading to higher CO_2 in the gas phase. This is also due to absence of Boudouard reaction caused by lack of carbon in the sample.

However, both H_2 and H_2O increase when PCB increases in the blend. H_2O composition increases from 0 kg/h when coal is used to about 9 kg/h when PCB is used during the smelting operation. This confirms that the hydrocarbons present in the PCB also take part in the reduction process as shown in Equation B.7. N_2 released however remained fairly the same between 3 kg/h and 4.2 kg/h.

4.6.2 Iron Smelting

As in chromite smelting, the iron recovery decreased with an increase in the mass percent of PCB in the blend (Figure 4.40). The optimum blend is less than 20% which was observed during the chromite smelting. It is believed that hydrocarbons also present in the PCB decompose to form carbon and hydrogen which are capable of reducing the ore. Carpenter (2010) investigated the use of coal and waste plastics in blast furnace and reported that the reduction by H_2 is less endothermic than direct reduction by carbon. Hence, there is a decrease in the energy requirement.

In Figure 4.41, it can be seen that both the evolved gas and the alloy content decreases while the slag composition increases as the mass percent of PCB in the blend increase similar to the

observation during chromite smelting. The slag is composed of FeO, SiO_2, Fe_2O_3 and CaO with small amount of Mn_2O_3, N_2O and MnO.

The composition of the gas (Figure 4.42) also followed a similar pattern as the gas composition during chromite smelting (Figure 4.39).

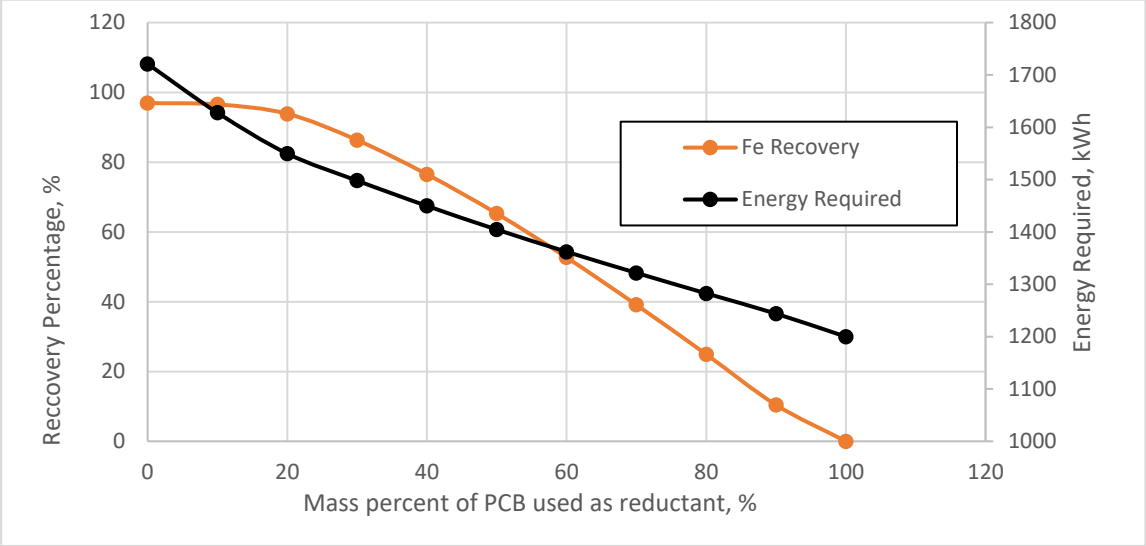

Figure 4.40: Metal recovery and energy required for iron smelting

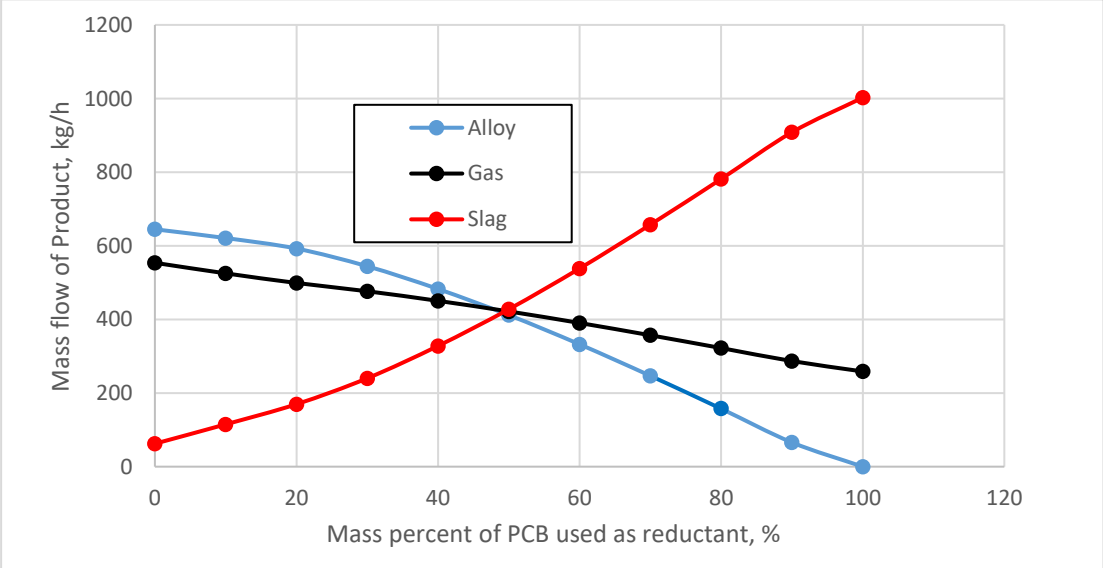

Figure 4.41: Products of iron smelting

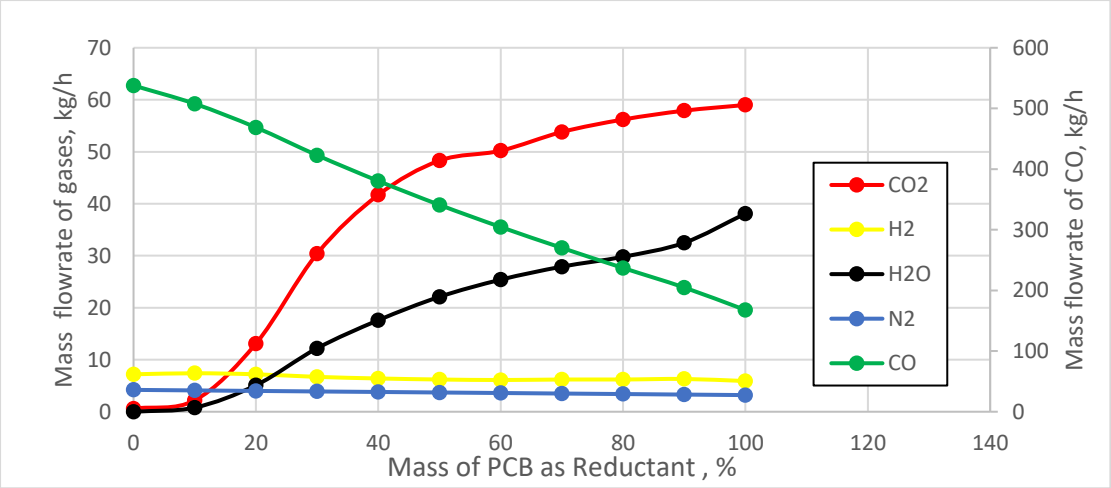

Figure 4.42: Mass flowrate of gases during Iron smelting

4.6.3 Smelting with Equivalent Total Mass of Carbon Content in PCB and Coal

In the previous scenario, smelting of both iron and chromite ore were simulated using 300 kg/h of reducing agent. Since PCB contains lesser carbon content compared to coal, the metal recovery decreases with the increase of PCB in the blend. In this scenario, smelting of chromite ore as well as iron ore were performed using reducing agents that contain 300kg/h of carbon. Table 4.9 shows the mass of PCB and coal used in each blend for the reduction of 1 ton of ore.

Table 4.9: Blends containing 300kg/h of equivalent carbon used in smelting simulation

Name of Blend	Mass of PCB, kg/h	Mass Of Coal, kg/h	Total Mass of reductant, kg/h
0%	0.00	374.53	374.53
10%	105.26	337.08	442.34
20%	210.53	299.63	510.15
30%	315.79	262.17	577.96
40%	421.05	224.72	645.77
50%	526.32	187.27	713.58
60%	631.58	149.81	781.39
70%	736.84	112.36	849.20
80%	842.11	74.91	917.01
90%	947.37	37.45	984.82
100%	1052.63	0.00	1052.63

4.6.3.1 Chromite Smelting

Since each of the blends contain the same mass of carbon, it was expected that the metal recovery remains constant for the reduction with each of the blends. However, with blends of PCB greater than 50%, the recovery decreases with increase in PCB. Although, the energy required for the smelting process was also expected to continuously increase since a higher mass input of reductant was used, the energy increase was only up to 30% blend. The energy constantly decreased with blends greater than 30%. It should be noted that since the mass percent of carbon and SiO_2 are nearly the same, increasing the mass of PCB to obtain the same mass of carbon in coal invariably increases the SiO_2 in the reductant. The increase in SiO_2 results in an increase in the slag formed. The slag content increased from around 0kg/h when only coal was used to about 1500 kg/h when only PCB was used as a reductant. The spinel in the product decreased from 200 kg/h when pure coal was used to 0 kg/h when at least 60% blend was used. The spinel content decreases because it is dissolved by the liquid slag. Also, the amount of oxygen in the reductant is increased as more PCB is used to achieve the same mass of carbon in coal. The oxygen is likely to react with the carbon in the PCB, thereby reducing the reduction potential of the PCB.

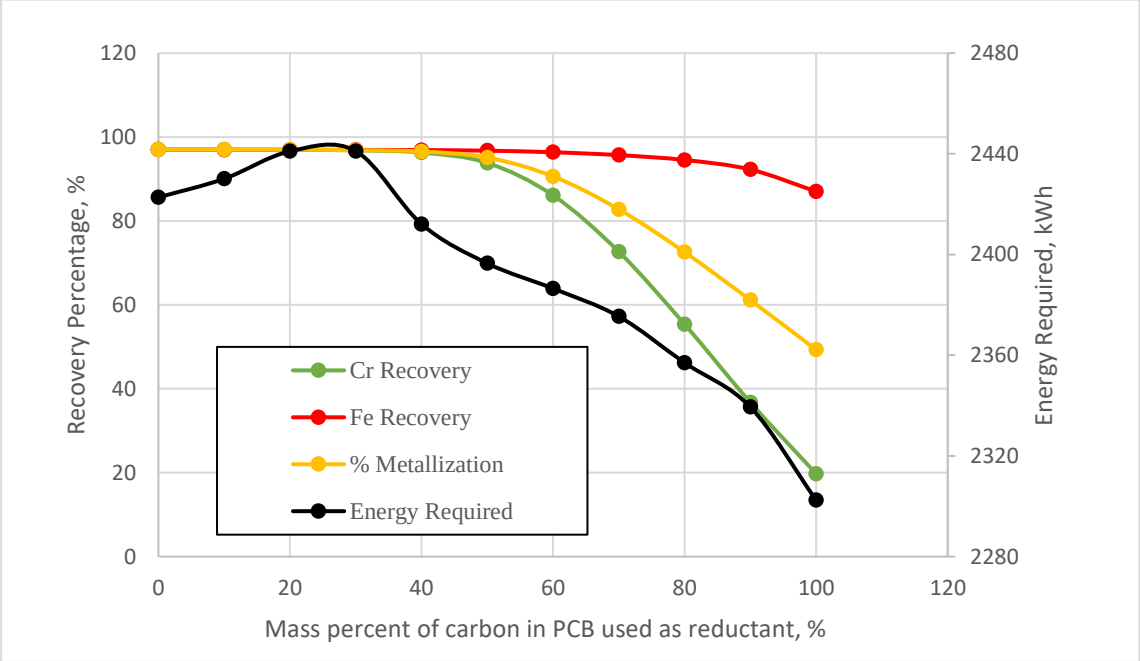

Figure 4.43: Metal recovery and energy required for chromite smelting

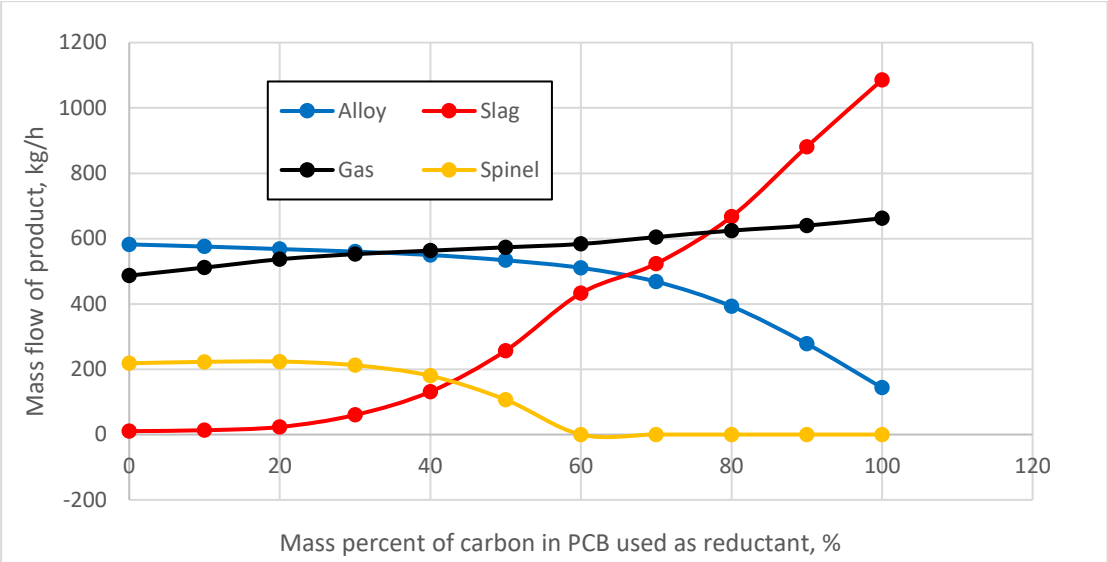

Figure 4.44: Products of chromite smelting

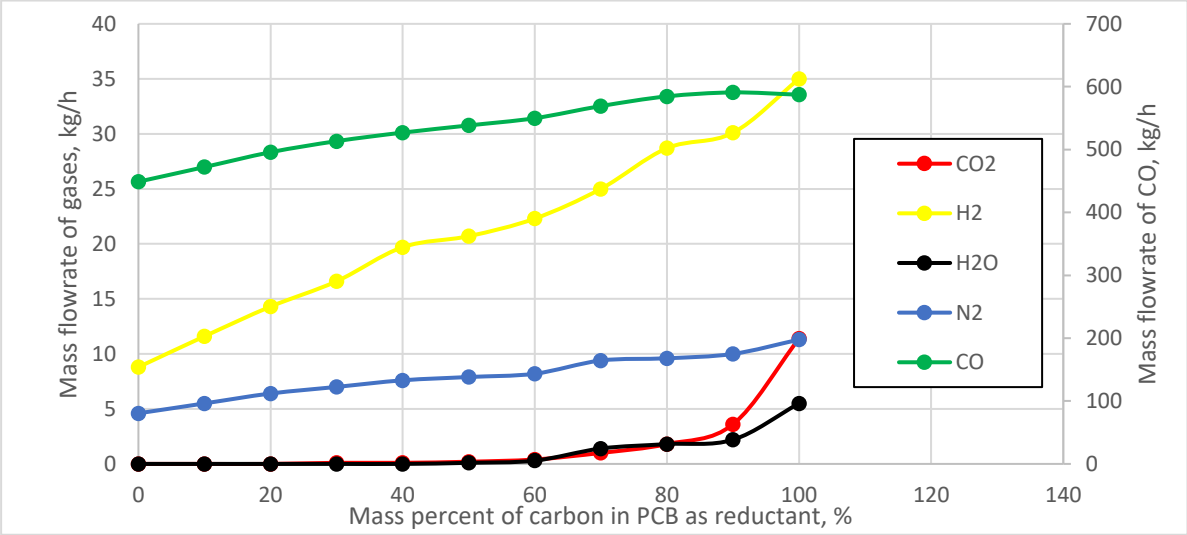

Figure 4.45: Mass flowrate of gases during chromite smelting

4.6.3.2 Iron Smelting

Smelting of iron using the same mass of carbon in each blend showed similar patterns as that of the chromite smelting. As shown in Figure 4.46 the metal recovery remained around 97% up to 40% blend after which it decreased to a value close to 50%. In the previous scenario, however, the metal recovery decreased to about 0%. This indicates that increasing the mass of PCB used as reductant in order to supply more carbon for a reduction process, only partially improves reduction.

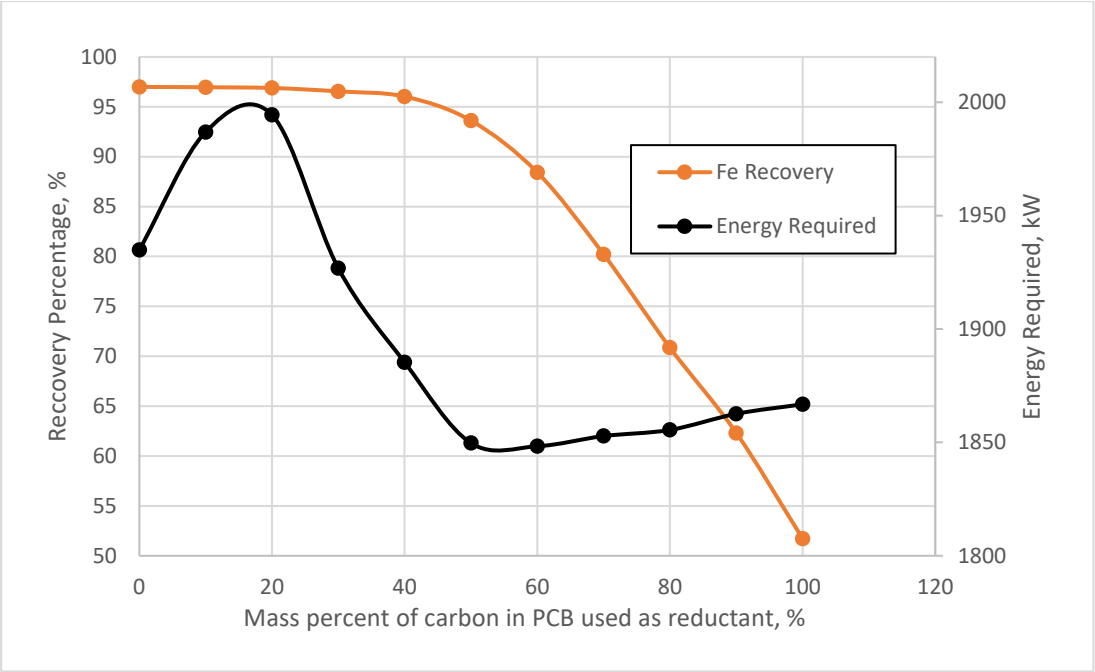

Figure 4.46: Metal recovery and energy required for iron smelting

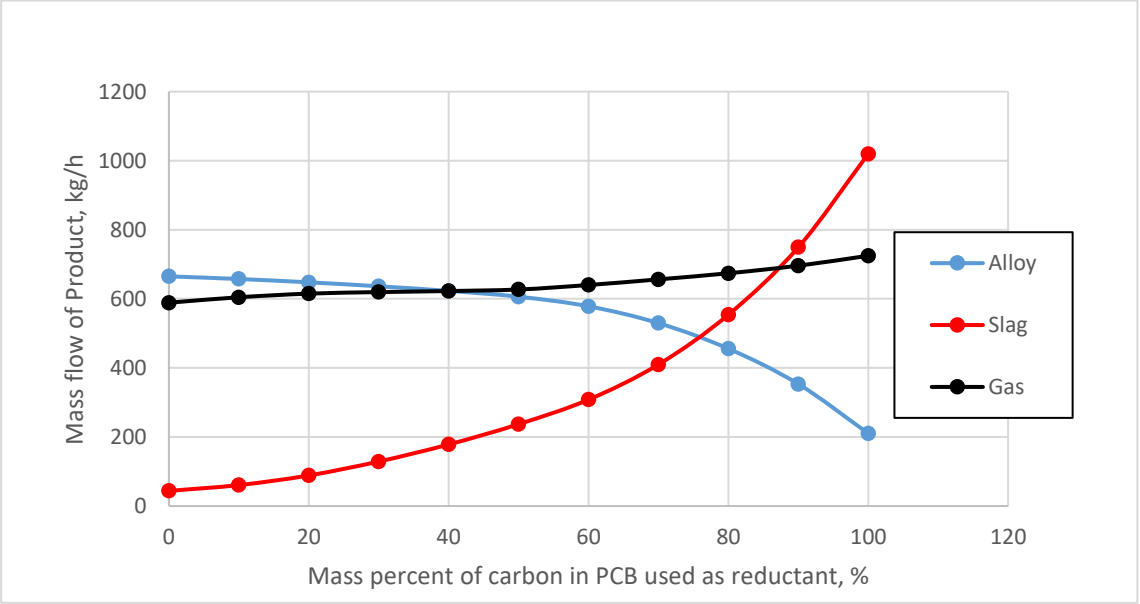

Figure 4.47: Products of iron smelting

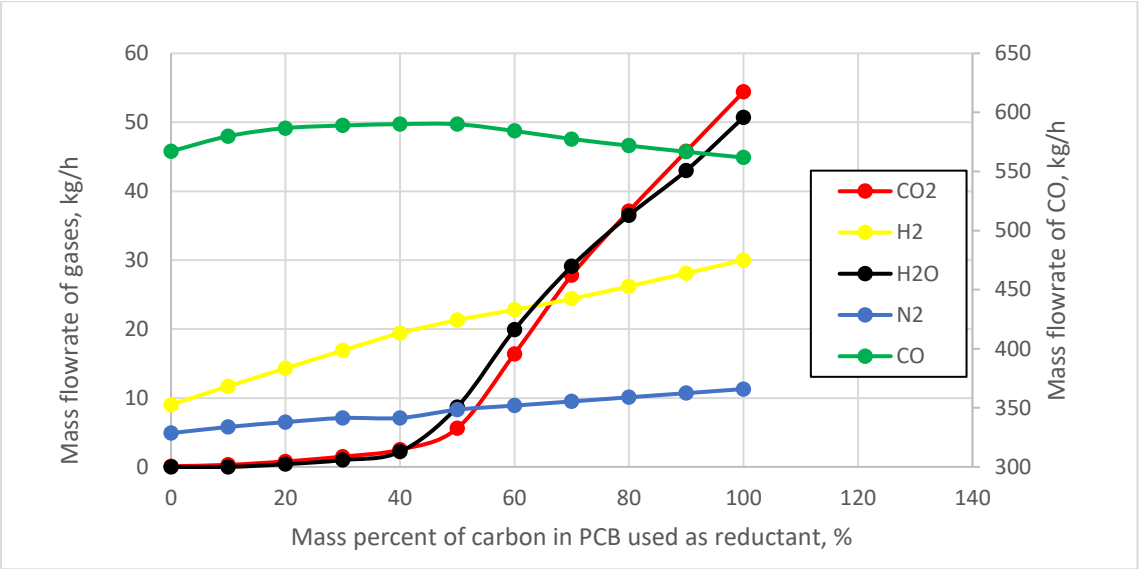

Figure 4.48: Mass flowrate of gases in off-gas during iron smelting

4.6.4 Effect of Temperature

The effect of temperature during smelting of PCB was investigated using EMSIM simulations. Iron ore smelting was carried out at different temperatures (Appendix A.2) to simulate the reduction of iron in blast furnace. Smelting of ore with coal, pure PCB and 20% blend (wt%) were considered for the study. The simulations were carried out from 900℃ to 1300℃ and also at 1700℃.

EMSIM simulations (Figure 4.49) revealed that when coal and 20% PCB are used as reducing agents, the metal recovery remain fairly constant at 97% and 96% respectively. These results are at equilibrium and do not necessarily reveal the kinetics of the operation. It is observed that PCB acts better at lower temperatures. At 900℃, when pure PCB was used as a reductant, a metal recovery of about 10% was observed whiles close to 0% iron was recovered at 1700℃ using pure PCB.

In addition, the energy required for iron ore smelting using each of the reductants increases as the temperature increases. The steeper slope observed between temperatures 1100℃ and 1200℃ may be attributed to the formation of liquid iron.

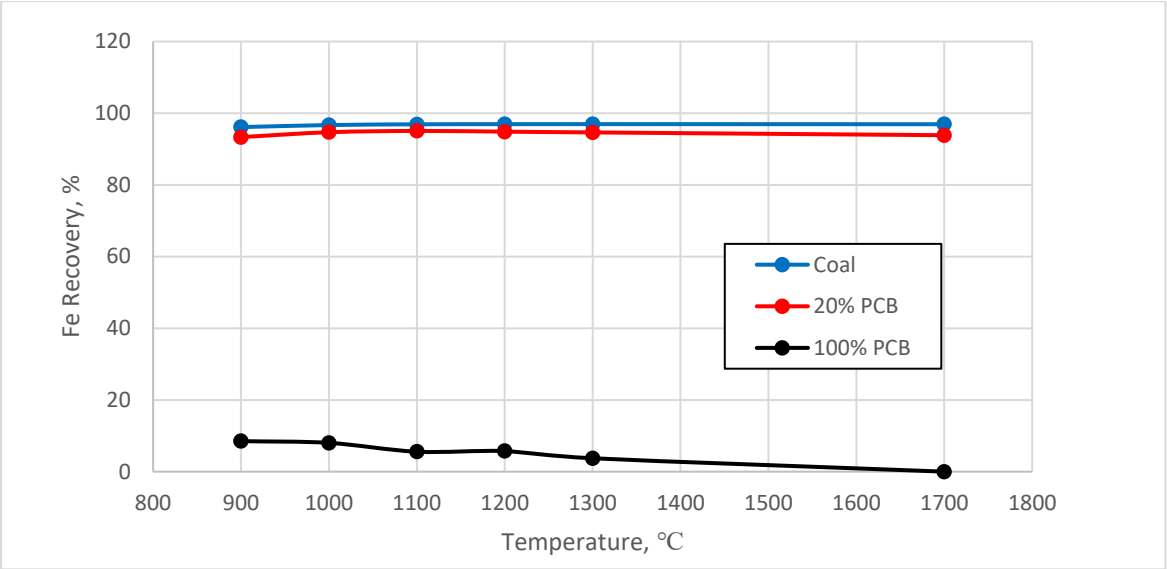

Figure 4.49: Iron recovery at different temperatures

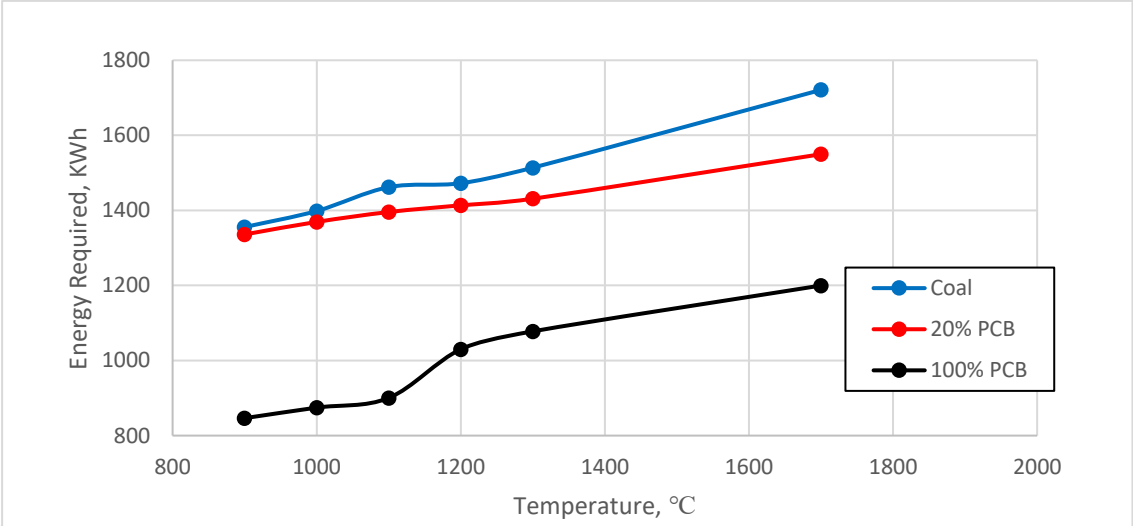

Figure 4.50: Energy required at different temperatures

4.6.5 Effect of Oxygen Present in PCB

The effect of percentage of oxygen was also studied using EMSIM. From the ultimate analysis, it was revealed that PCB contains about 20.72 wt% oxygen. The percentage of oxygen present in the PCB was varied and its effect on metal recovery, slag and CO_2 produced were compared to conventional coal. Three cases (as shown in Table 4.10) were considered and compared with the case where all the oxygen present in the PCB took part in the reduction process in order to understand the effect of the oxygen content of the PCB.

Table 4.10: Representations used in studying the effect of oxygen

Scenario	Wt% of oxygen in PCB that reacted	Meaning
Sc-A	20.72%	All the oxygen present in the PCB took part in smelting
Sc-B	16.576%	Only 80% of the oxygen present in the PCB took part in smelting
Sc-C	10.36%	Only 50% of the oxygen present in the PCB took part in smelting
Sc-D	0%	Oxygen present in the PCB did not take part in smelting

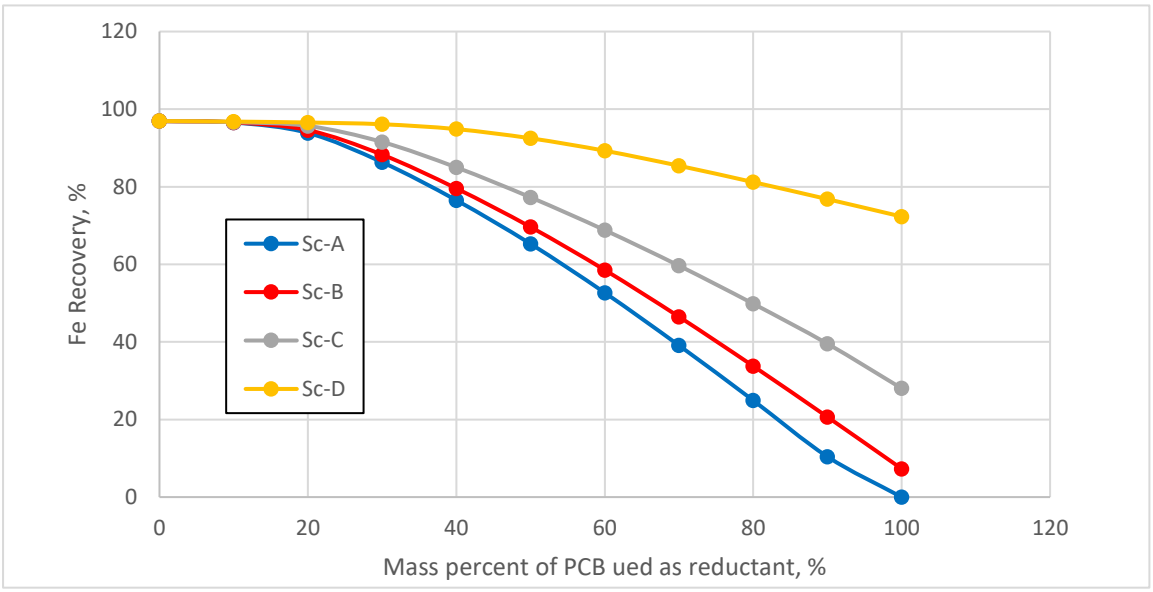

Figure 4.51: Effect of oxygen in PCB on the metal recovery

As shown in Figure 4.51, the oxygen content affects the recovery of iron. It can be seen that, when oxygen present in PCB do not take part in the reaction (Sc-D), about 73% of iron is recovered when pure PCB is used as reductant whereas with the case where all the oxygen takes part in the reaction (Sc-A), almost no iron is recovered when pure PCB is used during the reduction. Lotfian et al. (2016) reported that the presence of oxygen in some plastics like polyurethane (PU) and polyvinyl chloride (PVC) might affect their reduction potential when they are used as reducing agents. The simulation supports the study since there is a decrease in the recovery of iron when higher amounts of oxygen take part in the reduction.

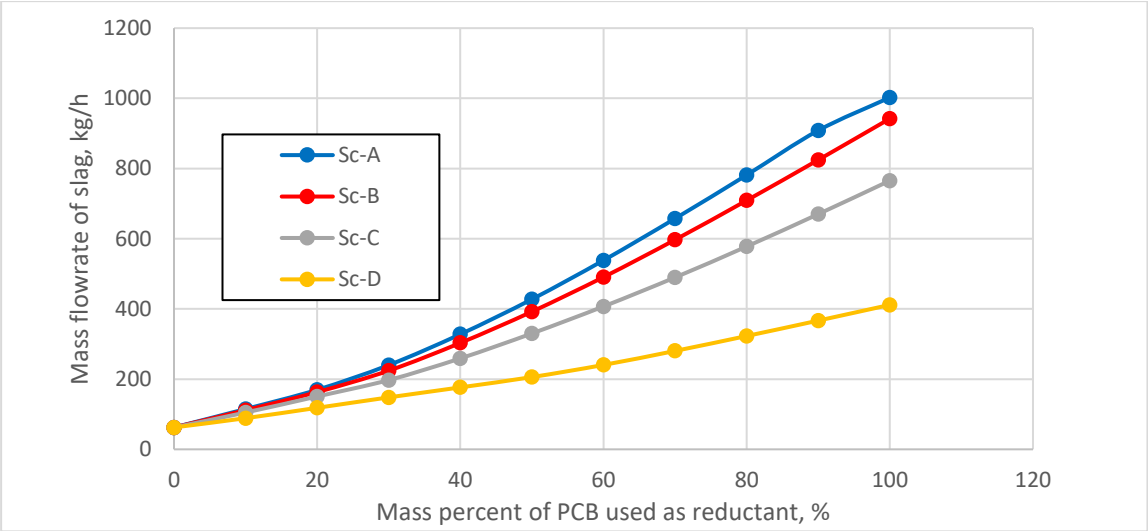

Figure 4.52: Effect of oxygen in PCB on the slag produced

The oxygen content also affects the amount of slag formed. The results (Figure 4.52) show that the presence of oxygen increases the slag content in the product. When PCB was used as a reductant, about 1000 kg/h slag was produced when all the oxygen present in PCB take part in the reduction whiles slightly over 400 kg/h slag was predicted when it was assume that none of the oxygen took part in the smelting operation.

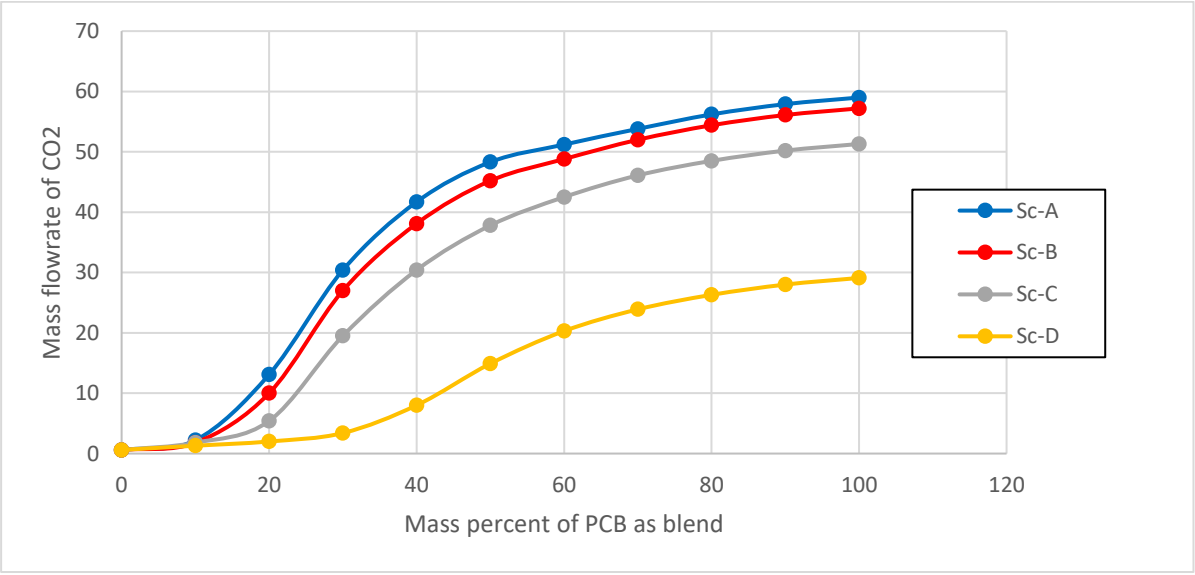

Figure 4.53: Effect of oxygen in PCB on the CO_2 present in off-gas

It is observed in Figure 4.53 that the oxygen present in the PCB contributes to the increase in the amount of CO_2 produced during reduction. When PCB is used as a reductant, a difference of about 30 kg/h is predicted by EMSIM if oxygen present in the PCB do not take part in the smelting of the ore relative to when all the oxygen in the PCB take part in the reduction.

5 Conclusions and Recommendations

In this study, the use of leached residue of PCB as a reducing agent in pyrometallurgical operations was investigated. The metal recovery, energy required as well as the slag produced when PCB was used as a reductant was compared with that of graphite/coal and PCB-graphite/coal blends.

A) The leached residue of PCB was characterized using XRD, XRF, FTIR as well as proximate and ultimate analysis and the following PCB characterization results were obtained:

   i. Proximate analysis revealed a higher volatile matter of about 44% relative to that of 5.1% present in coal. However, the fixed carbon of 11.5% present in the PCB was lower than coal which is 81.5%. The ash content of the PCB (40.1%) was higher than that of coal (11.7%).

   ii. The elemental analysis shows that PCB contains carbon and hydrogen content of 30.43% and 3.06% respectively. The carbon content is significantly less than that of coal (80%) whiles hydrogen composition is slightly greater than coal (1.6%). The oxygen content of PCB is shown to be 20.72% whiles that of nitrogen and sulphur is 1.42% and 0.63% respectively. The oxygen content in PCB is greater than that of coal (2.12%).

   iii. XRD results indicate that PCB is highly amorphous with trace amounts of titanium. The XRF corresponds with the ash analysis. Both show a high percentage of SiO_2 and the presence of CaO, Al_2O_3, Fe_2O_3 with trace amounts of TiO_2, MnO etc. In addition, the XRF shows the loss on ignition value of PCB as 59.8%

   iv. The calorific value of PCB was found to be 12.08 MJ/kg which is less than that of coal (30 MJ/kg). It is reported that the low calorific value is due to the presence of the glass fibres in the PCB.

B) Hematite reduction tests were performed in DSC-TGA and SPR.

   i. Non-isothermal reduction tests were carried out in the DSC-TGA which was coupled with QMS to analyse the gas released. The tests were carried out from ambient temperature to 1200℃ using high purity argon. The results show the pyrolysis of PCB at temperatures between 275℃ and 325℃. About 30% of the initial mass of the PCB was lost. QMS show the release of CO, CO_2, CH_4, HBr and other gases during the pyrolysis stage. In addition, it was revealed that the

reduction of hematite with PCB has faster kinetics than reduction with graphite due to the presence of hydrocarbons in PCB. The hydrocarbons were found to be reducing hematite at lower temperatures than pure carbon. Moreover, it is believed that plastics content present in the PCB forms a liquid phase which allows it to have more contact with the hematite during reduction experiments. The reduction degrees which were calculated from the mass loss showed that PCB and blends of PCB act as better reducing agents at lower temperatures.

ii. Isothermal reduction test were also carried out in SPR at 1000°C and 900°C. The volume percent of CO and CO_2 present in the off-gas were analysed and recorded. The results show that, at 900°C, PCB reduces hematite better than graphite. At 1000°C however, pure carbon proves to be a better reducing agent.

C) FactSage simulations were also carried out for validation of lab scale tests for solid state reduction of hematite. FactSage simulations predicted the formation of fayalite (Fe_2SiO_4) between 200°C and 800°C when PCB or blends of PCB are used as reducing agents. Moreover, the calculations predict the formation of solid iron at temperatures above 700°C. This is in good agreement with the experimental findings with respect to iron formation at 900°C.

D) Smelting of chromite ore and iron ore were simulated using EMSIM. Two scenarios were considered

i. In the first case, 1 ton of ore was smelted with the same mass of reductant and the following were established:

- As PCB in the blend increases, the amount of energy required for the smelting operation decreases
- Metal recovery decreased as the mass percent of PCB in the blend used as a reductant increased. The decrease in the metal recovery is ascribed to lower carbon content present in PCB relative to coal
- The optimum mass percent of PCB used in the blend is about 20% since about 200 kWh of energy is saved to achieve the same metal recovery. The decrease in the amount of energy required for the operation is also attributed to the higher volatile content of the PCB which also takes part in the reduction process
- As PCB in the blend increases, the slag produced increases. The slag increase is due to the relatively high content of SiO_2 present in the PCB

- Mass flow rate of the evolved gas was seen to decrease as PCB in the blend increased. This is because the hydrocarbons present in the PCB also take part in the reduction of the ore
- CO decreased while the CO_2 increased as the mass percent of PCB in the blend increased. The decrease in CO is due to the lower carbon content in the PCB whereas the CO_2 increase is due to the higher amount of oxygen in PCB

ii. A second scenario was simulated where the blends used in the smelting process contained the same mass of carbon

- EMSIM predicted that an increase in energy up to about 30% carbon from PCB blend after which the energy decreases. The recovery also decreased with blend higher than 40% carbon from PCB. In this scenario however, the mass flow rate of the evolved gas increase as PCB increases in the blend

E)

i. Mass and energy balance models showed that the energy required for smelting decreases when PCB or PCB blends are used as reducing agent. The economics of incorporating the non-metallic fraction of PCB could be studied

ii. Due to the high percentage of oxygen in the PCB sample, high amount of CO_2 was released when PCB was used as a reducing agent. Further studies could be done to investigate ways to reduce the CO_2 produced or capturing the CO_2 for other purposes

iii. The feasibility of using non-metallic fractions of PCB as reducing agent for hematite reduction showed that PCB has faster kinetics at lower temperatures than graphite. Further studies could be done to adequately comprehend the kinetic behaviour of PCB during reduction process.

iv. The study showed that pyrolysis of PCB occurs at a temperature around 300°C. Further investigations could be done to derive fuel and other products from the pyrolysis of the non-metallic fractions of PCB.

Contribution

Attah-Kyei, D., Akdogan, G., Dorfling, C., Erwee, M., Zietsman, J., Reynolds, Q., 2018. Printed circuit board leach residue as a reductant for pyrometallurgical operations, in: WasteCon 2018. Johannesburg, South Africa, pp. 1–11.

6 List of References

Albertyn, P. W., & Dorfling, C. (2017). *Ammonium thiosulphate leaching of gold from printed circuit board waste*. Stellenbosch University.

Baldé, C. P., Wang, F., Kuehr, R., & Huisman, J. (2015). *The Global E-Waste Monitor 2014*. *United Nations University, IAS – SCYCLE, Bonn, Germany*.

Bale, C. W., Bélisle, E., Chartrand, P., Decterov, S. A., Eriksson, G., Hack, K., … Petersen, S. (2008). FactSage Thermochemical Software and Databases – Recent Developments. *Calphad*, *33*(2), 295–311.

Bazargan, A., Bwegendaho, D., Barford, J., & McKay, G. (2014). Printed circuit board waste as a source for high purity porous silica. *Separation and Purification Technology*, *136*, 88–93. https://doi.org/10.1016/j.seppur.2014.08.026

Brouwer, P. (2010). *Theory of XRF*. *Theory of XRF* (3rd ed.). Almelo: PANalytical B.V.

Brown, M. E. (1989). Introduction to Thermal Analysis: Techniques and Applications. *Mineralogical Magazine*. https://doi.org/10.1180/minmag.1989.053.373.29

Bunaciu, A. A., Udriştioiu, E. gabriela, & Aboul-Enein, H. Y. (2015). X-Ray Diffraction: Instrumentation and Applications. *Critical Reviews in Analytical Chemistry*, *45*(4), 289–299. https://doi.org/10.1080/10408347.2014.949616

Cao, X., Prozorov, B., Koltypin, Y., Felner, I., & Gedanken, A. (1997). Synthesis of pure amorphous Fe2O3. *Journal of Materials Research*, *2*(Feb 1997), 2–6.

Carpenter, A. M. (2010). *Injection of coal and waste plastics in blast furnaces. Report CCC/166*. Retrieved from https://www.usea.org/sites/default/files/032010_Injection of coal and waste plastics in blast furnaces_ccc166.pdf

Cayumil, R., Khanna, R., Ikram-Ul-Haq, M., Rajarao, R., Hill, A., & Sahajwalla, V. (2014). Generation of copper rich metallic phases from waste printed circuit boards. *Waste Management*, *34*(10), 1783–1792. https://doi.org/10.1016/j.wasman.2014.05.004

Chatterjee, S. (2012). Sustainable Electronic Waste Management and Recycling Process, *2*(1), 23–33. https://doi.org/10.5923/j.ajee.20120201.05

Chen, H., Zheng, Z., Chen, Z., & Bi, X. T. (2017). Reduction of hematite (Fe2O3) to metallic iron (Fe) by CO in a micro fluidized bed reaction analyzer: A multistep kinetics study.

Powder Technology, *316*, 410–420. https://doi.org/10.1016/j.powtec.2017.02.067

Cui, H., & Anderson, C. G. (2016). Literature Review of Hydrometallurgical Recycling of Printed Circuit Boards (PCBs). *Journal of Advanced Chemical Engineering*, *6*(1), 1–11. https://doi.org/10.4172/2090-4568.1000142

Dankwah, J., Amoah, T., Dankwah, J., & Fosu, A. (2016). Recycling Mixed Plastics Waste as Reductant in Ironmaking. *Ghana Mining Journal*, *15*(2), 73–80. Retrieved from http://www.ajol.info/index.php/gm/article/view/127934

Dankwah, J. R., & Koshy, P. (2014). Reduction of FeO in EAF steelmaking slag by blends of metallurgical coke and waste polypropylene. *High Temperature Materials and Processes*, *4*(1), 274–279. https://doi.org/10.1515/htmp-2013-0035

Dankwah, J. R., Koshy, P., O'Kane, P., & Sahajwalla, V. (2012). Reduction of FeO in EAF steelmaking slag by blends of metallurgical coke and end-of-life tyre. *Steel Research International*, *83*(8), 766–774. https://doi.org/10.1002/srin.201200019

Delgado, A. C., Barruetabeña, L., & Salas, O. (2007). *Assessment of the Environmental Advantages and Drawbacks of Existing and Emerging Polymers Recovery Processes*. https://doi.org/10.2791/46661

Diaz, L. A., Lister, T. E., Parkman, J. A., & Clark, G. G. (2016). Comprehensive process for the recovery of value and critical materials from electronic waste. *Journal of Cleaner Production*, *125*, 236–244. https://doi.org/10.1016/j.jclepro.2016.03.061

Duan, H., Hou, K., Li, J., & Zhu, X. (2011). Examining the technology acceptance for dismantling of waste printed circuit boards in light of recycling and environmental concerns. *Journal of Environmental Management*. Elsevier Ltd. https://doi.org/10.1016/j.jenvman.2010.10.057

Evangelopoulos, P., Kantarelis, E., & Yang, W. (2015). Investigation of the thermal decomposition of printed circuit boards (PCBs) via thermogravimetric analysis (TGA) and analytical pyrolysis (Py-GC/MS). *Journal of Analytical and Applied Pyrolysis*, *115*, 337–343. https://doi.org/10.1016/j.jaap.2015.08.012

Fink, J. K. (1999). Pyrolysis and combustion of polymer wastes in combination with metallurgical processes and the cement industry. *Journal of Analytical and Applied Pyrolysis*, *51*(1), 239–252. https://doi.org/10.1016/S0165-2370(99)00019-4

Fisher, M. M. (2006). Feedstock recycling technologies in the sustainable recycling of plastics from end-of-life electrical and electronic products. *IEEE International Symposium on Electronics and the Environment, 2006*, 292–297. https://doi.org/10.1109/ISEE.2006.1650079

Franz, R. L. (2002). Optimizing portable product recycling through reverse supply chain technology. *IEEE International Symposium on Electronics and the Environment*, 274–279. https://doi.org/10.1109/ISEE.2002.1003279

Gallagher, P. (2008). *Handbook of Thermal Analysis and Calorimetry*. *Handbook of Thermal Analysis and Calorimetry* (Vol. 5). https://doi.org/10.1016/S1573-4374(13)60004-7

Guanghan, S., Zhu, X., Wenyi, Y., Chenglong, Z., & Wen, M. (2016). Recycling and disposal technology for non-mentallic materials from waste printed circuit boards (WPCBs) in China. *Procedia Environmental Sciences*, *31*, 935–940. https://doi.org/10.1016/j.proenv.2016.02.114

Guo, J., Guo, J., & Xu, Z. (2009). Recycling of non-metallic fractions from waste printed circuit boards: A review. *Journal of Hazardous Materials*, *168*(2–3), 567–590. https://doi.org/10.1016/j.jhazmat.2009.02.104

Guo, J., Tang, Y., & Xu, Z. (2010). Performance and thermal behavior of wood plastic composite produced by nonmetals of pulverized waste printed circuit boards. *Journal of Hazardous Materials*, *179*(1–3), 203–207. https://doi.org/10.1016/j.jhazmat.2010.02.080

Hadi, P., Ning, C., Ouyang, W., Xu, M., Lin, C. S. K., & McKay, G. (2015). Toward environmentally-benign utilization of nonmetallic fraction of waste printed circuit boards as modifier and precursor. *Waste Management*, *35*, 236–246. https://doi.org/10.1016/j.wasman.2014.09.020

Hattori, T. (2005). Recycling Technique of Waste Plastics as Carbon Material, *50*(1), 27–32.

Havlik, T., Orac, D., Petranikova, M., & Miskufova, A. (2011). Hydrometallurgical treatment of used printed circuit boards after thermal treatment. *Waste Management*, *31*(7), 1542–1546. https://doi.org/10.1016/j.wasman.2011.02.012

Höhne, G. W. H., Hemminger, W. F., & Flammersheim, H. J. (2003). Differential scanning calorimetry (p. 298). https://doi.org/10.1007/978-3-662-06710-9

Hotta, H. (2003). Recycling Technologies for Promoting Recycling-oriented Society, *88*(88).

Huang, K., Guo, J., & Xu, Z. (2009). Recycling of waste printed circuit boards : A review of current technologies and treatment status in China, *164*, 399–408. https://doi.org/10.1016/j.jhazmat.2008.08.051

Ida, H. (2006). Current Status of Plastics Recycling in Japan.

Jung, S. M., & Yi, S. H. (2013). A kinetic study on carbothermic reduction of hematite with graphite employing thermogravimetry and quadruple mass spectrometry. *Steel Research International*, *84*(9), 908–916. https://doi.org/10.1002/srin.201200310

Kadari, R., Velchuri, R., Malathi, M., Vithal, M., & Munirathnam, N. R. (2017). Degradation of organic pollutants by Ag , Cu and Sn doped waste non-metallic printed circuit boards. *Waste Management*, *60*, 629–635. https://doi.org/10.1016/j.wasman.2016.09.026

Kahhat, R., Kim, J., Xu, M., Allenby, B., Williams, E., & Zhang, P. (2008). Resources , Conservation and Recycling Exploring e-waste management systems in the United States, *52*, 955–964. https://doi.org/10.1016/j.resconrec.2008.03.002

Kanchanapiya, P., Pinyo, W., Jareemit, S., & Kwonpongsagoon, S. (2015). Recycling of non-metallic powder from printed circuit board waste as a filler material in a fiber reinforced polymer. *Environment Protection Engineering*, *41*(4), 151–166. https://doi.org/10.5277/epel50412

Kato, K., Nomura, S., & Uematsu, H. (2002). Development of waste plastics recycling process using Coke ovens. *ISIJ International*, *42*(87), 10–13. https://doi.org/10.4144/rpsj.50.182

Kaya, M. (2016). Recovery of metals and nonmetals from electronic waste by physical and chemical recycling processes. *Waste Management*, *57*, 64–90. https://doi.org/10.1016/j.wasman.2016.08.004

Khaliq, A., Rhamdhani, M., Brooks, G., & Masood, S. (2014). Metal Extraction Processes for Electronic Waste and Existing Industrial Routes: A Review and Australian Perspective. *Resources*, *3*(1), 152–179. https://doi.org/10.3390/resources3010152

Kim, B., Lee, J., Kim, B., Lee, J., Seo, S., Park, Y., & Sohn, H. Y. (2004). A Process for Extracting Precious Metals from Spent Printed Circuit Boards and Automobile Catalysts A Process for Extracting Precious Metals from Spent Printed Circuit Boards and Automobile Catalysts, (December 2015). https://doi.org/10.1007/s11837-004-0237-9

Kleynhans, E. L. J., Beukes, J. P., Van Zyl, P. G., Bunt, J. R., Nkosi, N. S. B., & Venter, M.

(2017). The Effect of Carbonaceous Reductant Selection on Chromite Pre-reduction. *Metallurgical and Materials Transactions B*, *48*(2), 827–840. https://doi.org/10.1007/s11663-016-0878-4

Legarth, J. B., Alting, L., & Baldo, G. L. (1995). Sustainability issues in circuit board recycling. *Proceedings of the 1995 IEEE International Symposium on Electronics and the Environment ISEE (Cat. No.95CH35718)*, 126–131. https://doi.org/10.1109/ISEE.1995.514963

Li, J., Duan, H., Yu, K., Liu, L., & Wang, S. (2010). Characteristic of low-temperature pyrolysis of printed circuit boards subjected to various atmosphere. *Resources, Conservation and Recycling*, *54*(11), 810–815. https://doi.org/10.1016/j.resconrec.2009.12.011

Lotfian, S., Ahmed, H., El-Geassy, A.-H. A., & Samuelsson, C. (2016). Alternative Reducing Agents in Metallurgical Processes: Gasification of Shredder Residue Material. *Journal of Sustainable Metallurgy*. https://doi.org/10.1007/s40831-016-0096-y

Luda, M. P. (2011). Recycling of Printed Circuit Boards. *Integrated Waste Management - Volume II*, 285–299. https://doi.org/10.5772/17220

Malan, W. T., Akdogan, G., & Bradshaw, S. (2014). *The recovery of platinum group metals from low- grade concentrates to an iron alloy using silicon carbide as reductant*. Stellenbosch University.

Mark, F. E., & Lehner, T. (2000). Plastics Recovery from Waste Electrical & Electronic Equipment in Non-Ferrous Metal Processes. *Technical Paper, Association of Plastics Manufacturers in Europe (APME)*.

Melorose, J., Perroy, R., & Careas, S. (2015). *Rate Processes of Extractive Metallurgy*. *Statewide Agricultural Land Use Baseline 2015* (Vol. 1). https://doi.org/10.1017/CBO9781107415324.004

Monazam, E. R., Breault, R. W., Siriwardane, R., Richards, G., Virginia, W., & Virginia, W. (2013). Kinetics of the reduction of hematite (Fe2O3) by methane (CH4) during chemical looping combustion: a global mechanism. *CHEMICAL ENGINEERING JOURNAL*, 1–28.

Motang, N. (Stellenbosch U. (2015). *In situ FTIR Measurements of the Kinetics of the Aqueous CO 2 - Monoethanolamine Reaction*. Stellenbosch University.

Muniyandi, S., Sohaili, J., Hassan, A., & Mohamad, S. (2013). Converting non-metallic printed

circuit boards waste into a value added product. *Journal of Environmental Health Science and Engineering*, *11*(1), 2. https://doi.org/10.1186/2052-336X-11-2

Naseska, M. (2016). Fourier Transform Infrared Spectroscopy. *University of Ljubljana*, 1–12. https://doi.org/10.1016/B978-0-323-46140-5.00004-2

Ning, C., Lin, C. S. K., Hui, D. C. W., & McKay, G. (2017a). Waste Printed Circuit Board (PCB) Recycling Techniques. *Topics in Current Chemistry*, *375*(2), 43. https://doi.org/10.1007/s41061-017-0118-7

Ning, C., Lin, C. S. K., Hui, D. C. W., & McKay, G. (2017b). Waste Printed Circuit Board (PCB) Recycling Techniques. *Topics in Current Chemistry*, *375*(2), 43. https://doi.org/10.1007/s41061-017-0118-7

Nourreddine, M. (2007). Recycling of auto shredder residue, *139*, 481–490. https://doi.org/10.1016/j.jhazmat.2006.02.054

Ogunniyi, I. O., & Vermaak, M. K. G. (2009). Froth flotation for beneficiation of rinted circuit boards comminution fines : An overview. *Mineral Processing & Extractive Metallurgy Review*, *7508*. https://doi.org/10.1080/08827500802333123

Ortun, N., Conesa, J. A., Molto, J., & Font, R. (2014). Pollutant emissions during pyrolysis and combustion of waste printed circuit boards, before and after metal removal. *Science of the Total Environment*, *499*, 27–35. https://doi.org/10.1016/j.scitotenv.2014.08.039

PlasticsEurope. (2009). Plastics Convert Iron Ore To Steel, 1–8.

Quan, C., Li, A., & Gao, N. (2012). Research on pyrolysis of PCB waste with TG-FTIR and Py-GC/MS. *Journal of Thermal Analysis and Calorimetry*, *110*(3), 1463–1470. https://doi.org/10.1007/s10973-011-2048-x

Quan, C., Li, A., & Gao, N. (2013). Combustion and Pyrolysis of Electronic Waste: Thermogravimetric Analysis and Kinetic Model. *Procedia Environmental Sciences*, *18*, 776–782. https://doi.org/10.1016/j.proenv.2013.04.104

Radebe, N. W. (2017). Coupling of Thermal Field-Flow Fractionation and FTIR Spectroscopy for the Fractionation and Analysis of Complex Polymers by, (December).

Rajagopal, R. R., Rajarao, R., Cholake, S. T., & Sahajwalla, V. (2017). Sustainable composite panels from non-metallic waste printed circuit boards and automotive plastics. *Journal of*

Cleaner Production, *144*, 470–481. https://doi.org/10.1016/j.jclepro.2016.12.139

Rajagopal, R. R., Rajarao, R., & Sahajwalla, V. (2016). High temperature transformations of waste printed circuit boards from computer monitor and CPU: Characterisation of residues and kinetic studies. *Waste Management*, *57*, 91–101. https://doi.org/10.1016/j.wasman.2015.11.016

Rajarao, R., Sahajwalla, V., Cayumil, R., Park, M., & Khanna, R. (2014). Novel Approach for Processing Hazardous Electronic Waste. *Procedia Environmental Sciences*, *21*, 33–41. https://doi.org/10.1016/j.proenv.2014.09.005

Rao, Y. K. (1971). The kinetics of reduction of hematite by carbon. *Metallurgical Transactions*, *2*(5), 1439–1447. https://doi.org/10.1007/BF02913373

Robinson, B. H. (2009). E-waste: An assessment of global production and environmental impacts. *Science of the Total Environment*. Elsevier B.V. https://doi.org/10.1016/j.scitotenv.2009.09.044

Sahajwalla, V., Zaharia, M., Kongkarat, S., Khanna, R., Rahman, M., Saha-Chaudhury, N., … Knights, D. (2012). Recycling end-of-life polymers in an electric arc furnace steelmaking process: Fundamentals of polymer reactions with slag and metal. *Energy and Fuels*, *26*(1), 58–66. https://doi.org/10.1021/ef201175t

Sahajwalla, V., Zaharia, M., Kongkarat, S., Khanna, R., Saha-Chaudhury, N., & O'Kane, P. (2010). Recycling plastics as a resource for electric arc furnace (EAF) steelmaking: Combustion and structural transformations of metallurgical coke and plastic blends. *Energy and Fuels*, *24*(1), 379–391. https://doi.org/10.1021/ef900875r

Schlotz, R., & Uhlig, S. (2006). Introduction to X-Ray Fluorescence (XRF) - Guide To XRF Basics. *Bruker AXS GmbH*, 62.

Sharma, A. K., Sharma, S., Bagdi, U., & Gautam, P. (2017). Copper extraction from the discarded printed circuit board by leaching, *3*(3), 634–637.

Shen, Y., Zhao, R., Wang, J., Chen, X., Ge, X., & Chen, M. (2016). Waste-to-energy: Dehalogenation of plastic-containing wastes. *Waste Management*, *49*, 287–303. https://doi.org/10.1016/j.wasman.2015.12.024

Shuey, S. A., & Taylor, P. (2005). Review of pyrometallurgical treatment of electronic scrap. In *SME Annual Meeting* (pp. 1–4). https://doi.org/10.1007/s11837-004-0237-9

Silvas, F. P. C., Jiménez Correa, M. M., Caldas, M. P. K., de Moraes, V. T., Espinosa, D. C. R., & Tenório, J. A. S. (2015). Printed circuit board recycling: Physical processing and copper extraction by selective leaching. *Waste Management*, *46*, 503–510. https://doi.org/10.1016/j.wasman.2015.08.030

Silvas, F. P. C., Jiménez, M. M., Caldas, M. P. K., Moraes, V. T. De, Espinosa, D. C. R., & Tenório, J. A. S. (2015). Printed circuit board recycling : Physical processing and copper extraction by selective leaching, *46*, 503–510. https://doi.org/10.1016/j.wasman.2015.08.030

Skoog, D. A., Holler, F. J., & Crouch, S. R. (1998). *Principles of Instrumental Analysis Sixth Edition*. *Thompson Brooks/Cole*. https://doi.org/10.1016/S0003-2670(00)84936-3

Sohaili, J., Muniyandi, S. K., & Mohamad, S. S. (2012a). A Review on Printed Circuit Board Recycling Technology. *Journal of Emerging Trends in Engineering and Applied Sciences*, *3*(1), 12–18.

Sohaili, J., Muniyandi, S. K., & Mohamad, S. S. (2012b). A Review on Printed Circuit Board Recycling Technology Corresponding Author : Johan Sohaili, *3*(1), 12–18.

Sohaili, J., Muniyandi, S. K., & Mohamad, S. S. (2012c). A Review on Printed Circuit Boards Waste Recycling Technologies and Reuse of Recovered Nonmetallic Materials. *International Journal Os Scientific & Engineering Research*, *3*(2), 1–7.

Sohn, I., & Fruehan, R. J. (2005). The reduction of iron oxides by volatiles in a rotary hearth furnace process: Part I. The role and kinetics of volatile reduction. *Metallurgical and Materials Transactions B: Process Metallurgy and Materials Processing Science*, *36*(5), 605–612. https://doi.org/10.1007/s11663-005-0051-y

Speight, J. G. (2005). *Handbook of Coal Analysis*. (J. D. Winefordner, Ed.). New Jersy: John Wiley & Sons, Inc. https://doi.org/10.1002/0471718513

Speyer, R. F. (Georgia I. of T. (1994). *Thermal Analysis of Materials*. *MARCEL DEKKER, INC*. NewYork.

Stewart, E. S., & Lemieux, P. M. (2003). Emissions from the incineration of electronics industry waste. *IEEE International Symposium on Electronics and the Environment, 2003.* https://doi.org/10.1109/ISEE.2003.1208088

Stokes, D. (2008). *Principles and Practice of Variable Pressure / Environmental Scanning*

Electron Microscopy (VP-ESEM). https://doi.org/10.1002/9780470758731

United States Environmental Protection Agency. (2012). Printed Circuit Board Recycling Methods. *Workshop Materials on WEEE Management in Taiwan*, *27*(October), 33–42.

Vasile, C., Brebu, M. A., Karayildirim, T., Yanik, J., & Darie, H. (2006). Feedstock recycling from plastic and thermoset fractions of used computers (I): Pyrolysis. *Journal of Material Cycles and Waste Management*, *8*(2), 99–108. https://doi.org/10.1007/s10163-006-0151-z

Verma, H. R. (1956). *Atomic and Nuclear Analytical Methods*. *Nuclear Physics*. https://doi.org/10.1016/0029-5582(56)90014-1

Wang, X., Guo, Y., Liu, J., Qiao, Q., & Liang, J. (2010). PVC-based composite material containing recycled non-metallic printed circuit board (PCB) powders. *Journal of Environmental Management*, *91*(12), 2505–2510. https://doi.org/10.1016/j.jenvman.2010.07.014

Wang, Z., Li, G., Sun, Y., & He, M. (2016). Reduction behavior of hematite in the presence of coke, *23*(11), 1244–1251. https://doi.org/10.1007/s12613-016-1345-6

Widmer, R., Oswald-krapf, H., Sinha-khetriwal, D., Schnellmann, M., & Bo, H. (2005). Global perspectives on e-waste, *25*, 436–458. https://doi.org/10.1016/j.eiar.2005.04.001

Xiang, D., Mou, P., Wang, J., Duan, G., & Zhang, H. C. (2007). Printed circuit board recycling process and its environmental impact assessment. *International Journal of Advanced Manufacturing Technology*, *34*(9–10), 1030–1036. https://doi.org/10.1007/s00170-006-0656-6

Xiang, Y., Wu, P., Zhu, N., Zhang, T., Liu, W., Wu, J., & Li, P. (2010). Bioleaching of copper from waste printed circuit boards by bacterial consortium enriched from acid mine drainage. *Journal of Hazardous Materials*, *184*(1–3), 812–818. https://doi.org/10.1016/j.jhazmat.2010.08.113

Yamane, L. H., de Moraes, V. T., Espinosa, D. C. R., & Tenório, J. A. S. (2011). Recycling of WEEE: Characterization of spent printed circuit boards from mobile phones and computers. *Waste Management*, *31*(12), 2553–2558. https://doi.org/10.1016/j.wasman.2011.07.006

Yang, X., Sun, L., Xiang, J., Hu, S., & Su, S. (2013). Pyrolysis and dehalogenation of plastics

from waste electrical and electronic equipment (WEEE): A review. *Waste Management*, *33*(2), 462–473. https://doi.org/10.1016/j.wasman.2012.07.025

Yokoyama, S., & Iji, M. (1997). Recycling of printed wiring boards with mounted electronic parts. *Proceedings of the 1997 IEEE International Symposium on Electronics and the Environment. ISEE-1997*, 109–114. https://doi.org/10.1109/ISEE.1997.605282

Zhang, C., Chen, S., Miao, X., & Yuan, H. (2009). Reduction experiment of iron scale by adding waste plastics. *Journal of Environmental Sciences*, *21*(SUPPL. 1), 48–51. https://doi.org/10.1016/S1001-0742(09)60035-8

Zhang, Y., Liu, S., Xie, H., Zeng, X., & Li, J. (2012). Current status on leaching precious metals from waste printed circuit boards, *16*, 560–568. https://doi.org/10.1016/j.proenv.2012.10.077

Zhang, Z., Zhao, X., Kown, E., & Calstaldi, M. J. (2010). Experimental Research on Microwave Induced Thermal Decomposition of Printed Circuit Board Wastes. In *Proceedings of the 18th Annual North American Waste-to-Energy Conference, NAWTEC18* (Vol. 7, pp. 1–7). Orlando, Florida: ASME.

Zhao, M., Zhao, C., Yu, L., Li, G., Huang, J., Zhu, H., & He, W. (2016). Prediction and analysis of WEEE in China based on the gray model. *Procedia Environmental Sciences*, *31*, 925–934. https://doi.org/10.1016/j.proenv.2016.02.113

Zhou, W., Apkarian, R. P., & Wang, Z. L. (2006). Fundamentals of Scanning Electron Microscopy. In *Fundamentals of scanning electron microscopy* (pp. 1–40). NewYork: Springer. https://doi.org/10.1007/978-0-387-39620-0_1

Zie, A., & Stanek, W. (2001). Forecasting of the energy effects of injecting plastic wastes into the blast furnace in comparison with other auxiliary fuels, *26*, 1159–1173.

Zietsman, J. H., Steyn, A., & Pretorius, W. (2018). Evaluating Pre-treatment and Smelting Options with EMSIM to Improve Production Efficiency, (February), 25–28.

Appendices

Appendix A. EMSIM Simulations

Appendix A.1 Creating EMSIM Models

In order to create the mass and energy balance models using EMSIM, the following steps are performed;

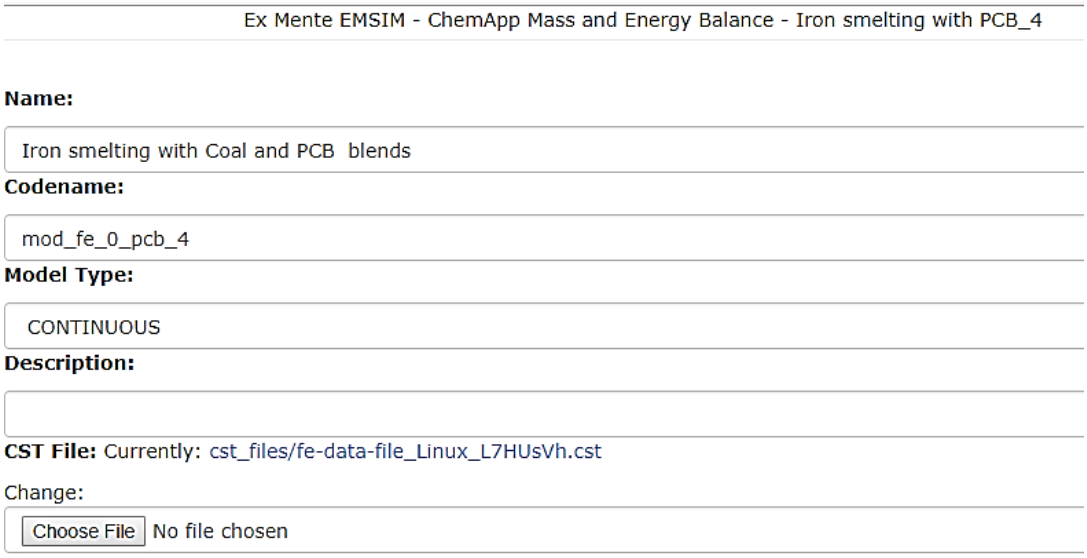

Figure A.1: Creating a new model

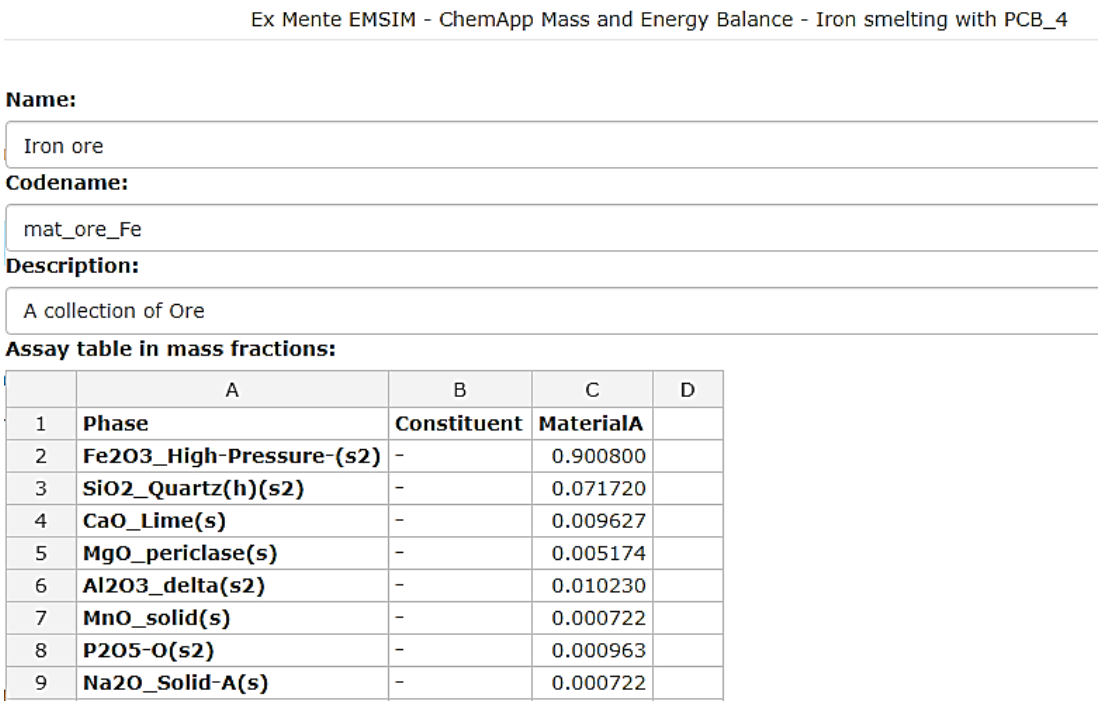

	A	B	C	D
1	**Phase**	**Constituent**	**MaterialA**	
2	**Fe2O3_High-Pressure-(s2)**	-	0.900800	
3	**SiO2_Quartz(h)(s2)**	-	0.071720	
4	**CaO_Lime(s)**	-	0.009627	
5	**MgO_periclase(s)**	-	0.005174	
6	**Al2O3_delta(s2)**	-	0.010230	
7	**MnO_solid(s)**	-	0.000722	
8	**P2O5-O(s2)**	-	0.000963	
9	**Na2O_Solid-A(s)**	-	0.000722	

Figure A.2: Composition of Iron ore

Name:

Reductant

Codename:

mat_red

Description:

PCB and other reductants

Assay table in mass fractions:

	A	B	C	D	E	F
1	**Assay Names**			**PCB**	**Coal1**	
2	**Proximate Assay**					
3	**Component**	**Basis**	**Units**			
4	Inherent moisture content	air-dried	mass %	3.600000	1.600000	
5	Ash content	air-dried	mass %	40.100000	11.700000	
6	Volatile matter content	air-dried	mass %	44.800000	5.100000	
7	Fixed carbon content	air-dried	mass %	11.500000	81.600000	
8	**Ultimate Assay**					
9	**Component**	**Basis**	**Units**			
10	C	air-dried	mass %	28.500000	80.100000	
11	H	air-dried	mass %	3.060000	2.290000	
12	O	air-dried	mass %	23.100000	2.120000	
13	N	air-dried	mass %	1.100000	1.450000	
14	**Forms of Sulphur Assay**					
15	**Component**	**Basis**	**Units**			
16	Pyritical S	air-dried	mass %	0.000000	0.000000	
17	Sulphatic S	air-dried	mass %	0.540000	0.740000	
18	Organic S	air-dried	mass %	0.000000	0.000000	
19	**Energy Content**					
20	**Parameter**	**Basis**	**Units**			
21	Gross Calorific Value	air-dried	MJ/kg	12.080000	30.490000	
22	**Ash Composition Assay**					
23	**Phase**	**Constituent**	**Units**			
24	SiO2_Quartz(l)(s)	-	mass %	84.000000	55.600000	
25	Al2O3_gamma(s)	-	mass %	6.280000	28.580000	

Figure A.3: Composition of Reducing agents

Ex Mente EMSIM - ChemApp Mass and Energy Balance - Iron smelting with PCB_4

Name:

Ambient Conditions

Codename:

pg_amb

Description:

This group contains parameters to describe ambient conditions relevant to the process described by the model.

Parameters (+ create a parameter)

Name	Codename	Default	Units	Calculation	Description	Actions
Pressure	pr_amb_P	1.0	atm	None	Ambient pressure.	
Temperature	pr_amb_T	25.0	°C	None	Ambient temperature.	

Figure A.4: Ambient parameters

Name:

Smelting Conditions

Codename:

pg_sml

Description:

Parameters (✚ create a parameter)

Name	Codename	Default	Units	Calculation	Description	Actions
Alloy Output Temperature	pr_sml_T_all	1600.0	°C	None		
Carbon Efficiency	pr_sml_y_c	0.85	g/g	None		
Dust loss	pr_sml_y_dst	0.03	g/g	None	The mass fraction ...	
Flux Feed Rate	pr_sml_q_flx	150.0	kg/h	None		
Gas Output Temperature	pr_sml_T_gas	850.0	kg/h	None		
Heat Loss	pr_sml_q_hls	500.0	kW	None	Heat loss from the...	
Ore Feed Rate	pr_sml_q_ore	1000.0	kg/h	None		
Reductant Feed Rate	pr_sml_q_red	300.0	kg/h	None		
Temperature	pr_sml_T	1700.0	kg/h	None	The temperature at...	

Figure A.5: Smelting conditions

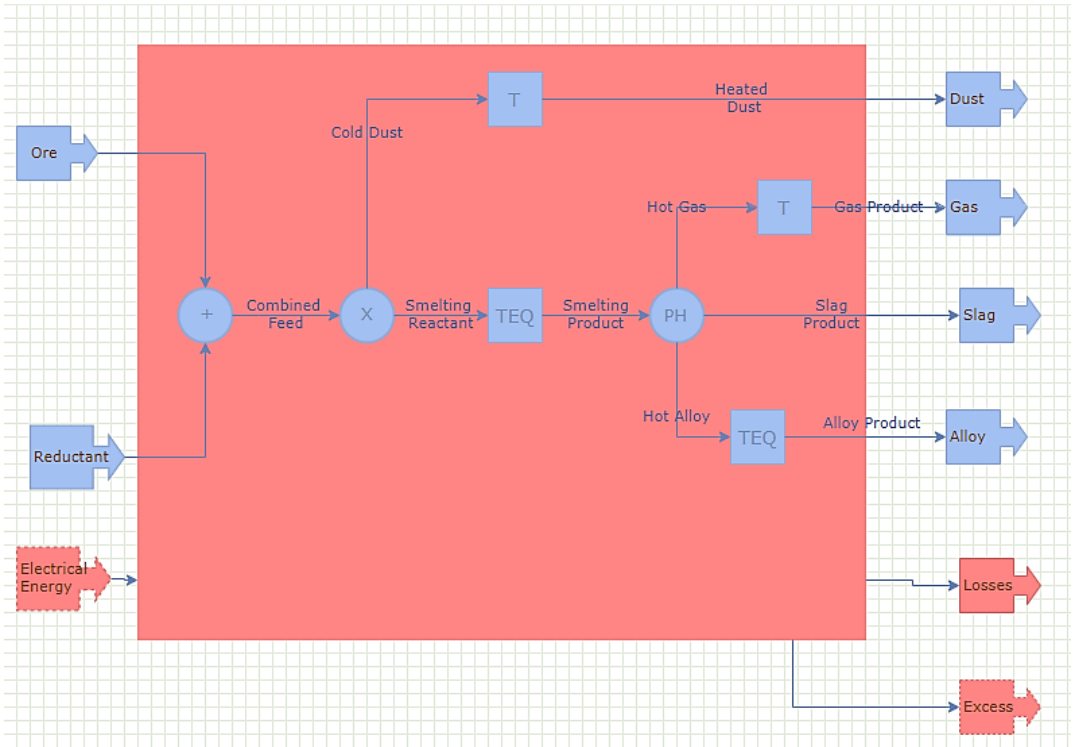

Figure A.6: Flowsheet for smelting operation

Energy nodes use a red colour, and material nodes and streams are shown in blue.

Table A.1: Energy Nodes for EMSIM flow sheet components

	Name	Description
	Input	This node brings a user-specified quantity of energy into the system.
	Output	This node removes a user-specified quantity of energy from the system.
	Energy Balance	This node calculates the system's energy balance.
	Energy Deficit	The energy balance associates an energy deficit with this node. An example would be the electrical energy required by a smelting furnace.
	Energy Excess	The energy balance associates an energy excess with this. An example would be energy released by an aluminothermic reaction.

Table A.2: Material Nodes for EMSIM flow sheet components

	Name	Description
	Input	This node brings a user-specified quantity of a specified material and specified composition into the system.
	Output	This node removes a user-specified quantity of material from the system.
	Combiner	This node combines two or more nodes into one.
	Fraction Splitter	This node splits a single input stream into two or more output streams based on user-specified fractions of phases and phase constituents.
	Phase Splitter	This node splits a single input stream into two or more output streams based on user-specified phase associations with the output streams.
	Temperature Setter	This node sets the temperature of a stream to a user-specified value.
	Isothermal Equilibrium	This node equilibrates a stream at a user-specified temperature.

Appendix A.2 EMSIM Simulations for Iron Smelting

Figure A.7 to Figure A.10 shows the metal recovery and the energy require for the smelting of iron different temperatures. The results follow similar pattern as reduction at 1700℃.

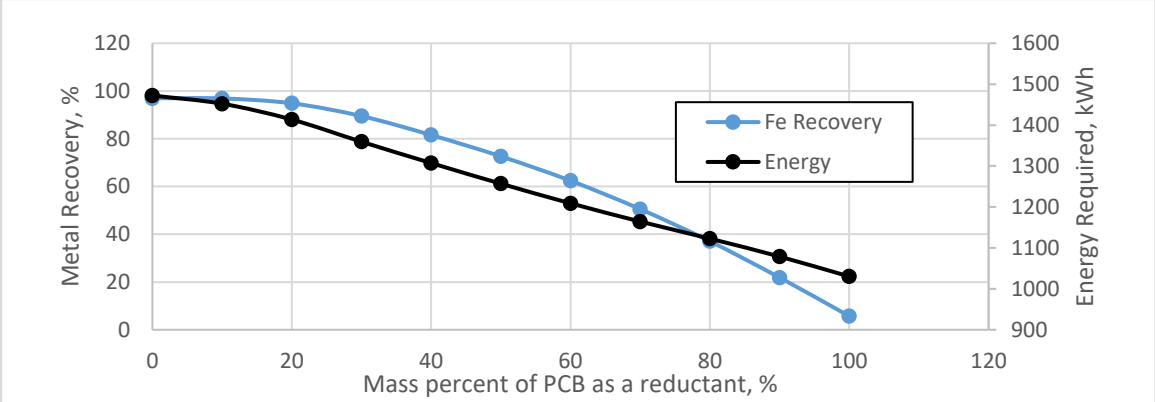

Figure A.7: Metal recovery and energy required for iron reduction at 1200℃

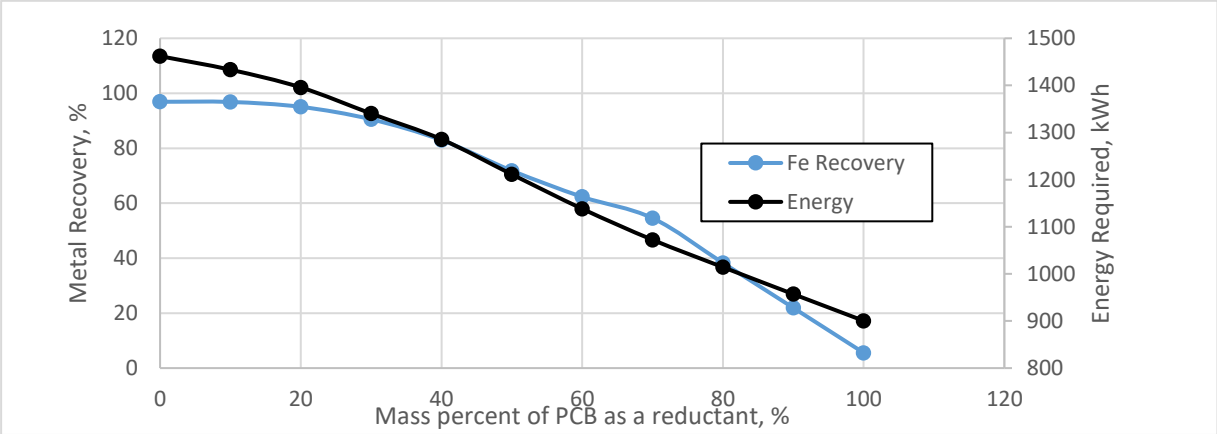

Figure A.8: Metal recovery and energy required for iron reduction at 1100℃

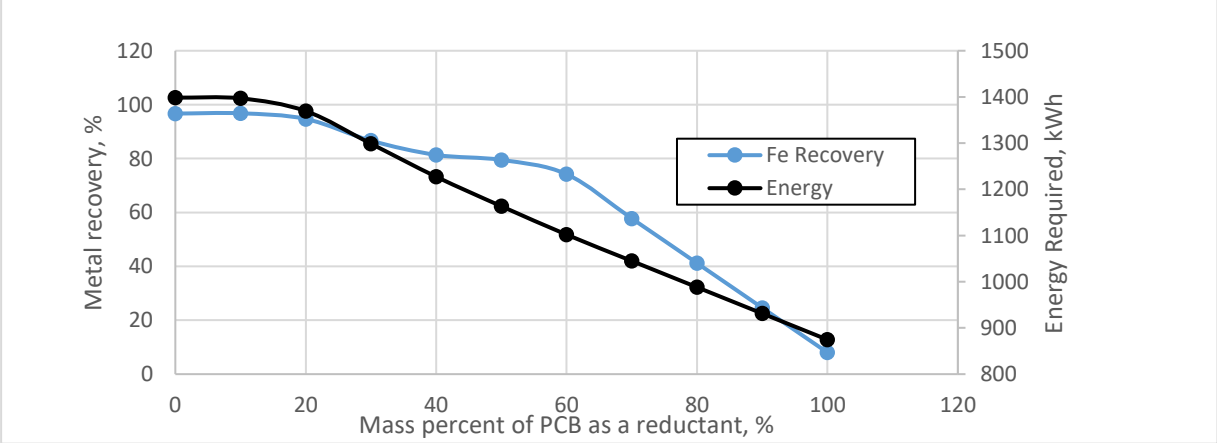

Figure A.9: Metal recovery and energy required for iron reduction at 1000℃

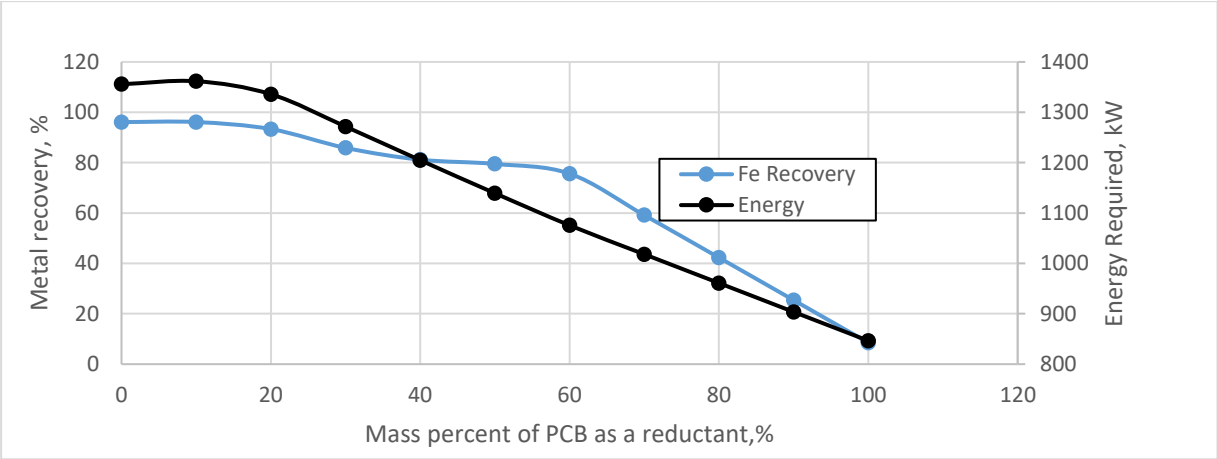

Figure A.10: Metal recovery and energy required for iron reduction at 900°C

During the smelting of iron at lower temperatures between 900°C and 1200°C, EMSIM revealed a decrease in the alloy content as well as the gas produced as the mass percent of PCB increases in the blend. In addition, higher mass of spinel is produced at low temperatures.

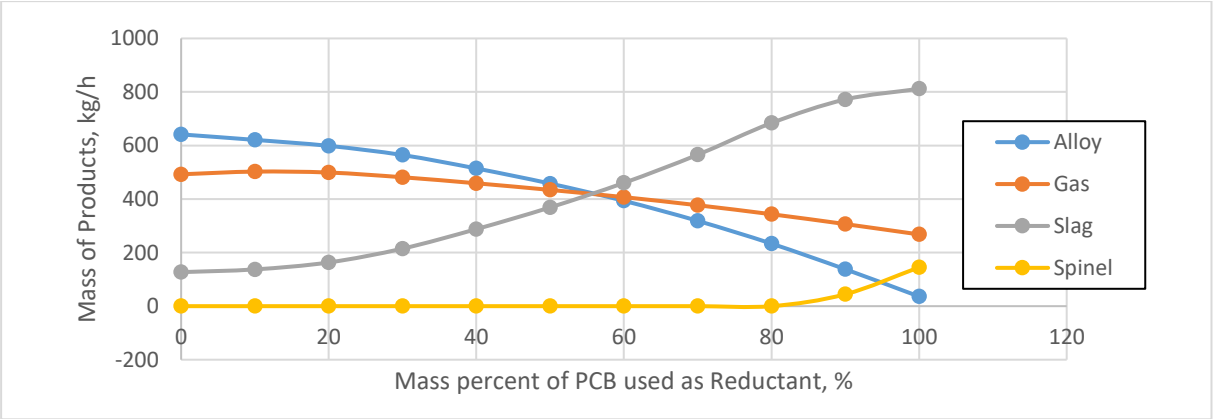

Figure A.11: Products of iron reduction at 1200°C

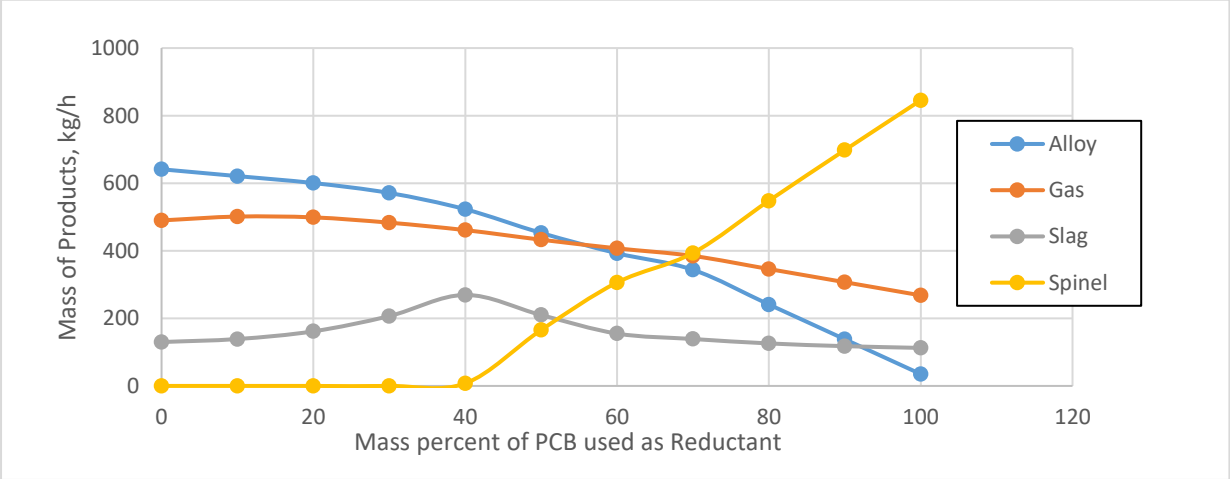

Figure A.12: Products of iron reduction at 1100°C

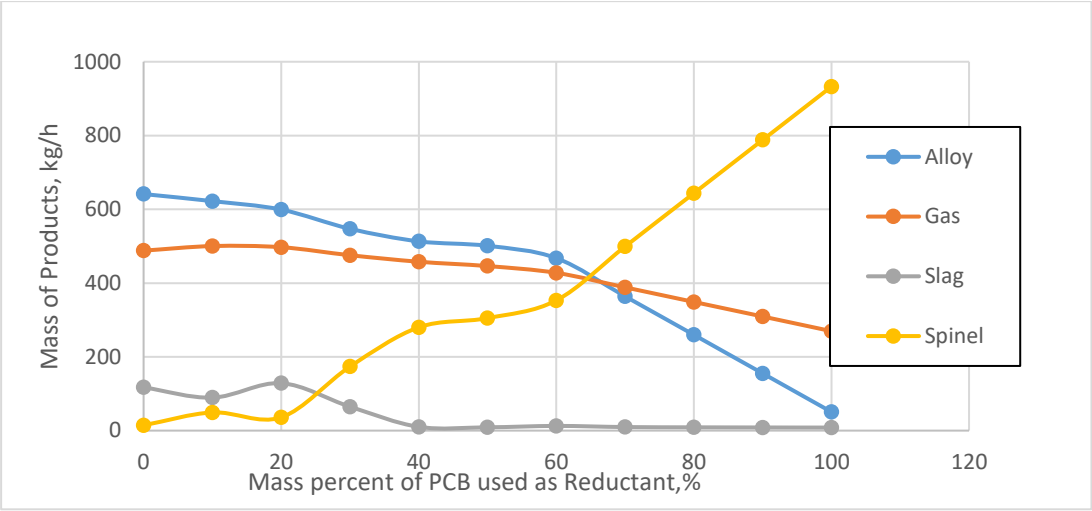

Figure A.13: Products of iron reduction at 1000°C

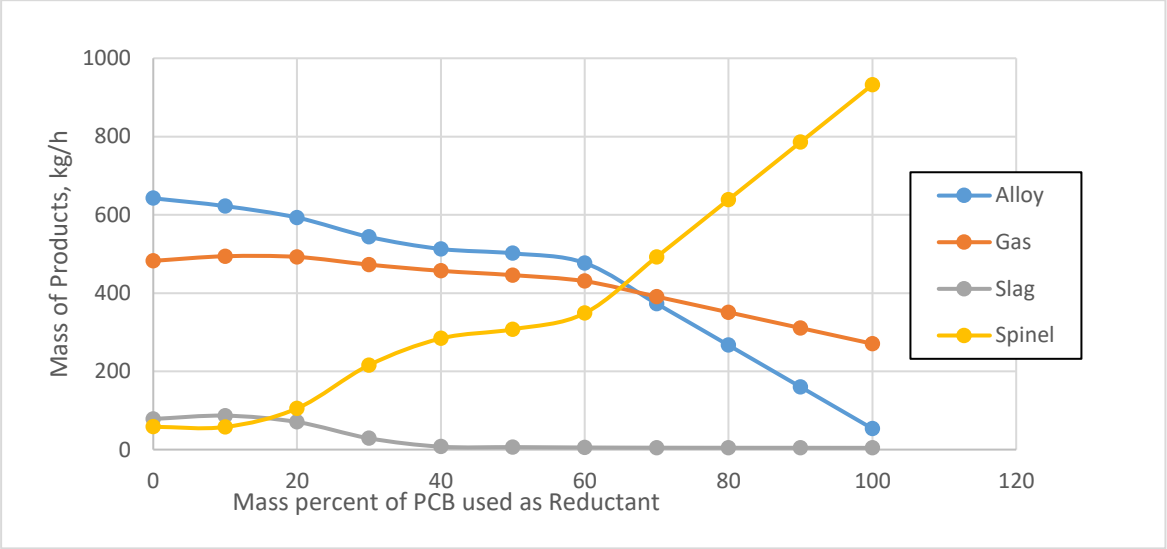

Figure A.14: Products of iron reduction at 900°C

EMSIM simulations revealed that at lower temperature, the mass flow rate of CO_2 also increases as PCB in the blend increases. The flow rate of CO, however, decreases as the mass of PCB in the blend increases.

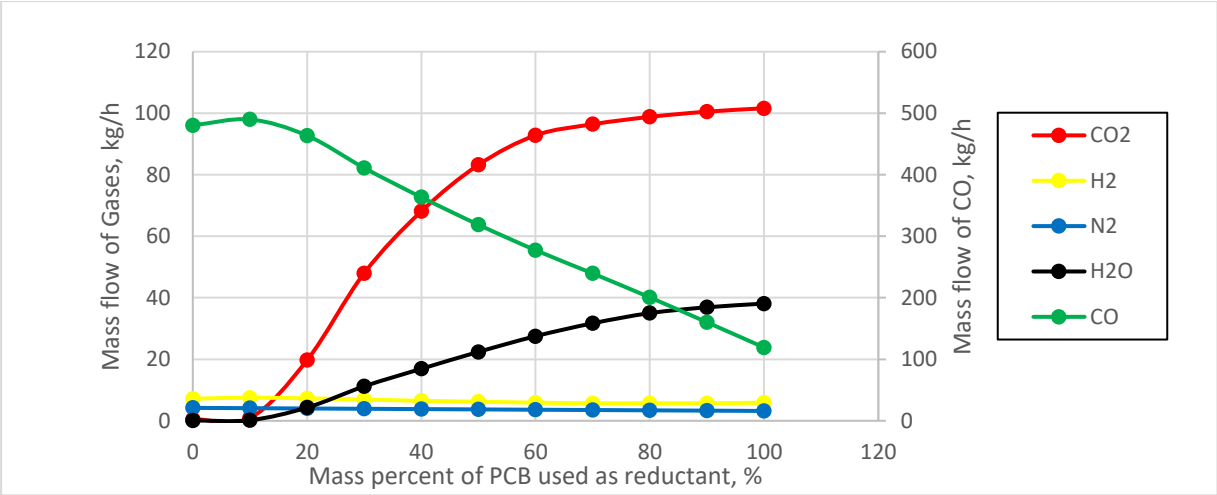

Figure A.15: Mass flowrate of gases during iron reduction at 1200°C

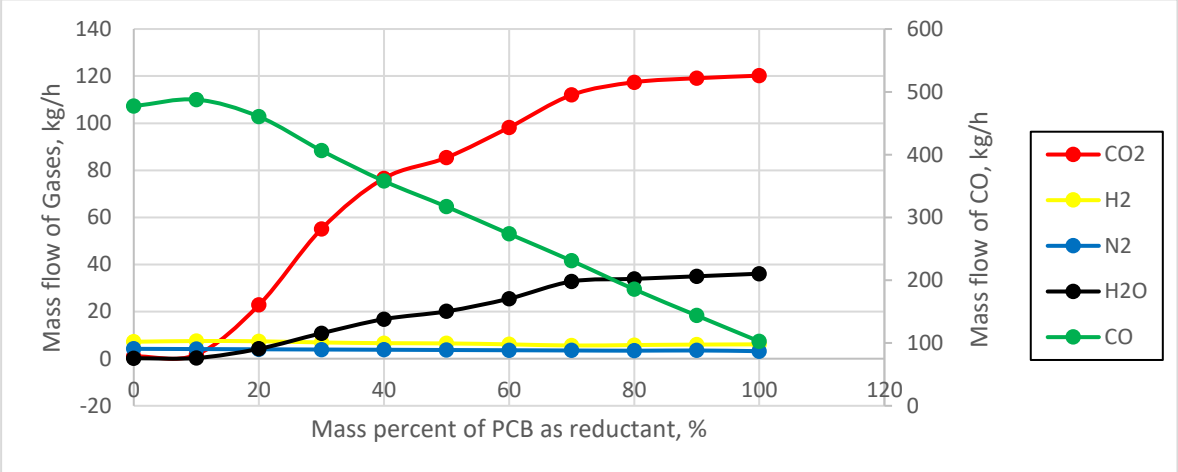

Figure A.16: Mass flowrate of gases during iron reduction at 1100°C

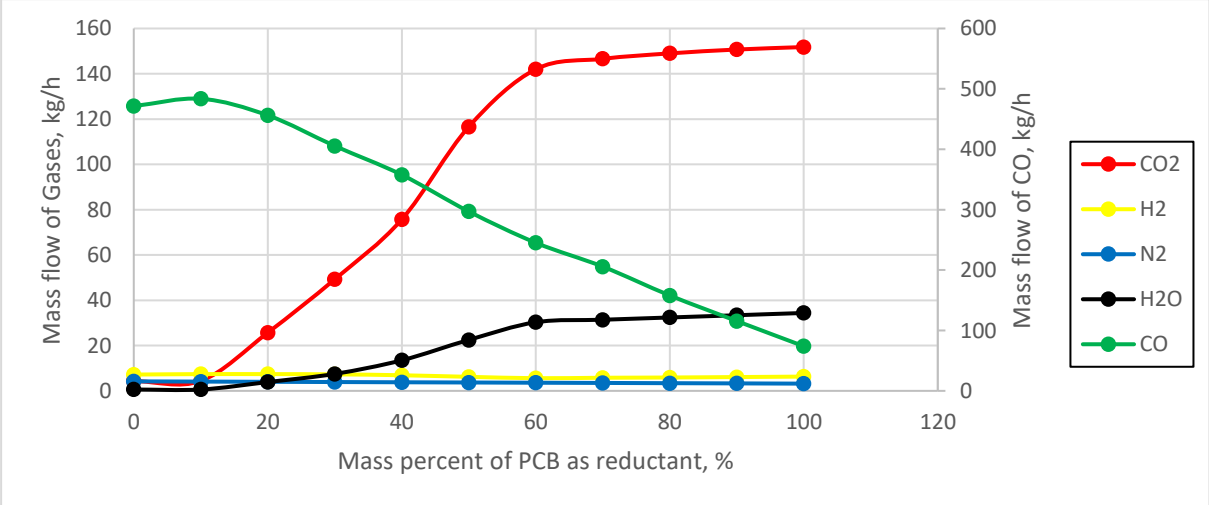

Figure A.17: Mass flowrate of gases during iron reduction at 1000°C

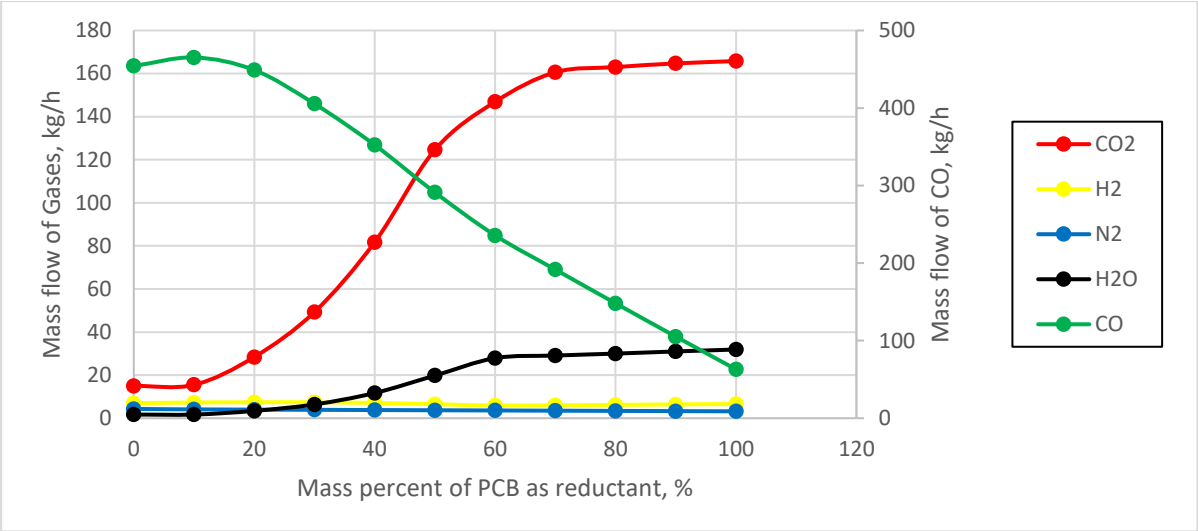

Figure A.18: Mass flowrate of gases during iron reduction at 900°C

Table A.3 and Table A.9 shows the mass and energy balance of the chromite smelting. It can be observed that in each of the smelting simulations the mass input is equal to the mass output. Table A.4 to Table A.8 and Table A.140 to Table A.14 shows the mass balance and energy balance respectively during the reduction of iron at different temperatures when blends of coal and PCB were used as reducing agents.

The energy balance was calculated using Equation A.1

$$Electrical\ Energy = \left[H_{f(alloy)} + H_{f(slag)} + H_{f(gas)} + H_{f(dust)} + heat\ lost\right] - \left[H_{f(ore)} + H_{f(reductant)}\right] \quad \text{Equation A.1}$$

Where $H_{f(x)}$ = the enthalpy of formation of x

It can be observed that as PCB in the blend increases, the mass flowrate of the alloy product decreases resulting in a decrease in enthalpy of formation of the alloy product. The slag products however increases as PCB in the blend increases. Since the enthalpy of formation of the slag is negative, the overall enthalpy of formation of the slag products increases in the negative direction as PCB increases in the blend. This results in a decrease in the amount of energy required for the smelting process.

Table A.3: Mass balance for chromite smelting

Stream	T, ℃	Mass flow rate, kg/h Mass percent of PCB in blend										
		0	**10**	**20**	**30**	**40**	**50**	**60**	**70**	**80**	**90**	**100**
Ore Feed	25.0	1,000.0	1,000.0	1,000.0	1,000.0	1,000.0	1,000.0	1,000.0	1,000.0	1,000.0	1,000.0	1,000.0
Reductant Feed	25.0	300.0	300.0	300.0	300.0	300.0	300.0	300.0	300.0	300.0	300.0	300.0
Total		1,300.0	1,300.0	1,300.0	1,300.0	1,300.0	1,300.0	1,300.0	1,300.0	1,300.0	1,300.0	1,300.0
Alloy Product	1,600.0	564.0	564.0	525.3	495.6	450.2	393.9	332.9	270.9	211.4	152.7	91.4
Dust Output	850.0	39.0	39.0	39.0	39.0	39.0	39.0	39.0	39.0	39.0	39.0	39.0
Gas Output	850.0	463.8	449.0	429.5	414.0	397.1	374.1	346.5	315.1	282.5	250.5	219.7
Slag Product	1,700.0	233.2	265.2	306.2	351.3	413.7	493.0	581.7	675.0	767.1	857.8	949.9
Total		1,300.0	1,300.0	1,300.0	1,300.0	1,300.0	1,300.0	1,300.0	1,300.0	1,300.0	1,300.0	1,300.0
Balance		0.0	0.0	0.0	0.0	0.0	0.0	0.0	0.0	0.0	0.0	0.0

Table A.4: Mass balance for Iron smelting at 1700℃

Stream	T, ℃	Mass flow rate, kg/h Mass percent of PCB in blend,%										
		0	**10**	**20**	**30**	**40**	**50**	**60**	**70**	**80**	**90**	**100**
Ore Feed	25.0	1,000.0	1,000.0	1,000.0	1,000.0	1,000.0	1,000.0	1,000.0	1,000.0	1,000.0	1,000.0	1,000.0
Reductant Feed	25.0	300.0	300.0	300.0	300.0	300.0	300.0	300.0	300.0	300.0	300.0	300.0
Total		1,300.0	1,300.0	1,300.0	1,300.0	1,300.0	1,300.0	1,300.0	1,300.0	1,300.0	1,300.0	1,300.0
Alloy Product	1,600.0	644.8	621.0	592.4	544.4	482.6	411.7	332.3	246.7	157.3	65.8	0.0
Dust Output	850.0	39.0	39.0	39.0	39.0	39.0	39.0	39.0	39.0	39.0	39.0	39.0
Gas Output	850.0	553.7	525.1	499.0	476.5	450.4	421.7	390.3	356.9	322.2	286.8	258.6
Slag Product	1,700.0	62.4	114.9	169.7	240.1	328.0	427.6	538.4	657.5	781.5	908.4	1,002.4

Total	1,300.0	1,300.0	1,300.0	1,300.0	1,300.0	1,300.0	1,300.0	1,300.0	1,300.0	1,300.0	1,300.0
Balance	0.0	0.0	0.0	0.0	0.0	0.0	0.0	0.0	0.0	0.0	0.0

Table A.5: Mass balance iron reduction at 1200°C

Stream	**T, °C**	**Mass flow rate, kg/h**										
		Mass percent of PCB in blend										
		0	**10**	**20**	**30**	**40**	**50**	**60**	**70**	**80**	**90**	**100**
Ore Feed	25.0	1,000.0	1,000.0	1,000.0	1,000.0	1,000.0	1,000.0	1,000.0	1,000.0	1,000.0	1,000.0	1,000.0
Reductant Feed	25.0	300.0	300.0	300.0	300.0	300.0	300.0	300.0	300.0	300.0	300.0	300.0
Total		1,300.0	1,300.0	1,300.0	1,300.0	1,300.0	1,300.0	1,300.0	1,300.0	1,300.0	1,300.0	1,300.0
Alloy Product	1,600.0	641.5	621.1	598.7	564.5	514.3	457.9	393.4	318.5	233.5	137.9	36.1
Dust Output	850.0	39.0	39.0	39.0	39.0	39.0	39.0	39.0	39.0	39.0	39.0	39.0
Gas Output	850.0	492.5	502.6	499.1	481.5	458.9	434.2	407.2	376.9	343.4	306.6	267.9
Slag Product	1,700.0	127.0	137.3	163.3	214.9	287.8	368.9	460.4	565.6	684.0	816.5	957.0
Total		1,300.0	1,300.0	1,300.0	1,300.0	1,300.0	1,300.0	1,300.0	1,300.0	1,300.0	1,300.0	1,300.0
Balance		0.0	0.0	0.0	0.0	0.0	0.0	0.0	0.0	0.0	0.0	0.0

Table A.6: Mass balance iron reduction at 1100°C

Stream	**T, °C**	**Mass flow rate, kg/h**										
		Mass percent of PCB in blend										
		0	**10**	**20**	**30**	**40**	**50**	**60**	**70**	**80**	**90**	**100**
Ore Feed	25.0	1,000.0	1,000.0	1,000.0	1,000.0	1,000.0	1,000.0	1,000.0	1,000.0	1,000.0	1,000.0	1,000.0
Reductant Feed	25.0	300.0	300.0	300.0	300.0	300.0	300.0	300.0	300.0	300.0	300.0	300.0
Total		1,300.0	1,300.0	1,300.0	1,300.0	1,300.0	1,300.0	1,300.0	1,300.0	1,300.0	1,300.0	1,300.0
Alloy Product	1,600.0	641.2	621.0	600.5	571.1	523.0	452.8	392.7	343.7	241.1	138.2	35.1
Dust Output	850.0	39.0	39.0	39.0	39.0	39.0	39.0	39.0	39.0	39.0	39.0	39.0
Gas Output	850.0	489.9	501.2	498.9	483.2	461.2	432.8	407.2	384.8	346.0	307.1	268.1

Slag Product	1,700.0	129.9	138.8	161.6	206.7	276.8	375.5	461.1	532.4	673.9	815.7	957.8
Total		1,300.0	1,300.0	1,300.0	1,300.0	1,300.0	1,300.0	1,300.0	1,300.0	1,300.0	1,300.0	1,300.0
Balance		0.0	0.0	0.0	0.0	0.0	0.0	0.0	0.0	0.0	0.0	0.0

Table A.7: Mass balance iron reduction at 1000°C

Stream	**T, °C**	**Mass flow rate, kg/h**										
		Mass percent of PCB in blend										
		0	**10**	**20**	**30**	**40**	**50**	**60**	**70**	**80**	**90**	**100**
Ore Feed	25.0	1,000.0	1,000.0	1,000.0	1,000.0	1,000.0	1,000.0	1,000.0	1,000.0	1,000.0	1,000.0	1,000.0
Reductant Feed	25.0	300.0	300.0	300.0	300.0	300.0	300.0	300.0	300.0	300.0	300.0	300.0
Total		1,300.0	1,300.0	1,300	1,300.0	1,300.0	1,300.0	1,300.0	1,300.0	1,300.0	1,300.0	1,300.0
Alloy Product	1,600.0	641.3	622.1	599.2	547.2	513.1	501.0	467.6	363.9	259.6	155.1	269.6
Dust Output	850.0	39.0	39.0	39.0	39.0	39.0	39.0	39.0	39.0	39.0	39.0	39.0
Gas Output	850.0	487.9	500.3	497.2	475.5	457.8	446.1	427.7	388.4	348.8	309.3	269.6
Slag Product	1,700.0	131.8	138.6	164.6	238.3	290.1	313.9	365.7	508.7	652.6	796.6	940.8
Total		1,300.0	1,300.0	1,300.0	1,300.0	1,300.0	1,300.0	1,300.0	1,300.0	1,300.0	1,300.0	1,300.0
Balance		0.0	0.0	0.0	0.0	0.0	0.0	0.0	0.0	0.0	0.0	0.0

Table A.8: Mass balance iron reduction at 900°C

Stream	**T, °C**	**Mass flow rate, kg/h**										
		Mass percent of PCB in blend										
		0	**10**	**20**	**30**	**40**	**50**	**60**	**70**	**80**	**90**	**100**
Ore Feed	25.0	1,000.0	1,000.0	1,000.0	1,000.0	1,000.0	1,000.0	1,000.0	1,000.0	1,000.0	1,000.0	1,000.0
Reductant Feed	25.0	300.0	300.0	300.0	300.0	300.0	300.0	300.0	300.0	300.0	300.0	300.0
Total		1,300.0	1,300.0	1,300	1,300.0	1,300.0	1,300.0	1,300.0	1,300.0	1,300.0	1,300.0	1,300.0
Alloy Product	1,600.0	642.1	622.2	592.9	543.6	512.7	501.5	476.9	372.9	266.7	160.2	53.6
Dust Output	850.0	39.0	39.0	39.0	39.0	39.0	39.0	39.0	39.0	39.0	39.0	39.0

Gas Output	850.0	482.3	494.1	492.3	472.6	456.8	448.8	430.3	390.9	350.8	310.7	270.5
Slag Product	1,700.0	136.5	144.6	175.8	244.7	291.5	313.8	353.8	497.2	643.5	790.1	936.9
Total		1,300.0	1,300.0	1,300.0	1,300.0	1,300.0	1,300.0	1,300.0	1,300.0	1,300.0	1,300.0	1,300.0
Balance		0.0	0.0	0.0	0.0	0.0	0.0	0.0	0.0	0.0	0.0	0.0

Table A.9: Energy balance for chromite smelting

Stream	**T, °C**	**Energy, kWh** **Mass percent of PCB in blend,%**										
		0	**10**	**20**	**30**	**40**	**50**	**60**	**70**	**80**	**90**	**100**
Ore Feed	25.0	-2,539.8	-2,539.8	-2,539.8	-2,539.8	-2,539.8	-2,539.8	-2,539.8	-2,539.8	-2,539.8	-2,539.8	-2,539.8
Reductant Feed	25.0	-110.5	-169.5	-228.5	-287.5.5	-346.6	-405.6	-464.6	-523.6	-582.7	-641.7	-700.7
Electrical Energy		2,124.7	2,042.1	1,966.5	1,915.8	1,864.2	1,799.1	1,723.0	1,636.5	1,541.7	1,449.1	1,368.1
Total		-525.5	-667.2	-801.8	-911.5	-1,022.1	-1,146.3	-1,281.4	-1,426.9	-1,580.8	-1,732.3	-1,872.4
Alloy Product	1,600.0	260.4	232.9	214.5	196.8	173.5	147.7	122.4	99.2	78.1	56.9	34.2
Dust Output	850.0	-69.8	-71.6	-73.4	-75.2	-77.0	-78.8	-80.6	-82.4	-84.2	-86.0	-87.8
Gas Output	850.0	-310.2	-319.9	-317.8	-307.8	-294.7	- 275.8	-252.7	-227.5	-203.9	-185.8	-173.3
Slag Product	1,700.0	-905.9	-1,008.6	-1,125.1	-1,225.3	-1,323.9	-1,439.4	-1,570.5	-1,716.3	-1,870.8	-2,017.4	-2,145.4
Heat loss*		500.0	500.0	500	500	500	500.0	500.0	500.0	500.0	500.0	500.0
Total		-525.5	-667.2	-801.8	-911.5	-1,022.1	-1,146.3	-1,281.4	-1,426.9	-1,580.8	-1,732.3	-1,872.4
Balance		0.0	0.0	0.0	0.0	0.0	0.0	0.0	0.0	0.0	0.0	0.0

Assumed Heat loss* is 500kWh

Table A.10: Energy balance for iron smelting at 1700°C

Stream	T, °C	Energy, kWh Mass percent of PCB in blend,%										
		0	**10**	**20**	**30**	**40**	**50**	**60**	**70**	**80**	**90**	**100**
Ore Feed	25.0	-1,580.1	-1,580.1	-1,580.1	-1,580.1	-1,580.1	-1,580.1	-1,580.1	-1,580.1	-1,580.1	-1,580.1	-1,580.1
Reductant Feed	25.0	-110.5	-169.5	-228.5	-287.5	-346.6	-405.6	-464.6	-523.6	-582.7	-641.7	-700.7
Electrical Energy		1,721.1	1,627.8	1,549.7	1,498.0	1,449.7	1,404.5	1,362.1	1,321.7	1,282.5	1,243.8	1,199.8
Total		30.5	-121.8	-259.0	-369.7	-477.0	-581.2	-682.7	-782.1	-880.3	-978.0	-1,081.0
Alloy Product	1,600.0	216.8	222.6	221.2	203.4	180.2	153.7	123.9	91.9	58.5	24.5	0.0
Dust Output	850.0	-40.9	-42.7	-44.5	-46.3	-48.1	-49.8	-51.6	-53.4	-55.2	-57.0	-58.8
Gas Output	850.0	-428.0	-407.6	-412.8	-437.5	-446.0	-442.6	-427.6	-403.6	-374.2	-341.5	-339.9
Slag Product	1,700.0	-217.5	-394.2	-522.9	-589.3	-663.1	-742.4	-827.4	-916.9	-1,009.5	-1,104.0	-1,182.3
Heat Loss*		500.0	500.0	500.0	500.0	500.0	500.0	500.0	500.0	500.0	500.0	500
Total		30.5	-121.8	-259.0	-369.7	-477.0	-581.2	-682.7	-782.1	-880.3	-978.0	-1,081.0
Balance		0.0	0.0	0.0	0.0	0.0	0.0	0.0	0.0	0.0	0.0	0.0

Table A.11: Energy balance iron reduction at 1200°C

Stream	T, °C	Energy, kWh Mass percent of PCB in blend,%										
		0	**10**	**20**	**30**	**40**	**50**	**60**	**70**	**80**	**90**	**100**
Ore Feed	25.0	-1,580.1	-1,580.1	-1,580.1	-1,580.1	-1,580.1	-1,580.1	-1,580.1	-1,580.1	-1,580.1	-1,580.1	-1,580.1
Reductant Feed	25.0	-110.1	-169.1	-228.2	-287.2	-346.2	-405.3	-464.3	-523.3	-582.4	-641.4	-700.5
Electrical Energy		1,450.2	1,452.3	1,413.6	1,359.4	1,307.3	1,256.9	1,209.0	1,164.4	1,122.7	1,078.9	1,030.2
Total		-240.0	-297.0	-394.7	-508.0	-619.0	-728.6	-835.5	-939.1	-1,039.8	-1,142.6	-1,250.4
Alloy Product	1,600.0	148.8	138.7	122.9	115.3	105.1	93.6	80.5	65.2	47.8	28.2	7.4
Dust Output	850.0	-40.9	-42.7	-44.5	-46.3	-48.0	-49.8	-51.6	-53.4	-55.2	-57.0	-58.8
Gas Output	850.0	-379.7	-387.8	-421.9	-465.8	-489.4	-504.3	-508.4	-498.1	-473.3	-433.6	-385.7
Slag Product	1,700.0	-468.2	-505.2	-551.2	-611.2	-686.7	-768.1	-855.9	-952.8	-1,059.0	-1,180.2	-1,313.3

Heat Loss*		500.0	500.0	500.0	500.0	500.0	500.0	500.0	500.0	500.0	500.0	500.0
Total		-240.0	-297.0	-394.7	-508.0	-619.0	-728.6	-835.5	-939.1	-1,039.8	-1,142.6	-1,250.4
Balance		0.0	0.0	0.0	0.0	0.0	0.0	0.0	0.0	0.0	0.0	0.0

Table A.12: Energy balance iron reduction at 1100°C

Stream	**T, °C**	**Energy, kWh**										
		Mass percent of PCB in blend,%										
		0	**10**	**20**	**30**	**40**	**50**	**60**	**70**	**80**	**90**	**100**
Ore Feed	25.0	-1,580.1	-1,580.1	-1,580.1	-1,580.1	-1,580.1	-1,580.1	-1,580.1	-1,580.1	-1,580.1	-1,580.1	-1,580.1
Reductant Feed	25.0	-110.1	-169.1	-228.2	-287.2	-346.2	-405.3	-464.3	-523.3	-582.4	-641.4	-700.5
Electrical Energy		1,462.0	1,433.3	1,395.7	1,340.2	1,285.6	1,211.2	1,138.1	1,072.2	1,014.2	957.0	900.4
Total		-228.3	-316.0	-412.6	-527.1	-640.8	-774.2	-906.3	-1,031.3	-1,148.3	-1,264.5	-1,380.2
Alloy Product	1,600.0	173.6	129.0	113.3	107.0	97.9	84.8	73.6	64.4	45.1	25.9	6.6
Dust Output	850.0	-40.9	-42.7	-44.5	-46.3	-48.0	-49.8	-51.6	-53.4	-55.2	-57.0	-58.8
Gas Output	850.0	-378.4	-388.1	-425.7	-475.2	-501.3	-499.3	-510.2	-534.6	-486.0	-437.0	-387.6
Slag Product	1,700.0	-482.7	-514.3	-555.8	-612.6	-689.3	-809.9	-918.1	-1,007.6	-1,152.2	-1,296.4	-1,440.4
Heat Loss*		500.0	500.0	500.0	500.0	500.0	500.0	500.0	500.0	500.0	500.0	500.0
Total		-228.3	-316.0	-412.6	-527.1	-640.8	-774.2	-906.3	-1,031.3	-1,148.3	-1,264.5	-1,380.2
Balance		0.0	0.0	0.0	0.0	0.0	0.0	0.0	0.0	0.0	0.0	0.0

Table A.13: Energy balance iron reduction at 1000°C

Stream	**T, °C**	**Energy, kWh**										
		Mass percent of PCB in blend,%										
		0	**10**	**20**	**30**	**40**	**50**	**60**	**70**	**80**	**90**	**100**
Ore Feed	25.0	-1,580.1	-1,580.1	-1,580.1	-1,580.1	-1,580.1	-1,580.1	-1,580.1	-1,580.1	-1,580.1	-1,580.1	-1,580.1
Reductant Feed	25.0	-110.1	-169.1	-228.2	-287.2	-346.2	-405.3	-464.3	-523.3	-582.4	-641.4	-700.5
Electrical Energy		1,398.5	1,396.9	1,369.4	1,298.7	1,227.3	1,163.4	1,102.0	1,044.9	988.1	931.3	874.6

Total		-291.7	-352.4	-438.9	-568.7	-699.1	-822.0	-942.5	-1,058.6	-1,174.4	-1,290.2	-1,406.0
Alloy Product	1,600.0	125.7	115.8	104.1	93.9	87.7	85.5	79.7	62.0	44.2	26.4	8.6
Dust Output	850.0	-40.9	-42.7	-44.5	-46.3	-48.0	-49.8	-51.6	-53.4	-55.2	-57.0	-58.8
Gas Output	850.0	-382.5	-392.1	-427.3	-446.6	-489.3	-561.0	-603.6	-552.4	-500.3	-448.0	-395.6
Slag Product	1,700.0	-494.0	-533.4	-571.2	-669.7	-749.5	-796.7	-866.9	-1,014.8	-1,163.1	-1,311.6	-1,460.2
Heat Loss*		500.0	500.0	500.0	500.0	500.0	500.0	500.0	500.0	500.0	500.0	500.0
Total		-291.7	-352.4	-438.9	-568.7	-699.1	-822.0	-942.5	-1,058.6	-1,174.4	-1,290.2	-1,406.0
Balance		0.0	0.0	0.0	0.0	0.0	0.0	0.0	0.0	0.0	0.0	0.0

Table A.14: Energy balance iron reduction at 900°C

Stream	**T, °C**	**Energy, kWh**										
		Mass percent of PCB in blend,%										
		0	**10**	**20**	**30**	**40**	**50**	**60**	**70**	**80**	**90**	**100**
Ore Feed	25.0	-1,580.1	-1,580.1	-1,580.1	-1,580.1	-1,580.1	-1,580.1	-1,580.1	-1,580.1	-1,580.1	-1,580.1	-1,580.1
Reductant Feed	25.0	-110.1	-169.1	-228.2	-287.2	-346.2	-405.3	-464.3	-523.3	-582.4	-641.4	-700.5
Electrical Energy		1,355.7	1,361.7	1,335.9	1,271.7	1,204.9	1,139.3	1,075.6	1,018.2	961.0	903.7	846.5
Total		-334.6	-387.6	-472.4	-595.7	-721.5	-846.1	-968.9	-1,085.3	-1,201.6	-1,317.8	-1,434.1
Alloy Product	1,600.0	115.3	105.4	95.9	85.9	78.0	73.8	69.2	54.1	38.6	23.2	7.7
Dust Output	850.0	-40.9	-42.7	-44.5	-46.3	-48.0	-49.8	-51.6	-53.4	-55.2	-57.0	-58.8
Gas Output	850.0	-395.9	-405.7	-425.6	-445.7	-491.5	-564.0	-618.3	-566.5	-511.7	-456.5	-401.2
Slag Product	1,700.0	-513.1	-544.6	-598.3	-689.6	-759.9	-806.1	-868.1	-1,019.4	-1,173.3	-1,327.5	-1,481.8
Heat Loss*		500.0	500.0	500.0	500.0	500.0	500.0	500.0	500.0	500.0	500.0	500.0
Total		-334.6	-387.6	-472.4	-595.7	-721.5	-846.1	-968.9	-1,085.3	-1,201.6	-1,317.8	-1,434.1
Balance		0.0	0.0	0.0	0.0	0.0	0.0	0.0	0.0	0.0	0.0	0.0

Appendix B. Reduction of Hematite

Appendix B.1 Mechanism of Solid State Reduction of Hematite at High Temperatures

The reduction of hematite is complex and takes place through a series of stages. Chen et al. (2017) studied the reduction of hematite to metallic iron in a micro fluidized bed. They stated that the reduction of hematite could be separated into two parts that proceed in series. In the first part, hematite is converted to magnetite in a single-step reaction which proceeds fast and covers a reduction degree of about 11%. The conversion of hematite occurs between 600 and 700℃ (Jung & Yi, 2013). A two-step reaction of magnetite to metallic iron takes place in the second part. This is a combination of two single step reaction; magnetite to wustite and wustite to iron; that occur in parallel to cover the conversion from 11% to 100%. Metallic iron is formed at temperatures between 900 and 1100℃ (Carpenter, 2010).

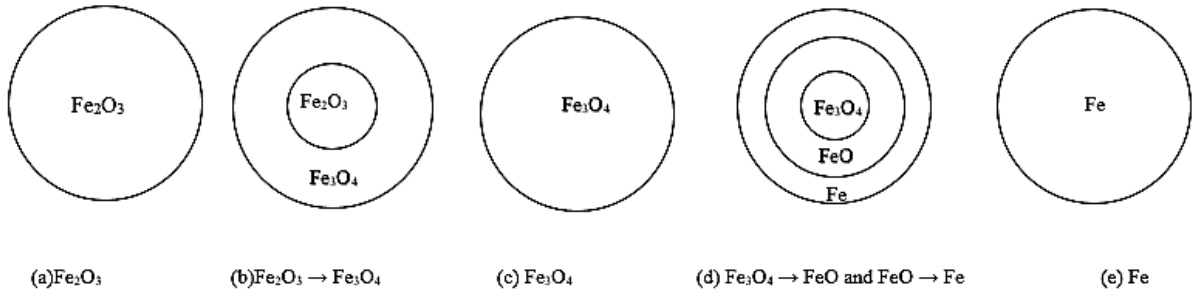

Figure B.1: Mechanism for the reduction hematite to iron reported by Chen et al., (2017)

According to Dankwah *et al.*, (2012) and Carpenter, (2010), the reactions that are believed to occur during reduction of hematite are divided into the following four categories: The removal of oxygen from the iron oxides takes place by a series of chemical reactions

1. Conversion of polymers into hydrocarbons (mainly CH_4)

$$\text{Polymers} = C_nH_{m(g)} \qquad \textbf{Equation B.1}$$

2. Decomposition of hydrocarbons into carbon and hydrogen:

$$C_nH_{m(g)} = C_{n(s)} + {}^{m}/_{2}H_{2(g)} \qquad \textbf{Equation B.2}$$

The hydrocarbon could also act as a sink for CO_2 gas, producing CO and H_2

$$C_nH_{m(g)} + nCO_{2(g)} = 2nCO_{(g)} + {}^{m}/_{2}H_{2(g)} \qquad \textbf{Equation B.3}$$

3. Reduction of iron oxide by hydrogen, carbon and carbon monoxide:

i. Hematite is reduced to Magnetite

$$3Fe_2O_3 + CO_{(g)} = 2Fe_3O_4 + CO_{2(g)} \quad \textbf{Equation B.4}$$

$$3Fe_2O_3 + H_{2(g)} = 2Fe_3O_4 + H_2O_{(g)} \quad \textbf{Equation B.5}$$

$$3Fe_2O_3 + C = 2Fe_3O_4 + CO_{(g)} \quad \textbf{Equation B.6}$$

ii. Magnetite is reduced to Wustite

$$Fe_3O_4 + CO_{(g)} = 3FeO + CO_{2(g)} \quad \textbf{Equation B.7}$$

$$Fe_3O_4 + H_{2(g)} = 3FeO + H_2O_{(g)} \quad \textbf{Equation B.8}$$

$$Fe_3O_4 + C = 3FeO + CO_{(g)} \quad \textbf{Equation B.9}$$

iii. Wustite is reduced to Iron

$$FeO + CO_{(g)} = Fe + CO_{2(g)} \quad \textbf{Equation B.10}$$

$$FeO + H_{2(g)} = Fe + H_2O_{(g)} \quad \textbf{Equation B.11}$$

$$FeO + C = Fe + CO_{(g)} \quad \textbf{Equation B.12}$$

4. Auxiliary reactions

i) Water gas shift reaction:

$$H_2O_{(g)} + CO_{(g)} = CO_{2(g)} + H_{2(g)} \quad \textbf{Equation B.13}$$

ii) Reaction of water vapour with C produced from the cracking of C_nH_m:

$$H_2O_{(g)} + C_{(s)} = CO_{(g)} + H_{2(g)} \quad \textbf{Equation B.14}$$

iii) Boudouard reaction:

$$CO_{(g)} + C_{(S)} = 2CO_{(g)} \quad \textbf{Equation B.15}$$

iv) Carbon dissolution into molten metal:

$$C_{(s)} = \underline{C} \quad \textbf{Equation B.16}$$

Hydrocarbon (C_nH_m) generated from a polymer can also directly reduce FeO and can be represented as

$$FeO + {}^{1}/_{n}C_nH_m = Fe + CO + {}^{m}/_{2n}H_2 \qquad \textbf{Equation B.17}$$

Appendix B.2 Repeatability of Reduction Tests

Each of the tests carried out in the DSC-TGA were repeated in order to establish the repeatability of the reduction experiments. Figure B2 to B6 shows the mass loss of the occurred during each test and their respective repeats.

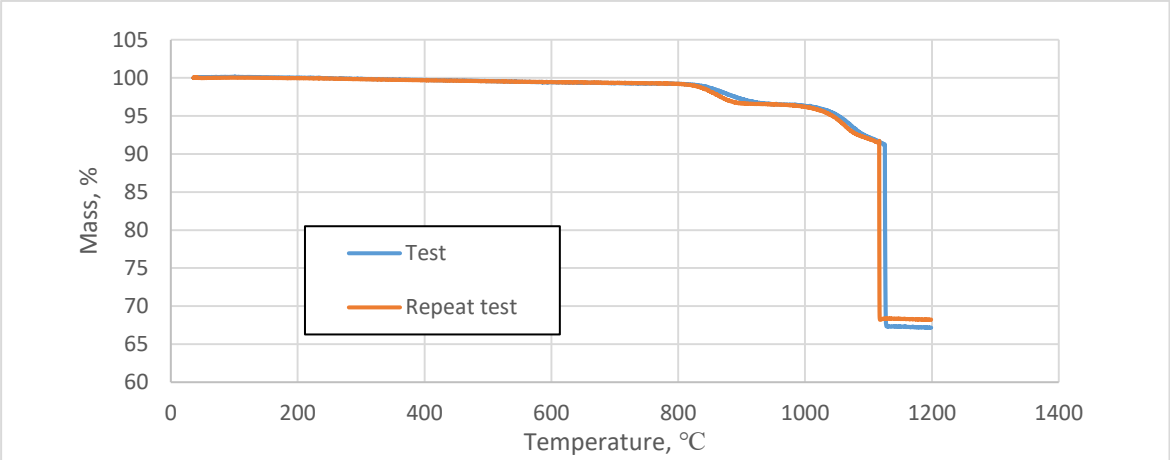

Figure B.2: Mass of sample during hematite-graphite reduction

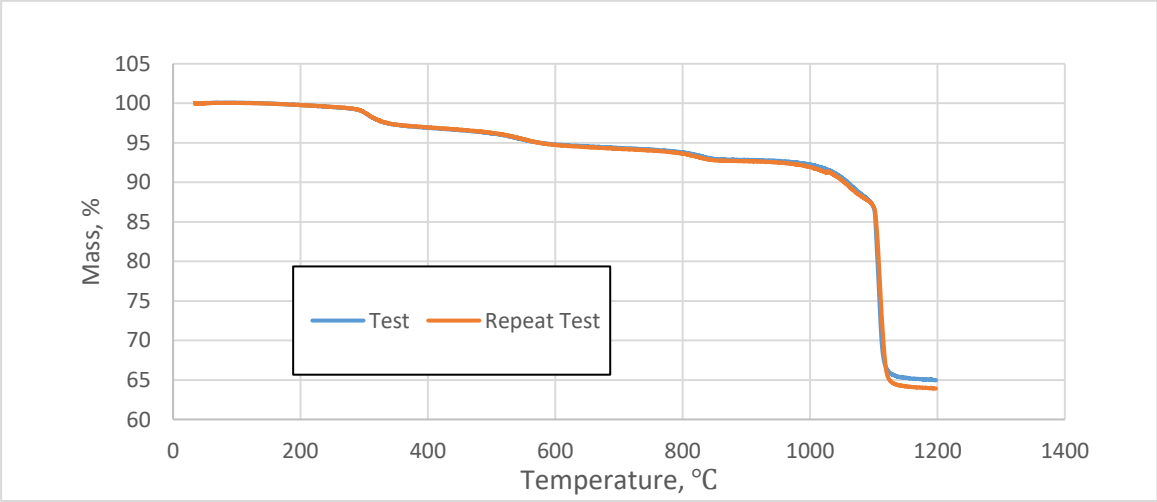

Figure B.3: Mass of sample during hematite-20%PCB reduction

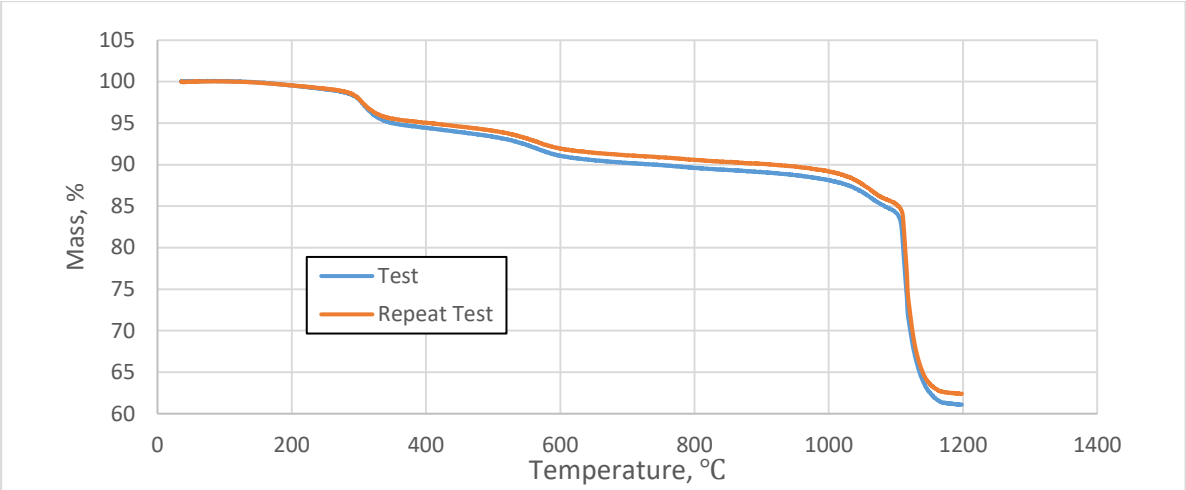

Figure B.4: Mass of sample during hematite-40%PCB reduction

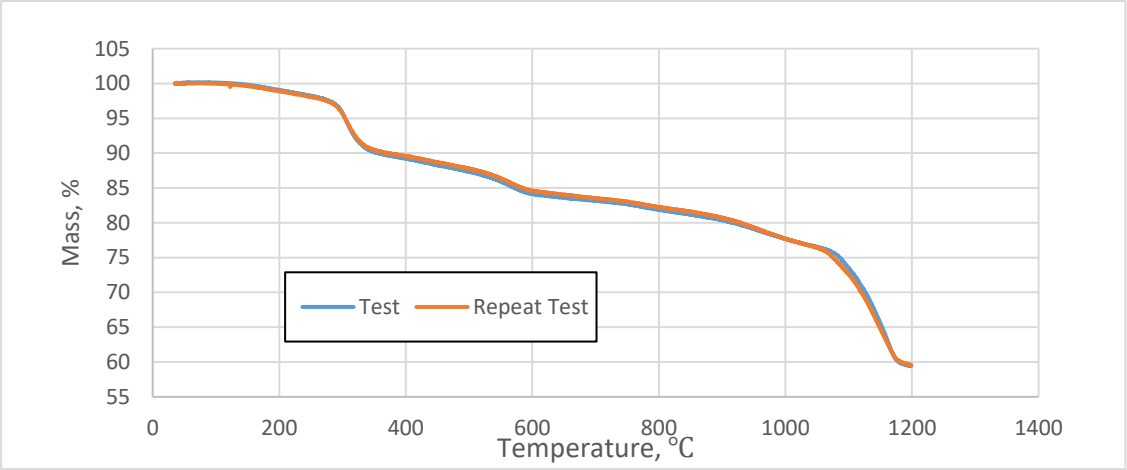

Figure B.5: Mass of sample during hematite-80%PCB reduction

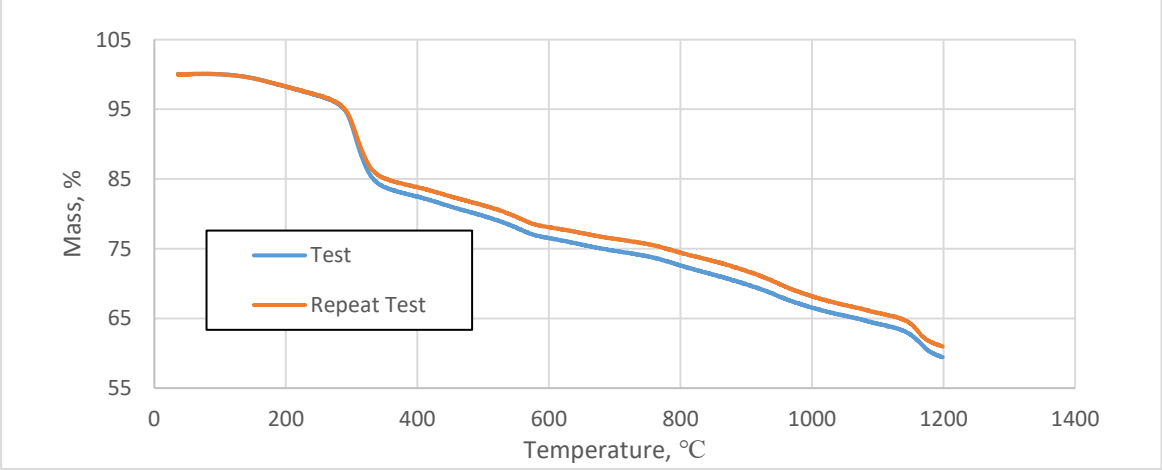

Figure B.6: Mass of sample during hematite-100%PCB reduction

The standard deviation at each of the temperatures were calculated. Table B1 to B5 shows the mass and the standard deviation at selected temperatures during reduction of hematite. Since each of the reduction tests has over 11600 data points, the temperatures 50℃ to 1200℃ with intervals 50℃ were selected. The average value for the standard deviation for all the data point is shown in Table B6.

Table B.1: Standard deviation at selected temperatures during Hematite-Graphite Reduction

Temperature, ℃	Mass, %	Mass of repeat, %	Standard deviation
50	100.0000	100.0000	0.00000
100	100.0000	100.0000	0.00000
150	100.0000	100.0000	0.00000
200	99.9900	99.9633	0.04355
250	99.9564	99.9109	0.02273
300	99.9025	99.8358	0.03334
350	99.7833	99.7624	0.01048
400	99.7256	99.6971	0.01422
450	99.6549	99.6360	0.00946
500	99.5889	99.5694	0.00975
550	99.4845	99.5080	0.01173
600	99.4344	99.4439	0.00477
650	99.3775	99.4045	0.01349
700	99.3113	99.3508	0.01972
750	99.2506	99.3016	0.02551
800	99.2287	99.2101	0.00934
850	98.6733	98.2523	0.21052
900	97.2268	96.6561	0.28534
950	96.5344	96.5270	0.00370
1000	96.3491	96.1948	0.07713
1050	95.1284	94.6324	0.24797
1100	92.2034	92.0059	0.09873
1150	67.2964	68.3465	0.52508
1200	67.1715	68.2305	0.52948

Table B.2: Standard deviation at selected temperatures during Hematite-20%PCB Reduction

Temperature, ℃	Mass, %	Mass of repeat, %	Standard deviation
50	100.0000	100.0000	0.00000
100	100.0000	100.0000	0.00000
150	99.9687	99.9509	0.00889
200	99.7724	99.7738	0.00073
250	99.5141	99.5344	0.01021
300	98.8396	98.8658	0.01310
350	97.2761	97.3076	0.01577
400	96.8953	96.9564	0.03057
450	96.5911	96.6590	0.03395
500	96.1972	96.2548	0.02884
550	95.3932	95.4656	0.03617

600	94.7758	94.7242	0.02578
650	94.5469	94.4475	0.04968
700	94.3432	94.2356	0.05379
750	94.1493	94.0238	0.06275
800	93.7844	93.6141	0.08515
850	92.9477	92.7841	0.08180
900	92.8138	92.6605	0.07667
950	92.6989	92.5022	0.09832
1000	92.2464	91.9188	0.16384
1050	90.5857	90.2509	0.16740
1100	86.7604	86.8953	0.06743
1150	65.2756	64.2022	0.53675
1200	65.0546	63.9511	0.55171

Table B.3: Standard deviation at selected temperatures during Hematite- 40%PCB Reduction

Temperature, °C	Mass, %	Mass of repeat, %	Standard deviation
50	100.0000	100.0000	0.00000
100	100.0000	100.0000	0.00000
150	99.9110	99.8772	0.01688
200	99.5359	99.5566	0.01037
250	99.0829	99.1556	0.03636
300	97.8435	97.9353	0.04589
350	94.9916	95.5478	0.27811
400	94.4399	95.0467	0.30337
450	93.9287	94.5880	0.32965
500	93.3632	94.0788	0.35781
550	92.3609	93.1550	0.39706
600	91.0641	91.9460	0.44097
650	90.5402	91.4359	0.44784
700	90.2058	91.1345	0.46439
750	89.9500	90.8912	0.47058
800	89.6041	90.5802	0.48807
850	89.3555	90.3236	0.48403
900	89.1034	90.0821	0.48938
950	88.7376	89.7363	0.49935
1000	88.1275	89.1834	0.52794
1050	86.6867	87.6391	0.47619
1100	84.2183	85.2815	0.53162
1150	62.6020	63.6320	0.51501
1200	61.1036	62.3952	0.64581

Table B.4: Standard deviation at selected temperatures during Hematite- 80%PCB Reduction

Temperature, °C	Mass, %	Mass of repeat, %	Standard deviation
50	100.0000	100.0000	0.00000
100	100.0000	100.0000	0.00000
150	99.8038	99.6225	0.09063
200	99.0554	98.8884	0.08350

250	98.2105	98.0728	0.06883
300	95.6976	95.6581	0.01977
350	90.1473	90.4498	0.15124
400	89.2190	89.5899	0.18547
450	88.2517	88.6885	0.21838
500	87.3416	87.7815	0.21996
550	85.9230	86.3573	0.21713
600	84.1260	84.5932	0.23357
650	83.5904	84.0252	0.21740
700	83.1470	83.5178	0.18542
750	82.6589	83.0009	0.17100
800	81.8667	82.2488	0.19103
850	81.1730	81.5773	0.20215
900	80.3704	80.7324	0.18103
950	79.1224	79.3041	0.09086
1000	77.6906	77.7014	0.00543
1050	76.4845	76.4219	0.03131
1100	73.4838	72.5920	0.44592
1150	65.5451	64.7734	0.38581
1200	59.3894	59.5567	0.08364

Table B.5: Standard deviation at selected temperatures during Hematite-100%PCB Reduction

Temperature, ℃	Mass, %	Mass of repeat, %	Standard deviation
50	100.0000	100.0000	0.0000
100	100.0000	100.0000	0.0000
150	99.4606	99.4436	0.00849
200	98.2715	98.2870	0.00774
250	96.9212	96.9908	0.03483
300	92.7655	93.1863	0.21041
350	83.8256	85.0906	0.63250
400	82.4732	83.8276	0.67718
450	81.0668	82.5002	0.71669
500	79.7074	81.2350	0.76380
550	78.0438	79.5861	0.77114
600	76.5129	78.0824	0.78477
650	75.5862	77.2421	0.82792
700	74.6797	76.3994	0.85986
750	73.9071	75.6693	0.88110
800	72.5879	74.4197	0.91586
850	71.2689	73.2247	0.97787
900	69.9128	71.8277	0.95743
950	68.1613	69.9614	0.90009
1000	66.5431	68.1814	0.81918
1050	65.3716	66.9381	0.78327
1100	64.2615	65.7838	0.76119
1150	62.6814	64.2272	0.77292
1200	59.4087	60.9357	0.76351

Table B.6: Average standard deviation of mass loss during hematite reduction

Sample	Average Standard Deviation
Hematite-Graphite	0.17073
Hematite-20%PCB	0.15880
Hematite-40%PCB	0.35381
Hematite-80%PCB	0.16001
Hematite-100%PCB	0.61890

Appendix B.3 Calculation of Reduction Degree

Reduction degree was calculated based on the mass loss during the test

$Fe_2O_3(s) + 3C = 2Fe + 3CO$

Reduction Degree = $\frac{\Delta W/W}{3MW_{CO}/(MW_{Fe2O3}+3MW_C)}$

Where,

W = Initial Mass; ΔW = Mass lost; MW = Molecular Weight

MW(C) = 12.010 g/mol; MW(O) = 15.999 g/mol; MW(Fe) = 55.845 g/mol

Mass of Fe_2O_3 = 1.00g

Molecular weight of Fe_2O_3 = 160g/mol

Amount of Fe_2O_3 = $\frac{1.00}{160}$ = 0.00625 mol

Mass of Reductant = 0.532 g

Amount of Graphite (C) = $\frac{0.532}{12}$ = 0.04433 mol

Moles of Graphite that took part in reduction = 3 × 0.00625 = 0.01875 mol

Excess Mass of Graphite = 0.532 – (0.01875 × 12) = 0.307 g = (57.71% of graphite used)

Assuming 100 g of Sample used

Initial Mass, W = 100 g

Mass of Hematite = $\frac{1}{1+0.532} \times 100$ = 65.359 g

Mass of Reductant present = 100 – 65.359 = 34.641 g

Excess graphite = 57.71% of 34.641 = 20g

Let X represent the mass loss

Mass lost, ΔW = X

Reduction Degree = $\frac{X/(100-20)}{84/196}$

Appendix C. XRF full Scan of PCB

Instrument: XRF Axios (PANalytical)

Crystals used: LIF220, LIF 200, Ge, PE, PX1.

The following elements were detected: Tellurium, Antimony, Tin, Palladium, Molybdenum, Zirconium, Strontium, Copper, Zinc, Tungsten, Nickel, Iron, Titanium, Barium, Calcium, Potassium, Chlorine, Suplhur, Posphorus, Silicon, Tantalum, Aluminium, Magnesium

Detection of small quantity need to be measured as the resolution of the scan is not small enough.

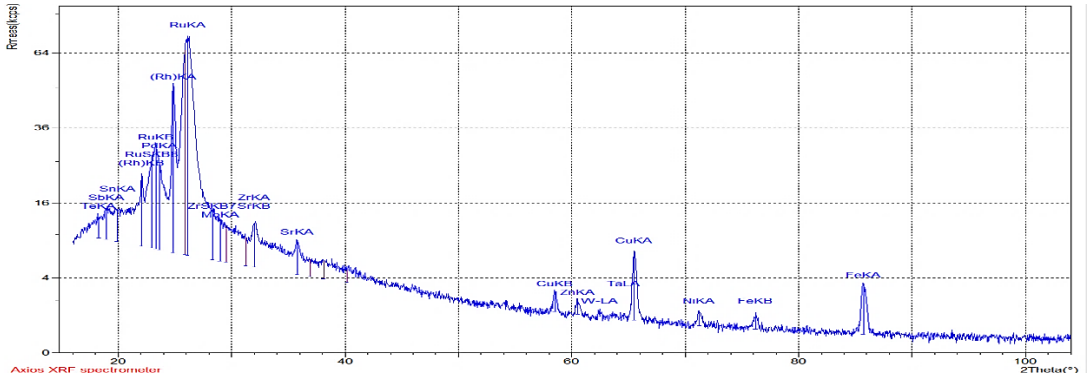

Figure C.1: XRF scan from angle 16 (2θ) to 110 (2θ), using LiF 220 crystal

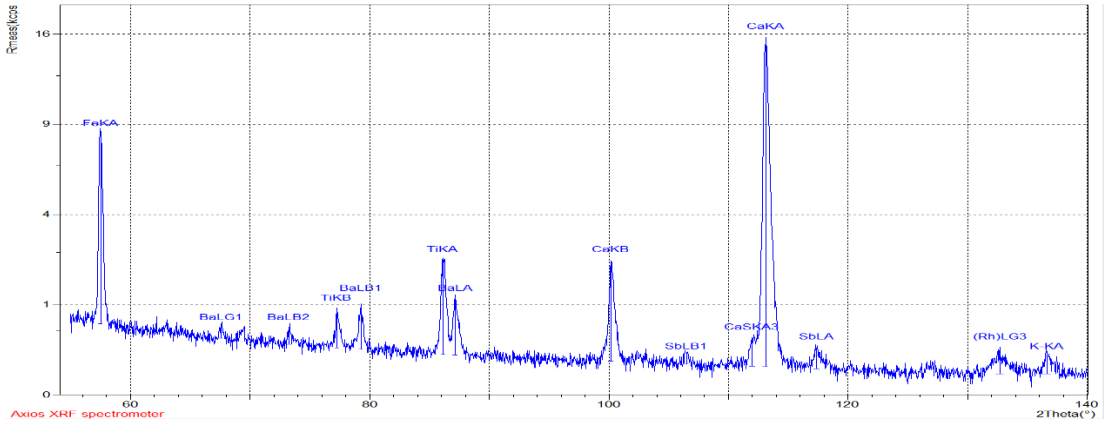

Figure C.2: XRF scan from angle 56 (2θ) to 140 (2θ), using LiF 200 crystal

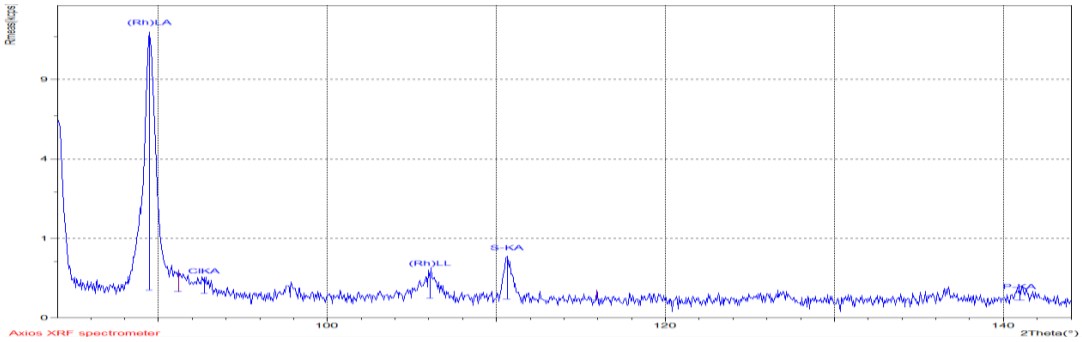

Figure C.3: XRF scan from angle 0 (2θ) to 160 (2θ), using Ge crystal

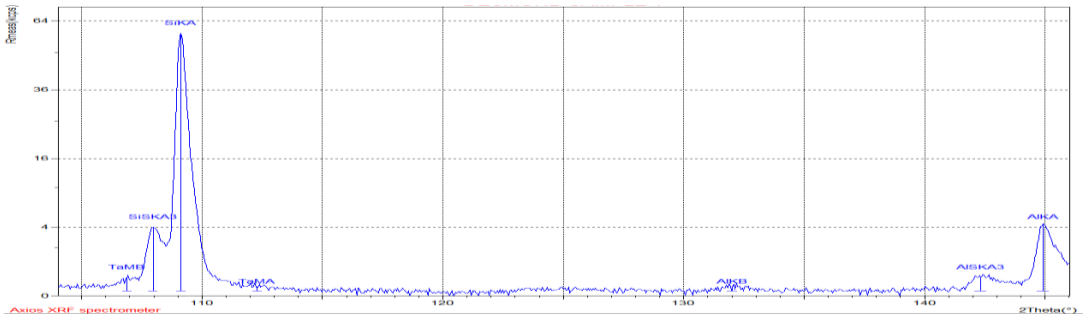

Figure C.4: XRF scan from angle 105 (2θ) to 146 (2θ), using PE crystal

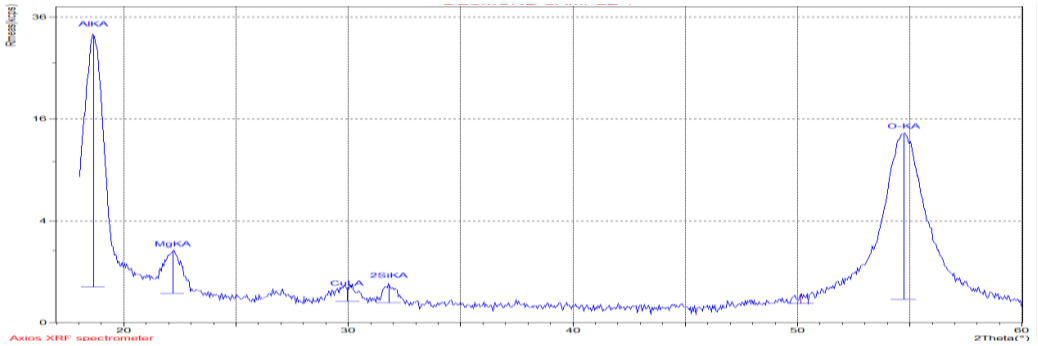

Figure C.5: XRF scan from angle 17 (2θ) to 60 (2θ), using PX1 crystal.

Appendix D. XRD Patterns from products of hematite reduction in SPR

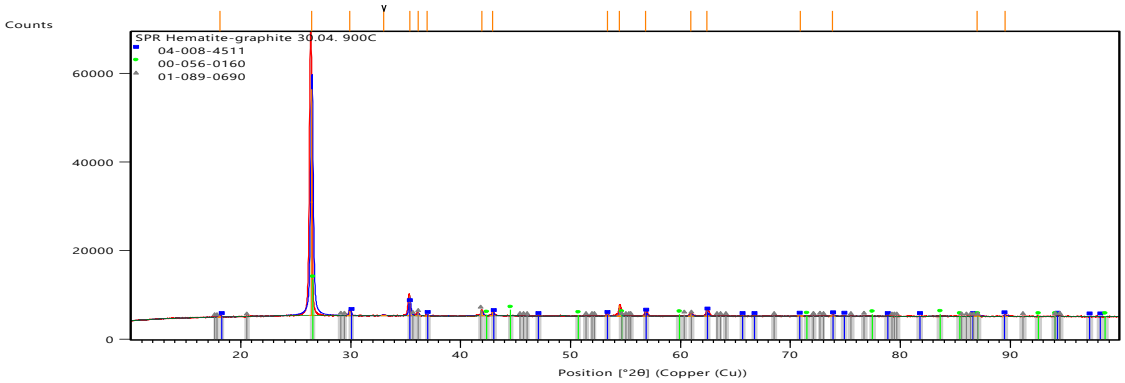

Figure D.1: XRD pattern from hematite-graphite reduction at 900°C

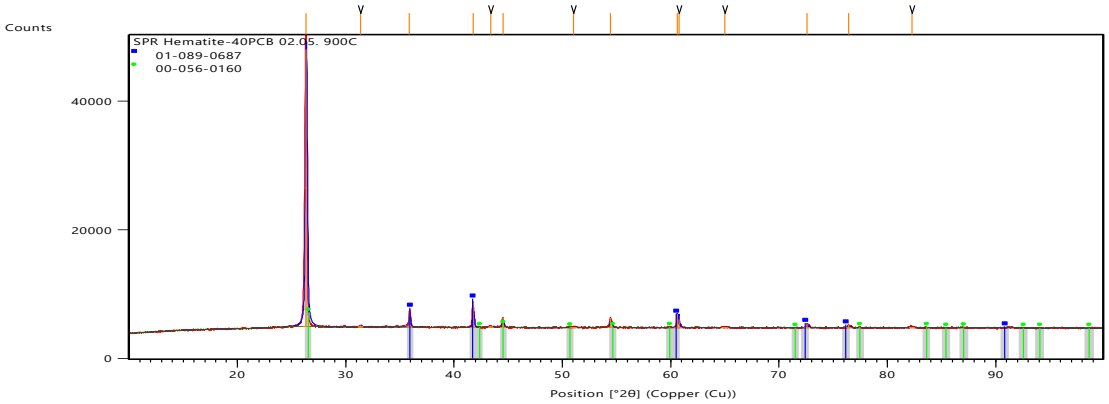

Figure D.2: XRD pattern from hematite-40%PCB reduction at 900°C

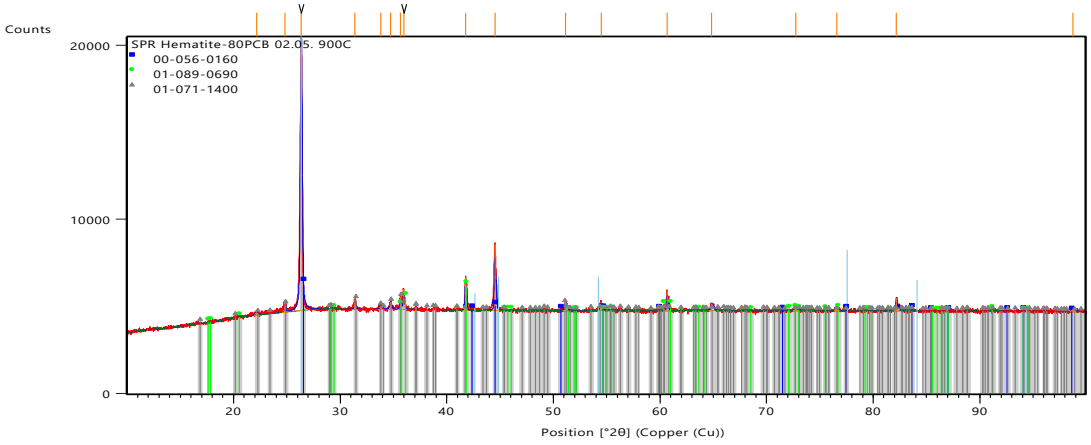

Figure D.3: XRD pattern from hematite-80%PCB reduction at 900°C

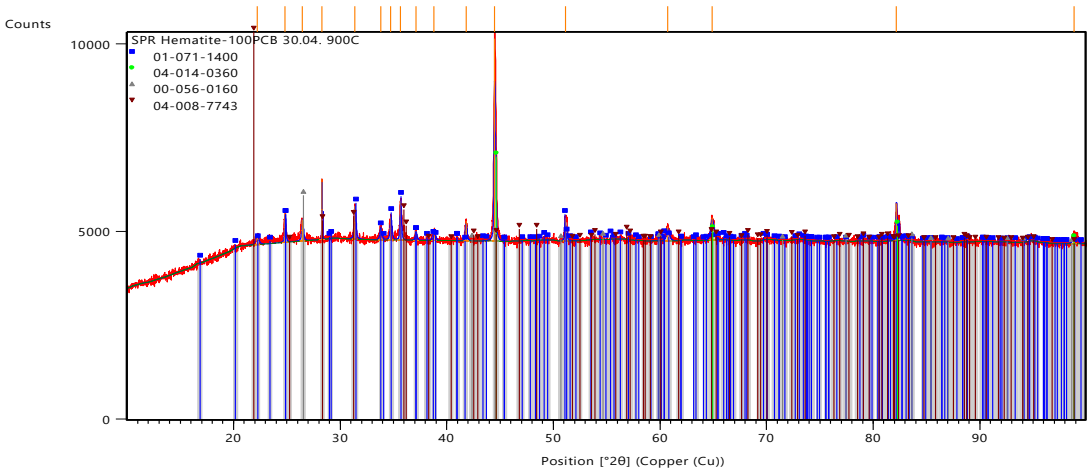

Figure D.4: XRD pattern from hematite-100%PCB reduction at 900°C

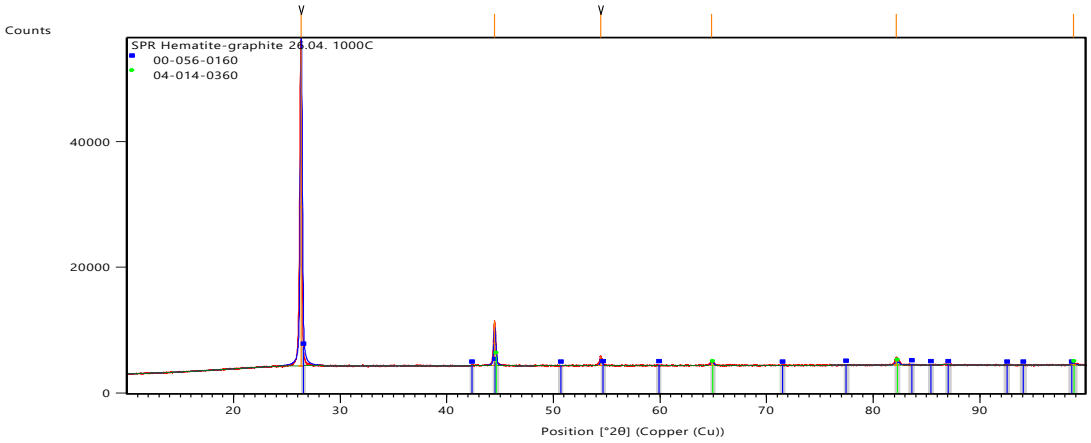

Figure D.5: XRD pattern from hematite-graphite reduction at 1000°C

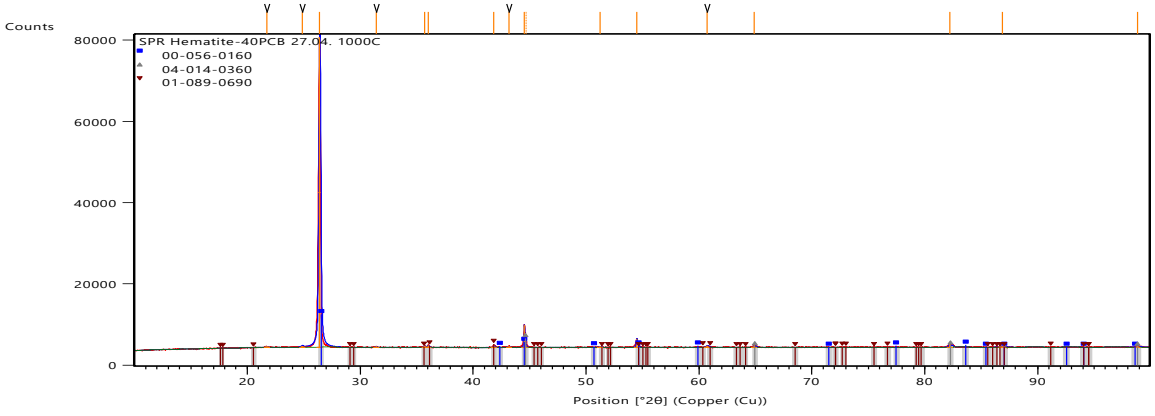

Figure D.6: XRD pattern from hematite-40%PCB reduction at 1000°C

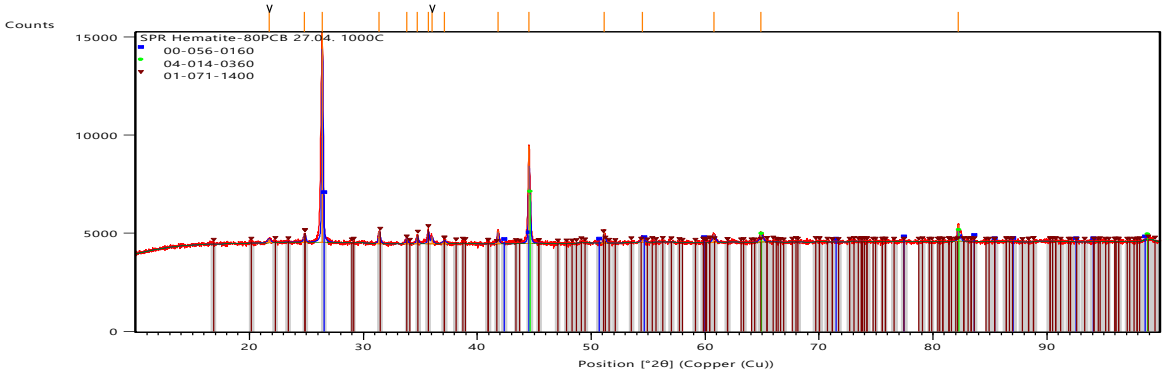

Figure D.7: XRD pattern from hematite-80%PCB reduction at 1000°C

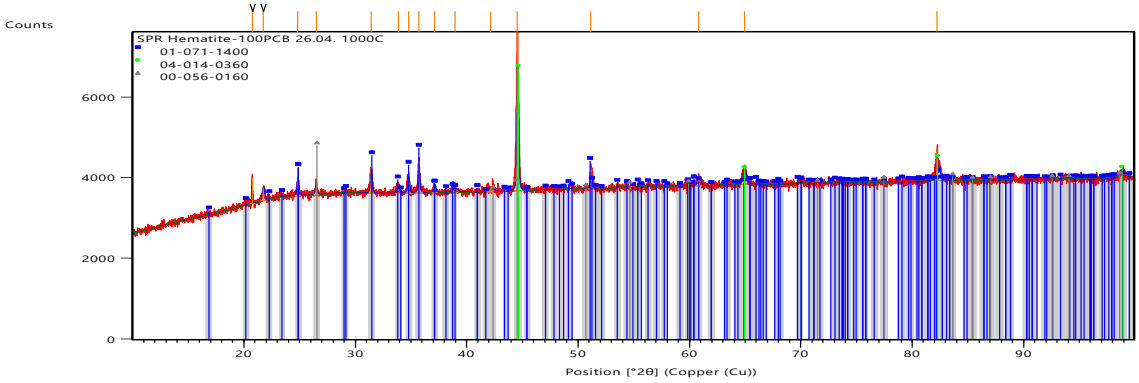

Figure D.8: XRD pattern from hematite-100%PCB reduction at 1000°C

Table D.1: Reference codes representing each compound in XRD patterns

Reference Code	Compound Name	Chemical Formula
04-008-4511	Iron Oxide	Fe_3O_4
00-056-0160	Graphite	C
01-089-0690	Iron Oxide	FeO
01-071-1400	Iron Silicate	Fe_2SiO_4
04-008-7743	Silicon Oxide	SiO_2
01-071-1400	Iron	Fe